UNIVERSITY OF OKLAHOMA

GRADUATE COLLEGE

DEVELOPMENT OF A NOVEL *EX VIVO* SCAFFOLD FOR THE REGENERATION OF PERIODONTAL TISSUES

A DISSERTATION

SUBMITTED TO THE GRADUATE FACULTY

in partial fulfillment of the requirements for the

Degree of

DOCTOR OF PHILOSOPHY

By

SELDA GOKTAS
Norman, Oklahoma
2011

DEVELOPMENT OF A NOVEL *EX VIVO* SCAFFOLD FOR THE REGENERATION OF PERIODONTAL TISSUES

A DISSERTATION APPROVED FOR THE
SCHOOL OF CHEMICAL, BIOLOGICAL
AND MATERIALS ENGINEERING

BY

_____
Dr. Lance L. Lobban, Chair

_____
Dr. Peter S. McFetridge

_____
Dr. Edgar A. O'Rear III

_____
Dr. Matthias U. Nollert

_____
Dr. Rong Z. Gan

_____
Dr. John J. Dmytryk

Acknowledgements

I am grateful to Dr. Lance Lobban, for being the chair of my doctoral committee and being a great supervisor to me especially during the very critical final phase of my Ph.D. Without his guidance and support, this project would not have been completed. I would like to express my appreciation to Dr. Peter McFetridge for his advice, valuable suggestions and constructive criticism. I also would like to thank Dr. John Dmytryk for his continuous guidance, very helpful suggestions and comments. I would also like to thank Dr. Edgar O'Rear, for his valuable support in my study, Dr. Rong Gan, for opening the gate to the amazing world of Biomechanics, Dr. Matthias Nollert, for his help, advice and suggestions whenever I needed.

I also would like to thank Dr. Barbara Safiejko-Mroczka for providing primary human gingival fibroblasts and being such a great person who is always willing to help in any way she could. I also would like to acknowledge the Birth Center in Norman Regional Hospital, Norman, OK for supplying the human umbilical cords used in this study.

Special thanks go to our wonderful technician, Alan Miles, for always making the impossible, possible in our research laboratory.

I would like to acknowledge the graduate students providing help and support for me in many ways- Roman Voronov, Rita Abousleiman, Brandon Engebretson, Brent Van Rite, Luis Filipe Neves, Nicholas Pierre, Maritza Rodriguez, Jaclyn Brennan, Jose Alvarez-Barreto, Samuel VanGordon, Koki Abe, Aravinda Buddhala, Pratik Kothary, Chiranth Srinivasan, Deepthi Konatham and Sivakumari Gnanasekar.

I also would like to acknowledge our staff Terri Colliver, Vernita Farrow, Donna King, Kelly Wilcox and Madena McGinnis for their kindness and very professional assistance**.**

Finally, I would like to thank my parents, Mustafa Goktas and Necla Goktas, and my "little" sister Semra Goktas Cengiz for their endless love, support and patience. I believe the good heart we share has brought us our happy lives.

Table of Contents

List of Tables

List of Figures

Abstract

Burgeoning knowledge of the principles of tissue engineering has enabled periodontal surgeons to evolve from resective therapies to more regenerative approaches to treat the periodontal diseases that afflict a large portion of the population. These investigations describe the development of a novel 3D *ex vivo* scaffold derived from the Human Umbilical Vein (HUV) and its potential as an alternative surgical barrier material for the regeneration of periodontal tissues.

Periodontal grafting materials should fulfill several requirements, of which the mechanical matching of the scaffold with the native residual tissue is crucial. However, little attention has been given to understanding the biomechanical behavior of oral soft tissues, and this represents an obstacle for the development of biomaterials that perform with appropriate biomechanical characteristics. With this as our motivation, an *in vitro* uniaxial mechanical analysis was performed on mammalian oral soft tissue to further our understanding of these complex tissues. Porcine oral soft tissues from both lingual and buccal sites were assessed to gain insight into human tissue performance and site-specific mechanical variation. Mechanical analysis was conducted on 3 different regions of the oral tissues – namely, the attached gingiva, alveolar mucosa, and buccal mucosa. Our hypothesis stated that a discrete quantitative mechanical analysis describing zonal behavior of each soft tissue region would correlate with published qualitative data. Results confirm the keratinized gingiva to have increased tensile strength and stiffness relative to non-keratinized mucosal regions, where densely arranged elastin fibers

contribute to a tissue with increased viscoelastic properties. These investigations quantify the biomechanical properties of these oral soft tissues and show region-to-region variation that provides important insight into structure-function relationships necessary to support masticatory and other oral forces.

Following the mechanical characterization of the porcine model system as reference, HUV were isolated from umbilical cords using a semi-automated machining technology, and decellularized using 1% sodium dodecyl sulphate (SDS). Uniaxial tensile testing, stress relaxation, and suture retention tests were performed on the acellular matrix to evaluate the HUV's biomechanical properties and human gingival fibroblasts (hGF) were seeded to assess adhesion, metabolic function and proliferation on the scaffold. Results show the scaffolds biomechanical properties were dependent upon the complex composition of the *ex vivo* scaffold, with the composite nature of the *ex vivo* tissue contributing to the biomechanical variability. Cell proliferation and metabolic activity were shown to be dependent upon the surface characteristics; in this case the lumen and ablumenal surfaces of the vascular derived scaffolds. hGF migration into the scaffold was also influenced by the organization of extracellular matrix (ECM) components, where the lumenal surface inhibits cell migration, acting as a barrier, whilst the ablumenal surface promotes cellular invasion. The results have shown the HUV bioscaffold with its unique biochemical and biomechanical properties represents a promising naturally derived surgical barrier for periodontal tissue regeneration.

In order to create functional HUV bioscaffolds for periodontal tissue engineering applications, *in vitro* 3D culture conditions were developed and optimized. The goal was

to assess the scaffolds' capacity to initiate the regeneration processes while mimicking the physiological conditions. The HUV scaffold was decellularized according to our previously described protocol in order to remove the cellular components that may cause any immune reactions by the host. The human gingival fibroblast (hGF) cells were cultured on the HUV grafts under both static and dynamic conditions for 7 and 28 days. We hypothesized that the flow conditions would enhance the cellular biological activities towards the achievement of periodontal regeneration. The adherence, migration and proliferation capacities of hGFs were evaluated over time. Investigations were also conducted to test the gene expression profiles of the hGFs cultured on the HUV scaffold. The data presented in this study reveals the dynamic culture conditions enhance the attachment and migration of hGFs on the HUV tissue matrix, as visualized with histological and immunohistochemical analyses. The cellular metabolic activity, proliferation rate and gene expression profiling also supported our hypothesis for this study.

CHAPTER 1

INTRODUCTION

Periodontal disease not only threatens the oral health of a large segment of the adult population, but has also been implicated as a contributor to major systemic disorders, such as cardiovascular disease.[1, 2] Several approaches have been adopted as treatment modalities among which periodontal tissue engineering has gained the most attention. One of the main goals of periodontal tissue engineering is to develop 3D tissue scaffolds that have the capacity to be remodeled and ultimately regenerate periodontal tissues that have been lost due to periodontal disease, specifically cementum, bone and periodontal ligament.

Periodontal tissue engineering employs two main scaffolding techniques to regenerate lost support: periodontal grafting materials and physical barriers. Numerous studies have been conducted that demonstrate the advantages and drawbacks with the use of periodontal grafting materials.[3, 4] However, the current golden standard for periodontal regeneration is the use of periodontal guided tissue regeneration (GTR) membranes, with or without the use of bone grafting materials.[5-7] The main concept of GTR membranes is that a physical barrier or membrane is used as a protective shield to prevent epithelial downgrowth and thus provides a favorable environment for progenitor cells to repopulate the defect site and ultimately differentiate into cells that will regenerate the periodontium.[8-10] Numerous cell types have been studied for their active roles in

periodontal GTR therapies, such as periodontal ligament cells and human gingival fibroblasts (hGFs) that have also been used *in vitro* for testing the biocompatibility of GTR membranes.[11, 12]

In the process of developing ideal GTR materials, however, further and detailed understanding of the complex interactions between the barrier and the native tissues is required. In order to achieve successful periodontal regeneration following reconstructive surgeries, biocompatibility, mechanical properties, and cell-selective characteristics of these barrier membranes must be optimally engineered in order to achieve predictable clinical outcomes.[13-15] In addition, the biochemical composition, biological characteristics and mechanical properties of the periodontal replacement graft should match those of the neighboring native tissues. Nevertheless, particularly in medical applications, the literature is replete with studies reporting graft failures due to mismatching of these characteristics and properties.[16-19]

In this study, we proposed that the human umbilical vein (HUV) would be a potential candidate periodontal GTR membrane. The HUV shows great resemblance to periodontal soft tissues, particularly, the gingival connective tissue.[20-28] In addition to its selected biochemical characteristics, the HUV with its internal void spaces that are larger in the outermost region of the scaffold, i.e., the Wharton's Jelly, may guide the fibroblasts to colonize the scaffold.[29] The loose structure of Wharton's Jelly surrounds the adventitial layer of the vein and comprises several growth factors.[30, 31] Thus, the unique composition and architecture of the HUV membrane may offer advantages for facilitating periodontal

wound healing and tissue regeneration. However, a reference material still remains to serve as baseline for the mechanical requirements for the HUV.

Therefore, one of the main focuses of this study was to characterize the biomechanics of a model oral soft tissue system. Porcine oral soft tissues were selected as the model system due to their resemblance in biochemical composition, histological organization and immunological properties to human tissues.[32, 33] In this investigation, we hypothesized that the porcine model could provide a valuable indication of how human tissues would react under similar stresses. Our aim with this study was also to understand the mechanical property requirements for our novel periodontal scaffold, the HUV, in order to match the biomechanics of the human oral tissues in surgical practice. Ideally, the mechanical properties of the GTR barrier implant should match the properties of the attached gingiva to provide a good seal between the wound site and the bacteria-rich oral environment.[34]

In order to create periodontal scaffolding materials with defined properties, the design of an *in vitro* model system that simulates the physiological conditions is essential. However, the literature still lacks such *in vitro* systems that would allow studies of the interactions between periodontal GTR membranes and the surrounding tissue environment. Bioreactors are important devices to provide suitable environments for further improvement of the scaffolds while maintaining the mechanical and biochemical stimulation at the desired level.[35, 36] Ideally, such a bioreactor system needs the harmonic functioning among the scaffold, cells and signaling factors, such as growth factors. Therefore, in this study, a model bioreactor system was designed to study the interactions

between hGFs seeded in the HUV-derived GTR membranes and the simulated 3D environment. In this study, it was hypothesized that the different conditions created within the bioreactor system would affect hGFs by altering their proliferative capacity and the synthesis of extracellular matrix (ECM) components.

In the light of the above-mentioned aspects, the objectives of the present research project were threefold:

1) To characterize the biomechanics of a model oral soft tissue system to better evaluate the mechanical response of the HUV-derived scaffold.
2) To characterize a novel *ex vivo* human umbilical vein (HUV)-derived scaffold to test its potential as a guided tissue regeneration (GTR) membrane. The ability of the HUV bioscaffold to provide a favorable environment for early wound healing events was assessed by examining the proliferation, migration and viability of human gingival fibroblasts (hGFs). The sustainability of the HUV biomatrix under applied mechanical stresses was also determined.
3) To examine the effects of the use of a novel pulsatile flow bioreactor system emulating the periodontal wound healing environment on hGF attachment, viability, proliferation and gene expression for various ECM proteins within the HUV scaffold.

In order to better understand the pathogenesis and treatment of periodontal disease, Chapter 2 gives a detailed background on the tissues, molecules and cells of the periodontium, and the biological processes related to the disease. Chapter 3 focuses on the concept of periodontal tissue engineering and the current scaffolding technologies

that are used in periodontal treatment. Chapter 4 covers the biomechanical characterization of a model soft oral tissue system to give periodontal tissue engineers the opportunity to contrast/compare their novel *ex vivo* periodontal GTR barrier membranes with actual oral tissues. Chapter 5 describes the investigations undertaken to introduce, modify and characterize our novel *ex vivo* material- the HUV. Chapter 5 concludes with a comparison of the mechanical properties of our novel barrier membrane with those of the model oral soft tissue system. Chapter 6 introduces a novel bioreactor system and describes experiments conducted with our HUV scaffold within an environment simulating the conditions during periodontal wound healing. Chapter 7 addresses the hypotheses and goals of the project stated in this chapter and provides the main conclusions to the study. Finally, Chapter 8 includes an overall summary and suggests important areas of further research based on the findings of the current study.

CHAPTER 2

PERIODONTAL DISEASE

2.1. INTRODUCTION

Periodontal disease is a mixed bacterial infection leading to a progressive destruction and loss of hard and soft connective tissue support of the teeth. Gingivitis and periodontitis are the two most common forms of periodontal disease. Formation of bacterial plaque biofilm on the tooth surface and calculus initiate the development of gingivitis. If treatment is not received, gingivitis could progress into the more serious later stage periodontitis. The indicator change for periodontitis is the downward migration of junctional epithelium and the consequent formation of a gingival pocket (Fig. 2.1). If untreated, periodontitis leads to periodontal disease and eventual loss of the teeth.

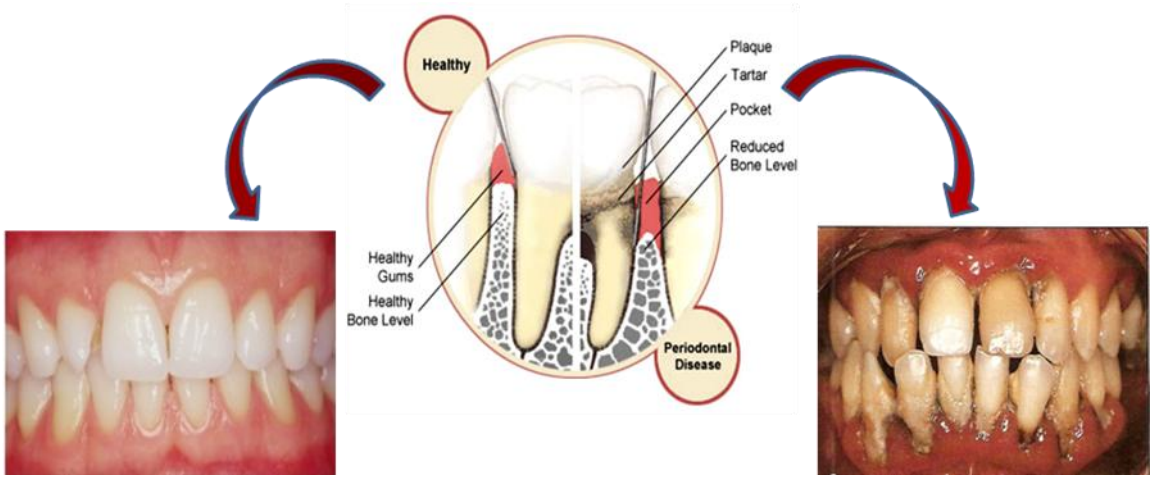

Figure 2.1. Clinical pictures showing the healthy periodontal tissues (left), and the resolution of periodontitis with associated anatomical deficiencies (right).[37]

Several factors may cause the periodontal disease, such as the long-term colonization of bacterial pathogens (such as *Actinobacillus actinomycetemcomitans*,[38, 39] *Porphyromonas gingivalis*,[40] and *Bacteroides forsythus*[41, 42]) on the root surfaces, smoking,[43, 44] alcohol,[45, 46] systemic and genetic disorders,[47-49] and stress[50, 51].

2.2. STRUCTURE OF NORMAL PERIODONTAL TISSUES

The periodontium consists of soft tissues (gingiva and periodontal ligament) and hard tissues (alveolar bone and cementum) and functions to support the teeth. Each of these periodontal components has distinct biochemical and biological composition and function. Fig. 2.2 illustrates the components of the periodontium – gingiva, cementum, periodontal ligament and alveolar bone.

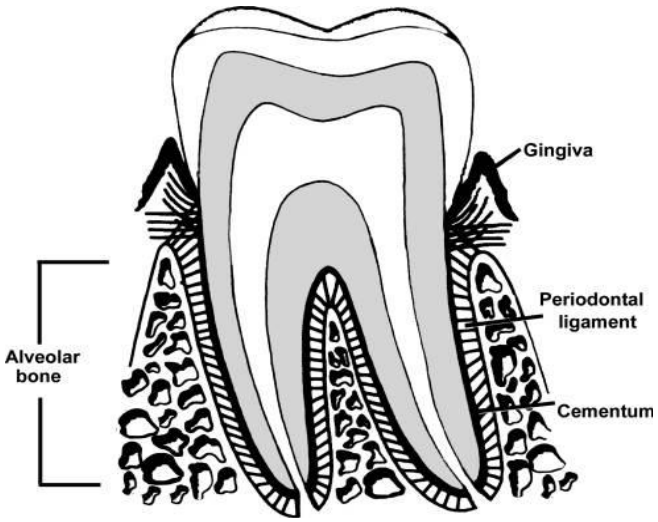

Figure 2.2. Schematic presentation of the tooth-supporting tissues of healthy periodontal tissues.[52]

2.2.1. Gingiva

The gingiva serves as the protective outermost tissue layer for the periodontium. Like all other oral mucosal tissues, gingival is composed of an upper epithelial layer (gingival epithelium) and the underlying gingival connective tissue layer (lamina propria). The structural transition between the two layers is achieved through a boundary layer, called the basement membrane (See Fig. 2.3). However, a definite sub-mucosa is absent in gingiva.

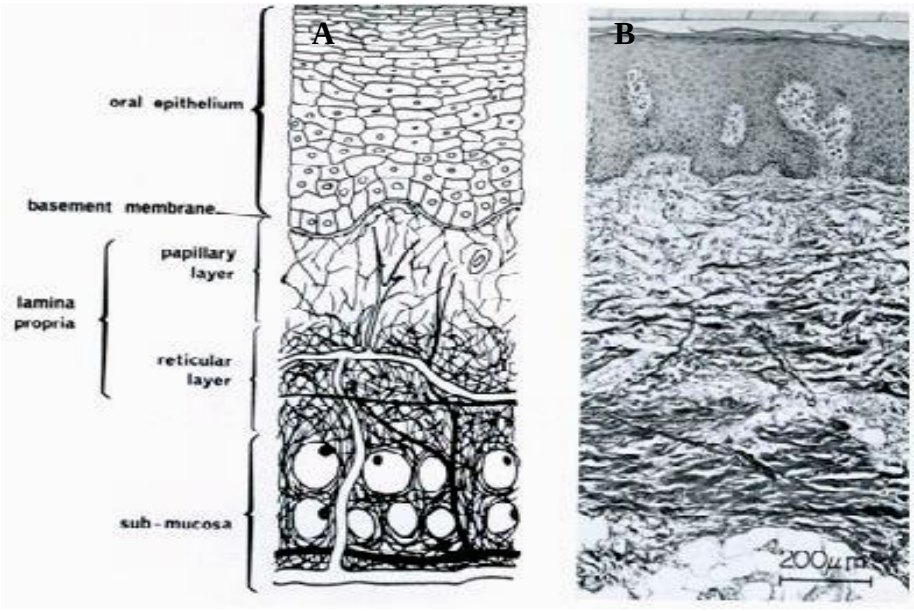

Figure 2.3. Structural features of the oral mucosal tissues **(A)** and the corresponding histological image **(B)**.[53]

2.2.1.1. *Gingival Epithelium*

Gingival epithelium is a stratified keratinizing layer acting as a protective barrier against the inflammatory and chemical substances, and mechanical stresses.[54] Gingival epithelium, with a matrix devoid of fibrous proteins, consists primarily of squamous epithelial cells, and depending on the presence of cell nuclei, this layer could be either orthokeratinized or parakeratinized. Gingival-epithelial proteoglycans and glycosaminoglycans comprise the primary non-fibrous proteins of this layer.[55, 56] Growth factors, such as platelet-derived growth factor and transforming growth factor-β, also exist in epithelium.[57]

2.2.1.2. *Gingival Connective Tissue (Lamina Propria)*

The connective tissue layer, i.e., the lamina propria, consists mainly of fibrous proteins embedded within a highly hydrated, non-fibrous tissue matrix composed primarily of hyaluronic acid, proteoglycans and glycoproteins.[58, 59] The collagen fibers responsible for the bulk tissue tensile properties are relatively thicker and more densely packed in the attached gingiva.[60] Healthy gingiva contains collagen type I (90%), collagen type III (8%), and collagen types IV, V, VI, and VIII (2%).[61]

On the other hand, elastic fibers that provide tissue flexibility for extension and twisting motions are abundant in the alveolar mucosal connective tissue with a progressive reduction in density toward the gingival connective tissue.[22, 62, 63] The network of elastic fibers is comprised of three different group of fibers, namely elastic, elaunin and oxytalan fibers. The elastic fiber is composed of two ultrastructurally distinct components – the

protein elastin and microfibrillar structures consisting of 10 to 12 nm in diameter.[64] Elastin constitutes 90% of the elastic fibers.[65] The elaunin is on the other hand composed of less mature elastin protein.[66] The oxytalan fibers are comprised of microfibrils lacking any elastic properties.[67, 68] By contrast the buccal mucosal connective tissues possess a loose fiber network sparsely populated with collagenous fibers but relatively abundant in elastic fibers.[69] In general, the epithelial layer undergoes higher deformation when subjected to load compared to the connective and submucosal tissue layers.[70]

Proteoglycans, hyaluronic acid and glycoproteins, on the other hand, resist applied compressive and tensional forces while maintaining tissue hydration.[71] The proteoglycans of the ECM of the gingiva are namely chondroitin sulfate (CS), dermatan sulfate (DS), and heparan sulfate (HS).[55, 72, 73]

The most abundant cell type in the gingival connective tissue layer are fibroblasts, comprising 5.6% of the total gingival volume.[74] Other cells residing in the lamina propria are mast cells, plasma cells, macrophages, and lymphocytes.[75] Capillaries constitute the vascular components within the gingival connective tissue layer.

2.2.2. Periodontal Ligament

Connective tissue of periodontal ligament (PDL) consists of collagen fibers (94% type I collagen and 16-18% type III collagen) that traverse from alveolar bone to cementum, proteoglycans, glycoproteins and progenitor cells that can differentiate into periodontal ligament fibroblast cells, osteoblasts and cementoblasts.[76-78] In addition, periodontal ligament contains blood and lymph vessels, and nerves.[79]

2.2.3. Alveolar Bone

Hydroxyapatite (HA) is the main mineral that constitutes most part of the alveolar bone.[52] On the other hand, collagen type I is the principal collagen constituting the organic part of the alveolar bone.[80] The vascular structure of alveolar bone comprises of cellular components such as osteoclasts, osteocytes and osteoblasts.[81] The noncollagenous matrix proteins found in alveolar bone are the complex glycoconjugates, such as glycoproteins, glycosaminoglycans and proteoglycans. The major proteoglycan in alveolar bone tissue is chondroitin sulfate, with the other proteoglycans hyaluronate, dermatan sulfate and heparin sulfate.[82]

2.2.4. Cementum

Cementum is an avascular, hard connective tissue consisting of approximately 50% hydroxyapatite (HA) and 50% organic matrix, mainly calcified collagen fibers (types I and III) that are contiguous with the PDL.[37, 83] Some of the important noncollagenous proteins present in cementum are laminin, fibronectin, osteonectin and glycosaminoglycans.[84-86] Cementoblasts and fibroblasts constitute the cellular part of cementum.[87] Cementum also comprises several growth factors, such as cementum-derived growth factor and fibroblast growth factor.[79, 88]

2.3. DISEASED PERIODONTAL TISSUES

Numerous factors have been mentioned in Section 2.1 that cause inflammatory periodontal disease. These factors could function through different stimulus-responsive pathways. In the case of inflammation caused by bacterial pathogens, lipopolysaccharides

(LPS), major surface components of almost all gram-negative bacteria, stimulate epithelial cells and monocytes to produce cytokine proteins interleukin-1 (IL-1), tumor necrosis factors-α (TNF-α), and prostaglandin E_2 (PGE_2).[37] The connective tissue fibroblasts interacting with LPS synthesize PGE_2 and interleukin-1 (IL-6). PGE_2 inhibits fibroblast proliferation and collagen synthesis, and triggers bone resorption with IL-6.[89] The synergistic action of cytokines IL-1 and TNF-α induce the periodontal tissue destruction through the synthesis of matrix metalloproteinase (MMP) enzyme.[90] Among the MMP family, MMP-1 plays a crucial role in the degradation of type I and III collagen of the ECM.[91]

Fig. 2.4 illustrates the possible mechanism in the progression towards the periodontal disease caused by the bacterial infection.

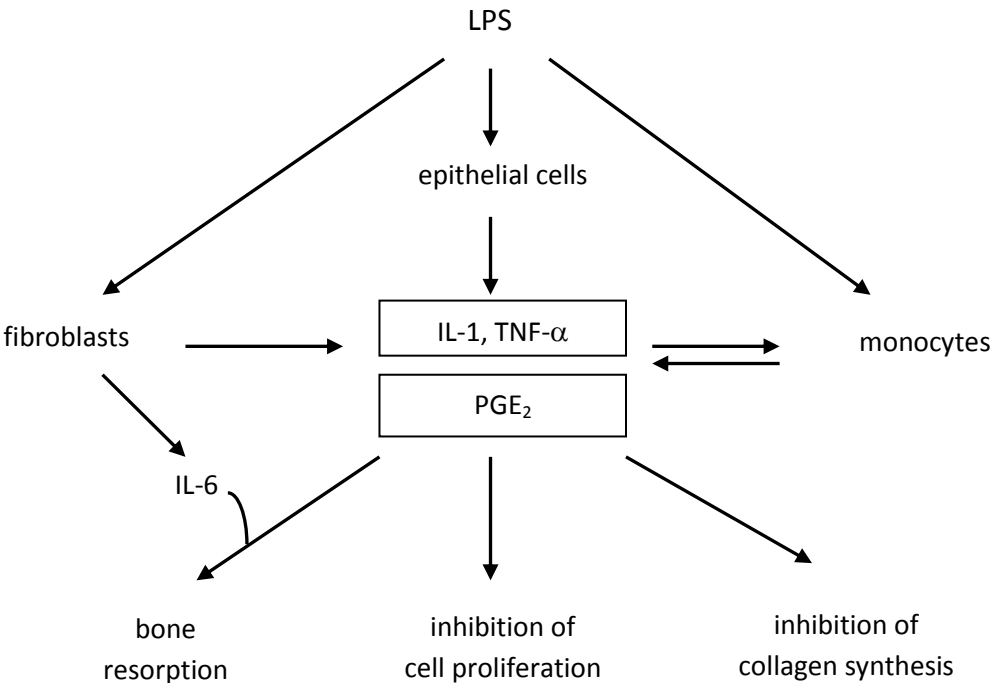

Figure 2.4. Possible mechanisms of connective tissue alterations during periodontal inflammation.[37]

Qualitative and quantitative changes occur in the periodontal connective tissues, especially in the gingiva, with the development of inflammatory periodontal diseases. Barnett *et al*. (1989), observed temperature pattern changes in inflamed gingival tissues and hypothesized that might be due to a result of variation in gingival microcirculation.[92] The gingival collagen becomes more soluble with disease, and relative ratios of collagen types start to change.[93] During the early phases of wound healing, the predominant collagen type is collagen type III, and is type I collagen when the healing is complete.[94] The total collagen content of gingiva has also been reported to decrease with the progression of the disease.[95, 96] Similarly, the proteoglycan types and their distribution also showed variation in gingival connective tissues for the diseased subjects.[97, 98] In addition, degradation of some gingival connective tissue proteoglycans and hyaluronic acid also occur during inflammation.[99]

2.4. PERIODONTAL WOUND HEALING PROCESSES

The healing cascade of periodontal wounds due to periodontal disease, like most of the connective tissues, occurs in three stages: inflammatory phase, granulation tissue formation phase and the matrix remodeling phase.

During the *inflammatory phase*, a blood clot which consists primarily of cross-linked fibrin and plasma fibronectin forms on the wound site.[100] The inflammatory cells start to migrate toward the wound site through this fibrin matrix. The blood clot also provides the suitable environment for the migration, proliferation and differentiation of the progenitor cells taking a role in the tissue repair. The cell migration process is mitigated by a series of events, mainly called chemotaxis. Chemotaxis is a chemical gradient-mediated

mechanism that attracts the healing accelerator cells to the wound site.[101] Chemoattractants and growth factors, with their specific interactions with cell surface receptors, play a vital role in promoting and directing the migration of different types of progenitor cells.[102]

The chemotactic secretory products, together with the inflammatory cells, fibroblasts and neovascular endothelium form a *granulation tissue*. As the healing progresses, granulation tissue develops further until the replacement tissue fully fills the wound space.

The granulation tissue formation is then followed by the *matrix remodeling phase*, in which the ingrowth of cells and neovascularization of the granulation tissue changes into a tissue matrix that is subject to continuous remodeling. During matrix remodeling, synthesis of ECM components occurs in concert with the degradation of the tissue matrix. Connective tissue fibroblasts and growth factors are primary factors in matrix synthesis. On the other hand, degradation of the matrix can progress through different routes, such as activation of the matrix metalloproteinases (MMPs) (i.e. matrix degrading enzymes), release of reactive oxygen species (ROS) such as superoxide radical and the hydroxyl radical, and phagocytosis of matrix components, mainly collagen by the phagocytic cells, especially neutrophils and macrophages.[103-106]

Periodontal wound healing is a complex biological process involving the interactions between different cell types (keratinocytes, fibroblasts, endothelial cells, macrophages and platelets),[107] a signaling network of several growth factors, proteoglycans, cytokines

and chemokines, and the extracellular matrix (ECM). Fig. 2.5 depicts the interaction of molecules with periodontal cells during periodontal regeneration.

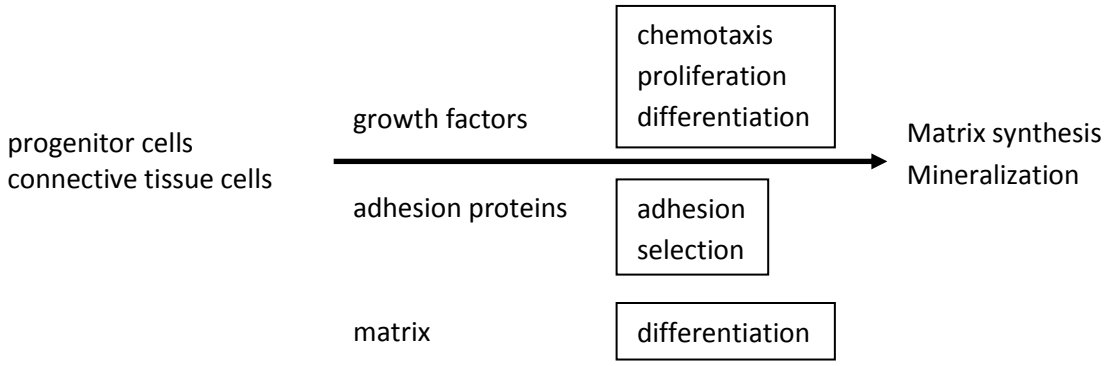

Figure 2.5. Interaction of molecules with periodontal cells and outcomes.[37]

The indicators for the healing of diseased periodontal tissues are the wound closure, cell migration and proliferation, connective tissue remodeling processes that involve the synthesis of extracellular components such as collagen, elastin, proteoglycans, and glycosaminoglycans.[108] The healing process for the diseased periodontal tissues is complete once tissue homeostasis, i.e., the dynamic equilibrium between the matrix synthesis and destruction, is attained.

2.4.1. Cells in Periodontal Wound Healing

Fibroblasts are the most important cell type during periodontal wound healing processes as they function as key modulators in wound contraction and ECM remodeling.[109] Another cell type, *macrophages*, start the formation of the granulation tissue and release

numerous types of cytokines and growth factors.[107] In addition, *monocytes* and *platelets* secrete platelet-derived growth factor (PDGF), which is essential for wound healing processes.[103] Other cells involved in periodontal wound healing and their functions are: *Inflammatory cells* (polymorphonuclear leucocytes, lymphocytes, and plasma cells) secrete polypeptide mediators that stimulate new matrix formation; *microvascular endothelial cells* initiate angiogenesis process; *myofibroblasts* activate the granulation tissue formation.[57, 110]

2.4.2. Growth Factors in Periodontal Wound Healing

Periodontal wound healing is a complex biological process and requires the employment of a growth factor cocktail. Growth factors are proteins or polypeptides that can enhance the ability of the wounded tissues to regenerate while improving cellular chemoattraction, proliferation and differentiation.[111] Growth factors regulate the biological processes during wound healing via binding to target cell surface receptors to activate transcription of specific genes through intracellular signaling pathways.[112, 113]

Growth factors, particularly platelet-derived growth factor (PDGF) and insulin-like growth factor (IGF), have been shown to be actively involved in periodontal wound healing processes while stimulating the periodontal regeneration.[108] PDGF is important in attracting neutrophils to the wound site to prevent bacterial contamination.[114] The other important growth factors playing key role in the periodontal wound healing and regeneration processes are epidermal growth factors (EGF), fibroblast growth factors (FGF), transforming growth factors (TGF) and vascular endothelial growth factor (VEGF).[115, 116]

2.4.3. Proteoglycans in Periodontal Wound Healing

Proteoglycans play a significant role in the matrix remodeling phase of periodontal wound healing.[117] Among these molecules, decorin and syndecan have been reported to contribute to healing processes while regulating the activity of the growth factors.[118, 119]

The cellular processes and key molecules that accelerate the healing process and improve periodontal wound repair are listed in Table 2.1.

TABLE 2.1. A SUMMARY OF THE MAJOR PROCESSES AND MOLECULES INVOLVED IN PERIODONTAL WOUND REPAIR[37]

Process	***Molecule***
Chemotaxis	PDGF, TGF-β, FGF, IL-1, matrix products
Adhesion	Fibronectin, collagens, laminin, vitronectin
Proliferation	PDGF, FGF, IGF-I
Differentiation	ECM, growth factors, hormones
Angiogenesis	FGF, VEGF, TGF-β, angiogenin
Matrix synthesis, remodeling	TGF-β, IFN-γ*, TNF-α, IL-1

* IFN-γ: interferon-gamma, a dimerized soluble cytokine.

CHAPTER 3

PERIODONTAL TISSUE ENGINEERING

3.1. INTRODUCTION

The aim of periodontal tissue engineering is to create and develop strategies to repair and regenerate the diseased tissues and form the replacement tissue. These strategies vary with the defect site, thus the tissue to be engineered. The periodontal tissue repair and regeneration techniques require the use of several cell types, scaffolds, growth factors and carefully designed bioreactor systems (Fig. 3.1). These components should all function in harmony to yield the desired outcome that enables tissue engineers to advance in the control of periodontal wound healing processes.

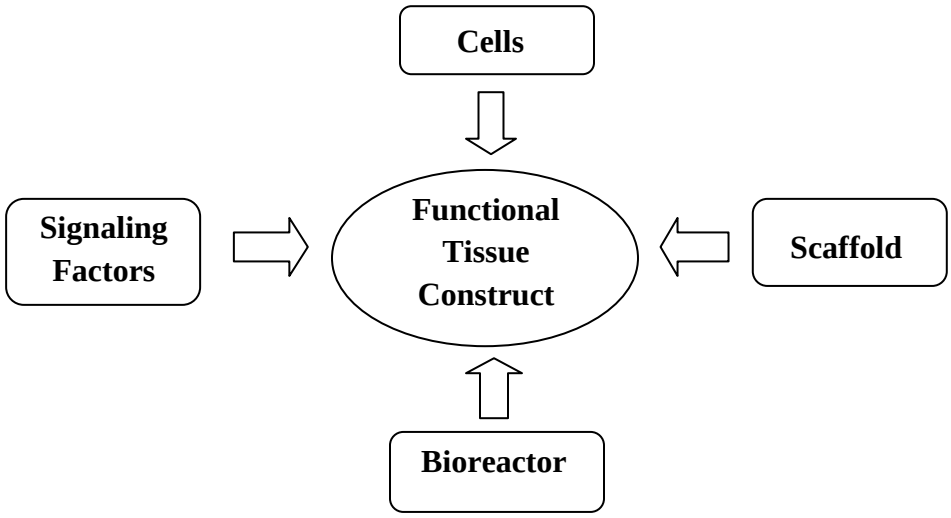

Figure 3.1. The main components in the creation of functional 3D tissue scaffolds. Appropriate cell sources, scaffold, signaling factors (e.g. growth factors, chemokines, cytokines) and the most suitable bioreactor system could help tissue engineers construct ideal replacement grafts.

Current periodontal tissue engineering principles are based on step-by-step treatment of the diseased tissues. As the prior step, removal of the infected parts and microbial cleaning of these areas is required. Diseased periodontal tissues are accompanied with the diseased root surfaces which do not support the regenerative processes. Therefore, chemical agents (e.g. citric acid and tetracycline) in conjunction with mechanical conditioning are currently used to create biocompatible root surfaces for a new connective tissue attachment.[120-122] The application of fibronectin on the acid-treated root surfaces has been reported to further enhance the attachment of fibroblasts onto root surfaces.[37]

Following the conditioning process, the appropriate combination of cells, scaffold, growth factors and bioreactor system is chosen to engineer the tissue construct with desired functions.

3.2. CELLS IN PERIODONTAL TISSUE ENGINEERING

Several types of cells have shown promise as candidate cells for periodontal tissue engineering, such as the cells derived from the gingiva, periodontal ligament (PDL) and alveolar bone,[123-127] bone marrow stromal cells (BMCs),[128] PDL stem cells,[129] cementoblasts,[130] bone mesenchymal stem cells (BMSCs)[131] and adipose-derived stem cells (ASCs)[132]. The soft and hard tissue repair processes require the synchronized functioning of gingival fibroblasts, gingival periodontal cells, PDL fibroblasts, cementoblasts and osteoblasts. The function of each cell type varies to a great extent, therefore, the specific focus will be given to the gingival fibroblasts and gingival epithelial cells in this section.

3.2.1. Gingival Fibroblasts

Human gingival fibroblasts (hGFs) constitute the major cell population in gingival connective tissue. These cells resemble the periodontal ligament fibroblasts (PDLFs) in their characteristic *in vivo* spindle shape morphology (Fig. 3.2) and growth rates, however their functioning in maintaining ECM structure and during inflammation differs significantly.[133-135] Somerman *et al*.[136] examined the *in vitro* behavior of the hGFs and PDLFs isolated from the same patient at the same passage number and found PDLFs synthesized more collagen and demonstrated higher alkaline phosphatase activity. The same authors also reported that the two cell types showed differences in their response to the cell attachment molecules.[137]

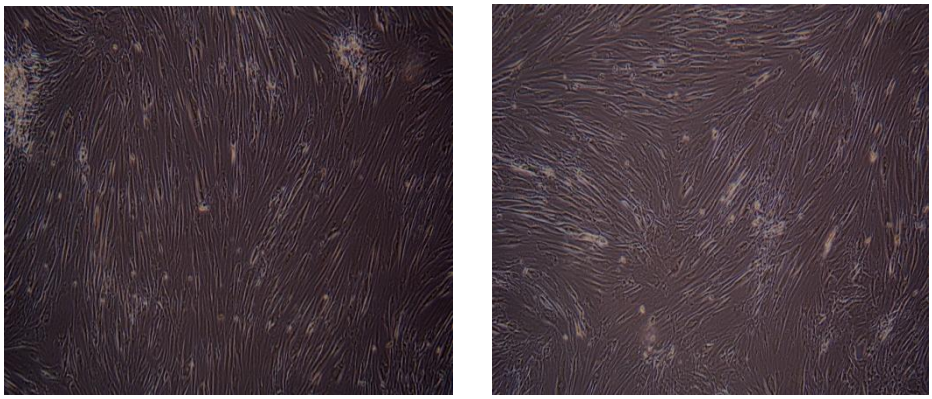

Figure 3.2. The spindle shape morphology of the hGFs as observed under light microscope. In culture, hGFs become very elongated when subconfluency is reached.

The degree of interaction of the hGFs with any scaffold surface is influenced greatly by several factors, such as the surface roughness and morphology of the scaffold,

intracellular cytoskeleton components of the ECM (e.g. microtubules, intermediate filaments and microfilaments) and the integrin receptors of the cells.[138-141] Pore size of the scaffold is also an important parameter, as currently it has been accepted that pore sizes smaller than 200 μm inhibit the attachment and migration of the fibroblasts.[142] However, pathogenic bacterial invasion may also accompany the migration of the fibroblasts within the scaffold, which is considered an important limiting factor for achieving predictable periodontal regeneration.[143]

The human gingival fibroblasts (hGFs), like all other cell types, regulate their activities by switching on and off the expression of their genes. The hGFs have been found to synthesize different ECM components (collagen, elastin, proteoglycans, etc.) as well as their degradation enzymes, such as collagenase, a matrix metalloproteinase (MMP). [144-147]

3.2.2. Gingival Epithelial Cells

Gingival epithelial cells rapidly migrate apically (downward) into the wound site and complicate early wound healing processes and compromise the ultimate success of the regenerative therapy. Therefore, periodontal regeneration therapies aim to seek ways to prevent the migration of epithelial cells towards the wound space, thus allowing the selective repopulation of the wound site with the progenitor cells from the adjacent healthy periodontal ligament and alveolar bone tissue.

On the other hand, gingival epithelial cells (keratinocytes), showing great resemblance to skin keratinocytes,[148] have attracted the attention of periodontal tissue engineers that are

specifically interested in engineering oral substitutes. The aim is to treat the periodontal defects by creating oral mucosal substitutes that could replace the diseased or damaged tissue. Several studies have been reported in the literature.[149-151] Basically, the tissue constructs are co-cultured with oral fibroblast cells and keratinocytes to fabricate oral tissue equivalents. Sanchez-Quevedo *et al*. (2007) populated their fibrin-agarose stromal substitutes with primary oral fibroblasts and keratinocytes by using the air-liquid culture technique (Fig. 3.3).[152] This methodology promoted the stratification of the oral mucosal constructs' epithelium while enhancing the healing process.

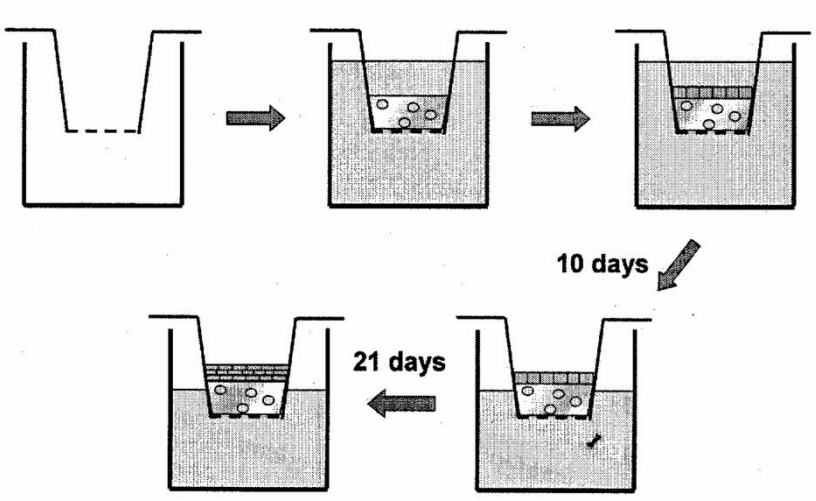

Figure 3.3. Air-liquid culture technique for the fabrication of oral mucosal substitutes.[152] The oral fibroblast-embedded scaffolds are placed on a porous membrane, and the keratinocytes are seeded on top. The cells are co-cultured using the air-liquid culture technique to produce oral mucosal constructs with stratified epithelium.

3.3. SCAFFOLDS IN PERIODONTAL TISSUE ENGINEERING

Periodontal tissue engineering seeks innovative ways to introduce, improve and apply scaffolds for the therapy of periodontal disease. Ideally, a periodontal scaffold should not cause immunologic responses beyond those enabling wound healing, should be resistant to infection and should withstand the physiological forces upon implantation. Such scaffold should enhance fibroblast adhesion, proliferation and differentiation.[153] The ideal scaffold should also have the desired surface/pore structure to promote migration/growth of cells, tissue in-growth, as well as the transport of nutrients and waste within the scaffold.[154, 155] The scaffold's ability to enhance vascular component formation for O_2 transport is another important issue. Additionally, the mechanical integrity of the scaffold should be in accordance with the biomechanical properties of the neighboring native tissue.[156] All these considerations should be carefully taken into account while designing an optimum periodontal scaffold for the treatment of the periodontal disease. Different scaffolding technologies have been introduced to periodontal tissue engineering.

3.3.1. Periodontal Grafting Materials

An ideal periodontal grafting material should evoke the biological processes required for the regeneration of the defected periodontal tissues, and maintain the formation of a new tissue attachment. Several grafting materials have been used for the treatment of periodontal defect sites.

3.3.1.1. *Autografts*

An autograft is a graft taken from one part of an individual and implanted to another part of the same individual. Cortical bone grafts and cancellous bone, marrow and bone blends are the commonly used periodontal autografts.[157, 158] These grafts have proven to accelerate healing in terms of osteogenicity, osteoinductivity and osteoconductivity.[52] However, the need for a secondary surgical site on the patient to harvest bone tissue makes the use of autografts one disadvantage compared to allografts and xenografts.

3.3.1.2. *Allografts*

Allografts are grafts transferred between different individuals of the same species. Three types of bone allograft materials have found their application in clinical studies: (1) cancellous bone and marrow, (2) freeze-dried bone allografts, (3) demineralized freeze-dried bone allografts.[37, 159] Bone allografts are advantageous over autografts as they do not require a second surgical site on the patient to extract bone. However, the processes applied on the bone allografts to remove the immunogenic constituents could lead to a decrease in the osteoinductive and osteoconductive potential of the grafts.[52] There is also a high incidence of pathogenic microorganism transfer with the use of allografts.[160]

3.3.1.3. *Xenografts*

Xenografts are surgical transplants taken from a different species. Bovine mineral matrix and bovine-derived hydroxyapatite (HA) are examples of commonly used xenografts in oral reconstructive surgeries.[161] However, the applicability of xenograft materials remains uncertain due to immune response problems.[162]

3.3.1.4. *Alloplasts*

Alloplasts are synthetic grafting materials used to treat the periodontal defect sites. The alloplastic materials commonly used in reconstructive periodontal surgery are the calcium phosphate ceramics- namely, the nonresorbable hydroxyapatites and the resorbable tricalcium phosphates.[163] The main advantages of alloplastic grafts are their off-the-shelf availability and non-immunogenic nature. However, it has been reported that alloplastic materials did not support the cementogenesis process.[164]

3.3.2. Guided Tissue Regeneration (GTR) Membranes

Natural and synthetic materials are now used routinely in a wide variety of surgical procedures to isolate tissue compartments, direct cell migration, and in some cases provide a source of bioactive molecules to promote wound healing or regeneration. The goal to direct tissue regeneration has been extensively studied in periodontal defect repair surgery, where the aim is to regenerate components of the tooth supporting apparatus that have been lost due to periodontal disease; specifically cementum, alveolar bone, and the periodontal ligament.[165, 166]

The feasibility of periodontal guided tissue regeneration (GTR) was demonstrated in a proof of principle study in 1982,[167] by employing a physical barrier interposed between the periodontal defect and overlying soft tissues (Fig 3.4). The concept was that the barrier provided a protected wound healing environment that excluded gingival epithelial and connective tissue cells that would regenerate soft tissues and inhibit bone repair. By limiting the wound site to undifferentiated mesenchymal cells that migrate from healthy

alveolar bone and the periodontal ligament, these cells are able to more effectively regenerate components of the tooth supporting apparatus.[168]

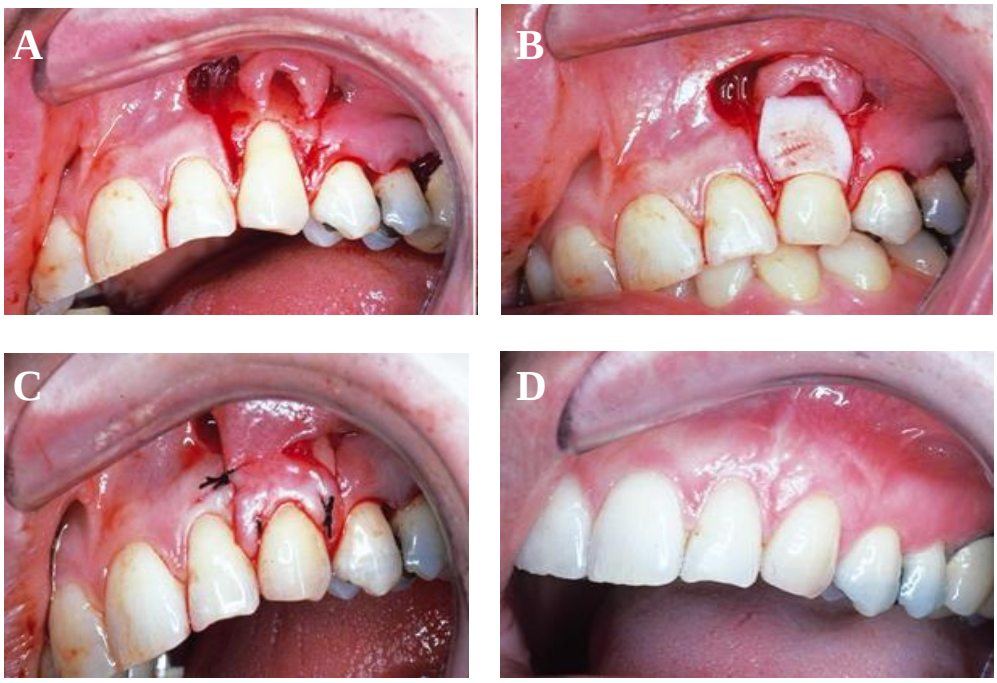

Figure 3.4. Surgical application of the GTR membranes. A gingival flap reflecting the exposed root recession and healthy bone is created **(A)**. Then, the barrier membrane is placed covering the root surface **(B)**. The gingival flap with the keratinized tissue is repositioned while completely covering the membrane and sutured in position **(C)**. Finally, the regeneration of the periodontal tissues, both physiologically and aesthetically, occurs with time **(D)** (www.dental-tribune.com).

3.3.2.1. *Non-Resorbable GTR Membranes*

A variety of non-resorbable materials have been used as physical barriers, the first being expanded poly-tetrafluoroethylene (e-PTFE) (Gore-Tex, W.L. Gore & Assoc., Inc., Flagstaff, AZ), a highly porous, synthetic graft with a long history of use in medical

applications. While this material has produced favorable clinical results in periodontal regeneration,[169, 170] it requires an undesirable second operative procedure for removal, and is associated with a high incidence of post-operative complications.[171-173]

3.3.2.2. *Resorbable GTR Membranes*

The second generation of physical barriers focused on resorbable membranes that avoid the need for a second surgical intervention while meeting the additional demands involved in the bioresorption process, such as Bioguide (Osteohealth Co., Shirley, NY) and Biomend (Sulzer Medica, Colla-Tec, Inc., Plainsboro, NJ), both of which consist of processed xenogenic collagen.[174, 175] More recent approaches have included human-derived intact tissue complexes including acellular dermal matrix (Alloderm, LifeCell Corp., Branchburg, NJ) and pericardium (Pericardium, Tutoplast, Neunkirchen, Germany).[176-180] Despite its favored polar structure allowing epithelial cell attachment on the basal side and fibroblast penetration and growth on the other side, the need for tissue donated from a human source remains a limiting factor with Alloderm.[181]

While a number of clinical studies have documented the effectiveness of periodontal GTR,[182-186] few studies have reported the long-term outcome of these therapies.[187] In addition, the predictability of these procedures is currently less than ideal, varying with local anatomy, patient characteristics, and other unknown factors.[188-190] Thus, the biological requirements for periodontal regeneration are not yet completely understood and the ideal materials to achieve this have yet to be developed.

3.4. GROWTH FACTORS IN PERIODONTAL TISSUE ENGINEERING

Various growth factors have been employed to stimulate the regeneration of periodontal defects. Platelet-derived growth factors (PDGF)[191] (PDGF-AA, PDGF-BB, PDGF-AB, vascular endothelial cell growth factor), epidermal growth factors (EGF) (epidermal growth factor, transforming growth factor-α, amphiregulin), fibroblast growth factors (FGF) (acidic fibroblast growth factor (FGF-1), basic fibroblast growth factor (FGF-2)[192]), insulin-like growth factors (IGF)[193] (IGF-I, IGF-II), transforming growth factors (TGF) (TGF-β,[194] bone morphogenetic proteins[195]) have been introduced as candidate growth factors for periodontal tissue engineering.

3.5. BIOREACTORS IN PERIODONTAL TISSUE ENGINEERING

Bioreactor technologies for dynamic culture of tissue constructs provide an aseptic culture environment where the temperature, pH, nutrients (e.g. glucose, amino acids), gases (O_2 and CO_2) and growth factors are homogenously distributed for the cells to proliferate and differentiate.[196] Besides their function to overcome the problems associated with the concentration gradients of these components, the mechanical stimulation created by such systems enable tissue engineers to develop various scaffolding materials for different applications.

While designing a bioreactor system, it is essential to keep the level of *in vitro* operating parameters close to physiological conditions. Bioreactor cultures with the appropriate design conditions have been reported to enhance the synthesis of the necessary ECM components by the seeded cells.[197] The perfusive flow created by these bioreactors

provided a culture environment where the ECM synthesis is enhanced, mass transfer limitations of the necessary nutrients and gases were reduced, and the appropriate physical stimuli contributed to the organization of the ECM components.[198]

To date, little emphasis has been placed on the design of a bioreactor system for the cultivation of oral mucosal substitutes or periodontal grafts,[199] as such exploration of ideal culture conditions and development of suitable periodontal grafts using advanced bioreactor technologies are necessary.

CHAPTER 4

CHARACTERIZATION OF PORCINE ORAL SOFT TISSUES AS A MODEL SYSTEM

4.1. INTRODUCTION

Oral soft tissues are complex biological systems with the components of their extracellular matrix (ECM) responding differentially to physiological stresses. These tissues are subjected to a wide variety of mechanical forces, including hydrodynamic forces, compression, elongation, friction, and shear generated during saliva flow, mastication, speech, toothbrushing, etc.[200-203] Periodontal tissues also react to some orthodontic tooth movements.[204]

Among the oral soft tissues, the attached gingiva, alveolar mucosa, and the buccal mucosa have attracted the most attention due to controversy among clinicians regarding the necessity and/or quantity of keratinized gingiva to support health around natural teeth and dental implants.[205-207] The mucogingival junction demarcates the attached gingiva from the alveolar mucosa, which, on the buccal side of the cheek, transitions to the buccal mucosa.[208] The surface of all three mucosal tissues is covered with a stratified squamous epithelium that is bound to the underlying connective tissues by a network of anchoring fibrils.[53, 209] Most gaseous and metabolic substance exchange is maintained through the junction between the epithelial and connective tissues.[210] On the other hand, the

epithelium represents the barrier to the oral tissues that limits the diffusion of the tissue fluids out, and prevents the migration of the toxic substances through the tissue.[211]

The ultrastructure of the different oral soft tissues is in accordance with their specific function within the oral cavity. The attached gingiva which is directly influenced by strong mechanical forces, especially during mastication, is firmly attached to the underlying cementum and alveolar bone.[212] In addition, the highly keratinized nature of the stratified epithelium enables the tissue to resist deformation forces.[213] Conversely, the alveolar and buccal mucosas, which have a reduced exposure to abrasive forces, are relatively loosely attached to the underlying bone and possess a non-keratinizing epithelium.[214, 215]

Besides the ultrastructural changes between the attached gingiva and the adjacent alveolar mucosa, the existence of a temperature gradient through the mucogingival junction has also been reported.[216] Volchansky *et al*. (1994) also reported a difference in temperature between the oral mucosal tissue and the underlying bone.[217]

From both materials development and clinical perspectives, a quantitative mechanical analysis of oral soft tissues is essential if new materials are to be developed that mimic the behavior of natural tissues. This is particularly important from a clinical perspective where there is ongoing debate regarding the necessity of a band of keratinized gingival tissue to surround natural teeth and dental implants.

In the current literature, an extensive research has been conducted on the mechanical properties of the periodontal ligament (PDL) and the bone tissue.[218, 219] However, there is

little descriptive analysis of the oral soft tissues, especially details of the biomechanical properties and regional variations in performance. Kydd *et al*. (1967) investigated the *in vitro* tensile properties of human gingiva using an extensometer and reported the low and high elastic moduli of the human ginviva to be 2.76 ± 0.95 and 10.20 ± 0.40 dynes/cm^2 (mean ± standard deviation (SD)), respectively.[220] This study aims to characterize the *in vitro* biomechanical behavior of porcine tissues as a representative model system due to the morphological and histological resemblance of porcine oral soft tissues to human oral tissues.[221]

4.2. Material and Methods

4.2.1. Sample Preparation

The lower jaws of 25 freshly slaughtered 6-9 month-old pigs were obtained from Animal Technologies Inc. (Tyler, Texas). Oral tissues, including the buccal attached gingiva (BAG), buccal alveolar mucosa (BAM), buccal mucosa (BM), lingual attached gingiva (LAG), and lingual alveolar mucosa (LAM) were excised using sharp dissection from porcine lower jaws within 24 hours of animal sacrifice (Figs. 4.1A, 4.1B). The complete soft tissue complex was dissected from epithelium to bone, including the periosteum. The excised tissue was stored in phosphate-buffered saline (PBS) containing 0.03 M potassium phosphate monobasic (Merck, Darmstadt, Germany), 0.12 M sodium phosphate dibasic (Mallinckrodt Baker, Inc., Phillipsburg, NJ), and 0.2% penicillin (Invitrogen Corp., Grand Island, NY) (pH 7.4) at 4°C for no more than 3 days before the mechanical analysis.

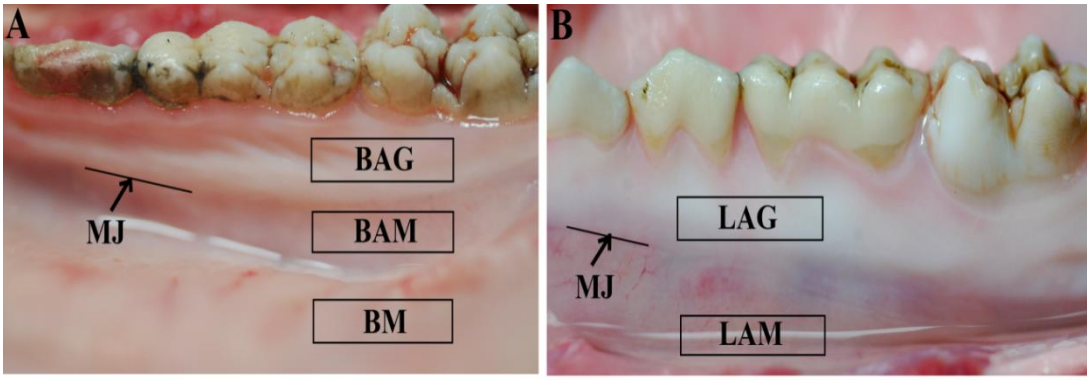

Figure 4.1. Porcine oral soft tissues extracted from the buccal **(A)** and lingual **(B)** aspects of porcine lower jaws. BAG, buccal attached gingiva; BM, buccal mucosa; MJ, mucogingival junction; LAG, lingual attached gingiva; and LAM, lingual alveolar mucosa.

4.2.2. Uniaxial Mechanical Testing

The mechanical properties (tensile, viscoelasticity, and dynamic compressive) of the porcine oral soft tissues were assessed using an Instron mechanical testing machine. For the dynamic compression tests, the tensile testing rig of the Instron mechanical tester was replaced with top and bottom compression plates (Fig. 4.2).

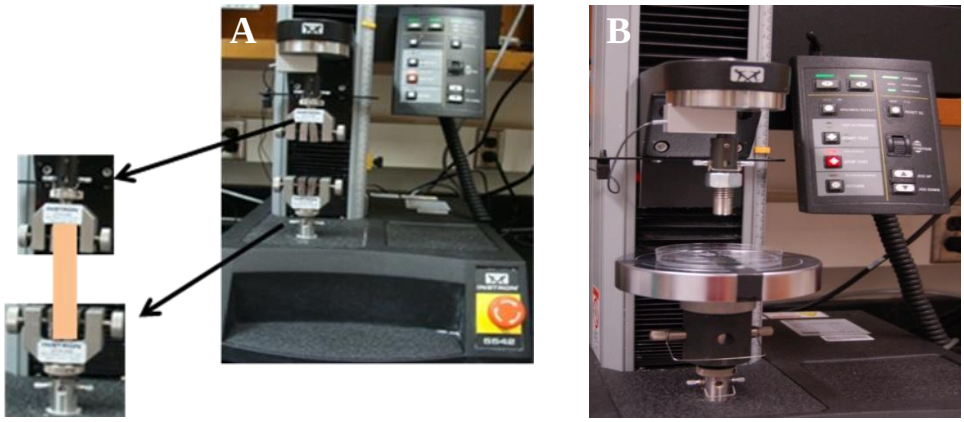

Figure 4.2. The tensile **(A)** and compression testing **(B)** of the porcine oral soft tissues was performed using the grips and compression plates of the Instron uniaxial mechanical tester.

4.2.2.1. *Tensile Testing*

Tensile analysis was carried out using an Instron 5543 testing machine (Instron Corp., Norwood, MA) equipped with a 50-N load cell. Tissue strips 3 x 30 mm (n = 9) were maintained in PBS until the mechanical testing to prevent dehydration.[222] Samples were secured in the grips of the tensile testing rig using #100 grit sandpaper with cyanoacrylate adhesive (Loctite, Henkel Loctite Co., Ireland).[223] The aspect ratio of the tissue strips was maintained at a minimum of 6:1 to ascertain a homogeneous stress-strain state.[224] Tissue strips were preloaded to 0.003 N at a cross-head velocity of 5 mm/min, then preconditioned to achieve a steady response with 5 repeated load/unload cycles at an extension rate of 5 mm/min.[225, 226] Finally, the strips were stretched to failure at an extension rate of 5 mm/min.[227] Load and displacement data was the recorded, with the stress-strain relationship and tensile properties of the HUV strips deduced from the acquired data.

Prior to testing, the thickness of the tissue strips (n = 9) was measured as 1.31 ± 0.26 mm (mean ± standard deviation (SD)) (lingual attached gingiva), 1.60 ± 0.20 mm (buccal attached gingiva), 1.95 ± 0.42 mm (lingual alveolar mucosa), 2.45 ± 0.25 mm (buccal alveolar mucosa), and 2.96 ± 0.38 mm (buccal mucosa).

From the load-displacement data, tensile stress (MPa) was calculated by normalizing the tensile load (N) to the tissue cross-sectional area (3 mm × tissue thickness). Tensile strain was computed by normalizing the displacement data to the tissue section's original gauge length. Young's modulus (MPa) was calculated as the slope of the linear region of the stress-strain curve, whereas the ultimate tensile strength (MPa) was determined as the

maximum attainable stress of the stress-strain curve. Failure load (N) was expressed as the maximum load sustained at fracture, and the strain at failure was computed from the displacement corresponding to failure load.

4.2.2.2. *Stress Relaxation*

Regional variation in tissue viscoelasticity was assessed by stress relaxation analysis. Each tissue strip was mounted in the mechanical testing machine and preconditioned, as described above. Samples (n = 8) were loaded to one-third of the force at fracture at an extension rate of 30 mm/min and then the cross-head was stopped immediately to unload the sample.[226] Stress was normalized to the initial stress and plotted versus time. The initial stress, σ_o at t = 0 and the equilibrium stress, σ_∞ were recorded after relaxation was initiated. The contribution of the viscoelastic stress to the total stress, $(\sigma_o-\sigma_\infty)/\sigma_o$ was assessed to characterize the viscoelasticity of each region.[222]

During tensile and stress relaxation tests, the porcine specimens were maintained in a hydrated state to mimic the physiological state by spraying PBS on all surfaces of the tissue.[228]

4.2.2.3. *Dynamic Compression*

In order to mimic the chewing movement of mammalians, dynamic compression tests were performed on the porcine tissues.[229] Using the same uniaxial mechanical testing machine, tissue sections were compressed between the two metal compression plates by cyclic displacements of the top indentor. Dynamic behavior of the tissues was assessed with a triangular waveform at strain amplitudes of 5%, 10%, and 15%, and loading

frequencies, 0.1 Hz, 0.5 Hz, and 1 Hz. 5 mm-diameter tissue disks were excised from each location and glued onto a Petri dish which was then filled with PBS until the tissue was covered. The mean thickness of the unloaded disks (n = 6) was the same as stated in the uniaxial testing section. The tissue thickness within each tissue region group was kept the same since it has been reported that the degree of recovery of the tissue upon compression was significantly dependent on the tissue thickness.[230] Then, excess moisture was removed from the bottom surface of the specimen, then glued using cyanoacrylate adhesive onto a Petri dish (which was glued onto the bottom compression plate). The Petri dish was then filled with PBS (0.15 M, pH 7.4) until the sample was covered in order to mimic the hydrated physiological environment. Compressive force and displacement was measured instantaneously with a sampling rate 500 ms; range 50 N, and accuracy ± 0.25%. Compressive strain, ε, was defined as the displacement of the top indenter (Δh) relative to the initial thickness of the disk between the compression plates (h_0). Compressive stress, σ, was computed as $\sigma = F/A$, where F and A represent the compressive load and the tissue cross-sectional area, respectively.[231]

The time dependency of the tissue behavior was assessed after 25 compression cycles, then after a recovery time of 5 min, a trial series of tests was conducted under different amplitude-frequency combinations. The series was repeated in reverse order for the same region. Both series showed similar results indicating the testing order and time had no effect on the tissue stress-strain relationship.

The dynamic compressive properties, instantaneous modulus (E_{int}) and steady modulus (E_s) were computed as the peak stress values at the first and last compression cycle relative to the corresponding compressive strain.[232]

4.2.3. Histological Analysis Using Light Microscopy

Tissue samples from different regions (n = 6) were fixed in 3.7% formalin (tissue:solvent ratio was 1:40 (v:v)) overnight. The samples were placed in 70% ethanol (EtOH) solution in distilled water until the analysis. Prior to analysis, the sections were put in tissue cassettes and the cassettes were labeled. The tissue sections in cassettes were subjected to a dehydration step at 45°C (80% EtOH (1×), 95% EtOH (2×), 100% EtOH (3×), 30 min for each step). After the dehydration step, tissue sections were placed in Clear-Rite reagent to clear the tissue (2×, 30 min for each). The sections were then infiltrated with melted paraffin at 60°C (2×, 1 hr for each). This was followed by soaking the tissue samples in paraffin bath under vacuum for 1 hr to ensure paraffin penetration within the tissue. The tissue sections were then removed from the cassettes and paraffin-embedded using a Tissue-Tek II Tissue Embedding Center (Miles Laboratories, Inc., Westmont, IL). Paraffinized samples were gradually freezed down to -80°C and were kept at that temperature until sectioned (at least 24 hr). Samples were sectioned to 5 µm on a Leitz 1512 microtome (Leitz, Oberkochen, Germany). The tissue sections were placed on 38°C water bath and mounted on glass slides, and then kept in 60°C for 2 hours. The samples were then deparaffinized by soaking in Clear-Rite (3×, 3 min each), and rehydrated through decreasing alcohol concentrations (100%, 95%, 80%, 70% EtOH, 1 min each). The sections were then stained with Hematoxyline (Richard-Allan Scientific, Kalamazoo,

MI) for 7 min, cleared in 1% acid alcohol solution (hydrochloric acid (HCl)/EtOH) for 5-10 sec and immersed in 0.2% ammonia-water solution for 20 sec, and counterstained with Eosin-Y (Richard-Allan Scientific, Kalamazoo, MI) with a few drops of glacial acetic acid (J.T. Baker, Phillipsburg, NJ) for 5 sec. The stained sections were then dehydrated through increasing alcohol concentrations (95% EtOH, 2×, 1 min each, 100% EtOH, 2×, 1 min each), and immersed in Clear-Rite (2×, 1 min each). The stained sections were mounted and secured with cover slips and left at room temperature overnight. The sections were then histologically assessed to visualize structural variation using a Nikon Eclipse E800 Epifluorescent upright microscope (Nikon, Melville, NY). The analysis of the histological images was done using the MetaMorph software V6.2 (Molecular Devices, Downingtown, PA).

4.2.4. Data Analysis

Statistical analyses were performed using the SPSS 15.0 software (SPSS Inc., Chicago, IL). One-way univariate analysis of variance (ANOVA) was used to test for significant differences among multiple test groups. Multiple comparisons between groups were performed with the Games-Howell or Tukey *post hoc* tests depending on homogeneity of variance tested with Levene's test. A three-way univariate ANOVA was also carried out to demonstrate the interaction between region, strain frequency (0.1, 0.5, and 1 Hz), and strain amplitude (5, 10, and 15%) affecting the instantaneous modulus (E_{int}) and steady modulus (E_s). Statistical significance was set at $p < 0.05$ for all tests. All values are expressed as mean ± SD.

4.3. RESULTS

4.3.1. Assessment of Tissue Mechanics

4.3.1.1. *Tensile Properties*

The representative stress-strain curves (Fig. 4.3) exhibited characteristic behavior of soft connective tissues.[233] Stress-strain data was derived from the load-displacement data by normalizing the force values with the tissues cross-sectional area.

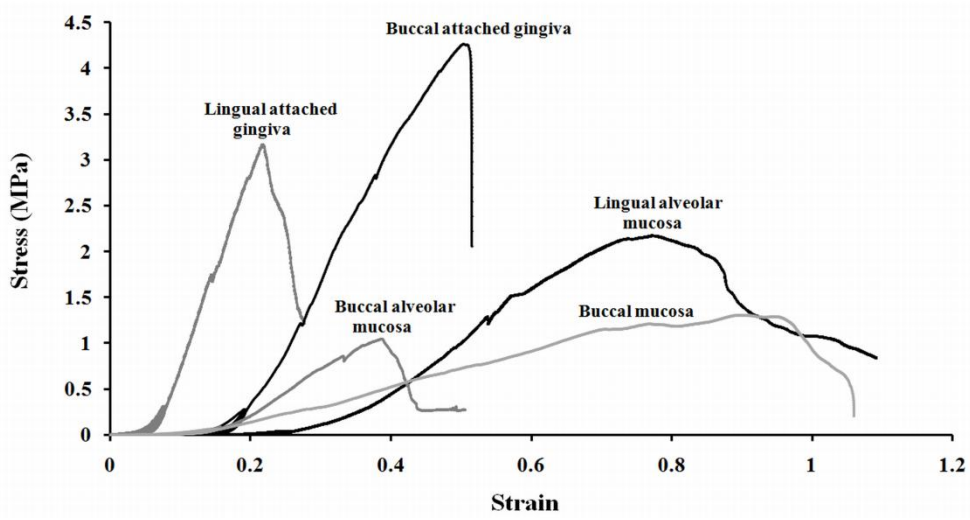

Figure 4.3. Representative stress-strain curves for different regions of porcine oral mucosal tissue in uniaxial tensile testing (n = 9).

The ultimate tensile strength of the buccal attached gingiva (3.94 ± 1.19 MPa) was similar to that of the lingual attached gingiva and this strength value was significantly higher than all other regions of oral mucosa tested ($p < 0.005$) (Fig. 4.4).

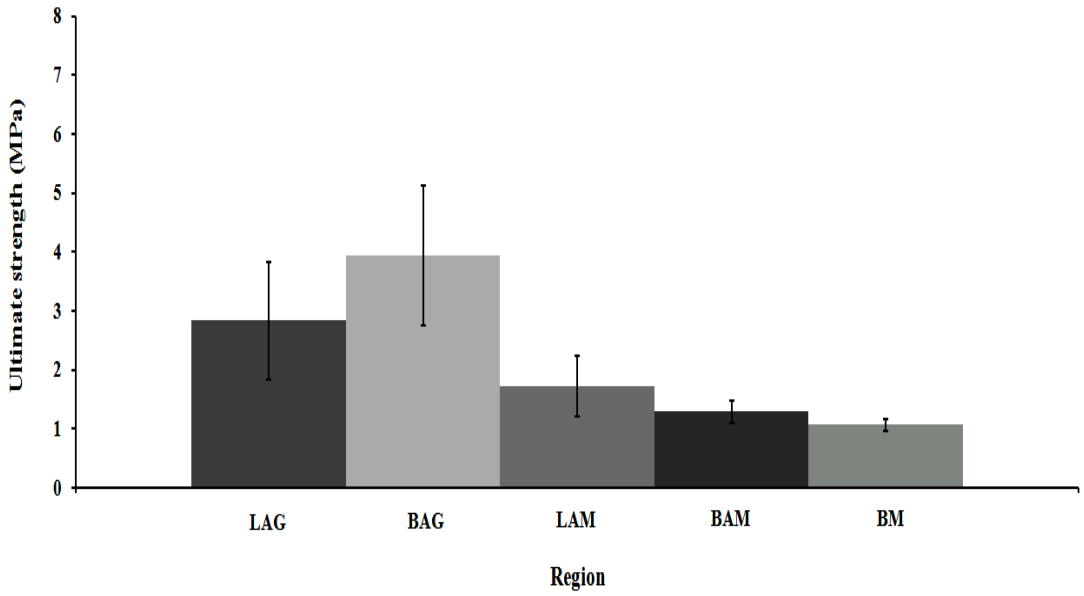

Figure 4.4. Ultimate tensile strength. Attached gingiva demonstrated the highest ultimate strength among all the regions tested (n = 9, Games-Howell, $p < 0.05$). LAG, lingual attached gingiva; BAG, buccal attached gingiva; LAM, lingual alveolar mucosa; BAM, buccal alveolar mucosa; BM, buccal mucosa.

The buccal attached gingiva exhibited the highest stiffness with a Young's modulus value of 19.75 ± 6.20 MPa, which was significantly higher than the alveolar mucosa (of both lingual and buccal aspects), as well as the buccal mucosa ($p < 0.005$). However, there was no significant difference in stiffness between the lingual and buccal aspects of the attached gingiva, nor between the lingual and buccal alveolar mucosa sections (Table 4.1).

TABLE 4.1. TENSILE PROPERTIES OF THE PORCINE ORAL SOFT TISSUE

REGION	TENSILE PROPERTIES*		
	Young's Modulus (MPa)	**Strain at Failure**	**Failure Load (N)**
Lingual attached gingiva (LAG)	$18.83 \pm 5.98^{c,d,e}$	$0.29 \pm 0.05^{c,d,e}$	10.89 ± 2.74^{b}
Buccal attached gingiva (BAG)	$19.75 \pm 6.20^{c,d,e}$	$0.35 \pm 0.07^{c,d,e}$	$19.74 \pm 5.04^{a,c-e}$
Lingual alveolar mucosa (LAM)	$4.79 \pm 2.54^{a,b}$	$0.88 \pm 0.19^{a,b,d}$	10.54 ± 2.18^{b}
Buccal alveolar mucosa (BAM)	$5.74 \pm 1.15^{a,b,e}$	$0.51 \pm 0.08^{a-c,e}$	8.93 ± 2.06^{b}
Buccal mucosa (BM)	$2.48 \pm 0.37^{a,b,d}$	$0.94 \pm 0.06^{a,b,d}$	9.08 ± 1.66^{b}

* Data are mean ± standard deviation (n = 9). Pairwise comparisons (statistical significance set at $p < 0.05$) are reported between the groups: [a] versus LAG; [b] versus BAG; [c] versus LAM; [d] versus BAM; [e] versus BM.

4.3.1.2. *Viscoelasticity*

Stress relaxation curves for the porcine tissue (Fig. 4.5) displayed a typical nonlinear viscoelastic oral soft tissue response, as the stress within the tissue decayed over time until equilibrium values were reached.[234, 235] The normalized stress reached a steady value by the end of 360 s for all the regions tested in this study.

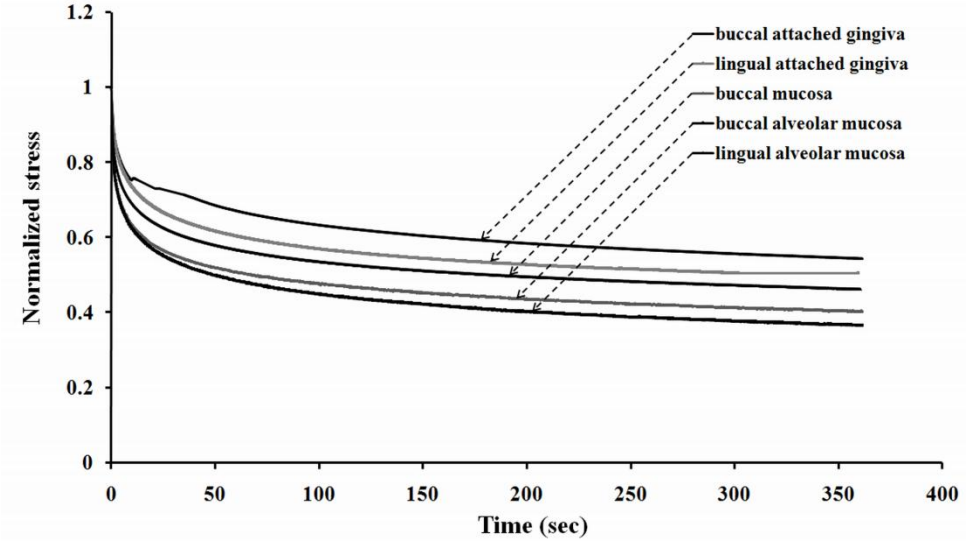

Figure 4.5. Normalized stress relaxation curve. The stress at each time point was divided by the maximum stress to yield the normalized stress values for the relaxed tissue strips. Lingual alveolar mucosa demonstrated significantly higher viscoelasticity compared to the lingual and buccal attached gingiva, and buccal mucosa (n = 8, Games-Howell, $p < 0.05$).

The lingual alveolar mucosa demonstrated a significantly higher viscoelasticity compared to the attached gingiva (lingual and buccal), as well as the buccal mucosa (n = 8, $p < 0.05$). The viscoelastic properties of the lingual and buccal alveolar mucosa were found to be statistically similar**.** The mean (± SD) values for the initial stress (σ_o), equilibrium stress (σ_∞) and $(\sigma_o-\sigma_\infty)/\sigma_o$ ratio, a measure of tissue viscoelasticity, were tabulated in Table 4.2.

TABLE 4.2. STRESS RELAXATION DATA OF THE PORCINE ORAL SOFT TISSUE

REGION	STRESS RELAXATION DATA*		
	Initial Stress, σ_0 (MPa)	**Equilibrium Stress, σ_∞ (MPa)**	**$(\sigma_0 - \sigma_\infty)/ \sigma_0^+$**
Lingual attached gingiva (LAG)	$1.88 \pm 0.11^{c\text{-}e}$	$0.97 \pm 0.08^{c\text{-}e}$	$0.48 \pm 0.02^{c,d}$
Buccal attached gingiva (BAG)	$1.84 \pm 0.23^{c\text{-}e}$	$0.96 \pm 0.14^{c\text{-}e}$	$0.47 \pm 0.06^{c,d}$
Lingual alveolar mucosa (LAM)	$0.25 \pm 0.03^{a,b,e}$	$0.1 \pm 0.01^{a,b,e}$	$0.59 \pm 0.04^{a,b,e}$
Buccal alveolar mucosa (BAM)	$0.21 \pm 0.02^{a,b,e}$	$0.09 \pm 0.01^{a,b,e}$	$0.56 \pm 0.06^{a,b}$
Buccal mucosa (BM)	$0.39 \pm 0.03^{a\text{-}d}$	$0.19 \pm 0.03^{a\text{-}d}$	0.51 ± 0.04^{c}

*Data are mean ± standard deviation (tensile, n = 9; stress relaxation, n = 8). Pairwise comparisons (statistical significance set at $p < 0.05$) are reported between the groups: [a] versus LAG; [b] versus BAG; [c] versus LAM; [d] versus BAM; [e] versus BM.
+ represents the contribution of the viscous components relative to the total stress.

4.3.1.3. *Dynamic Compressive Properties*

A representative graph of compressive stress versus time is shown in Figure 4.6A. At 10% strain and 1 Hz frequency the buccal attached gingival displayed the highest peak stress values, after which the stress of each subsequent cycle decreased to a steady-state value. The percent strain remained constant for the subsequent cycles (Fig. 4.6B).

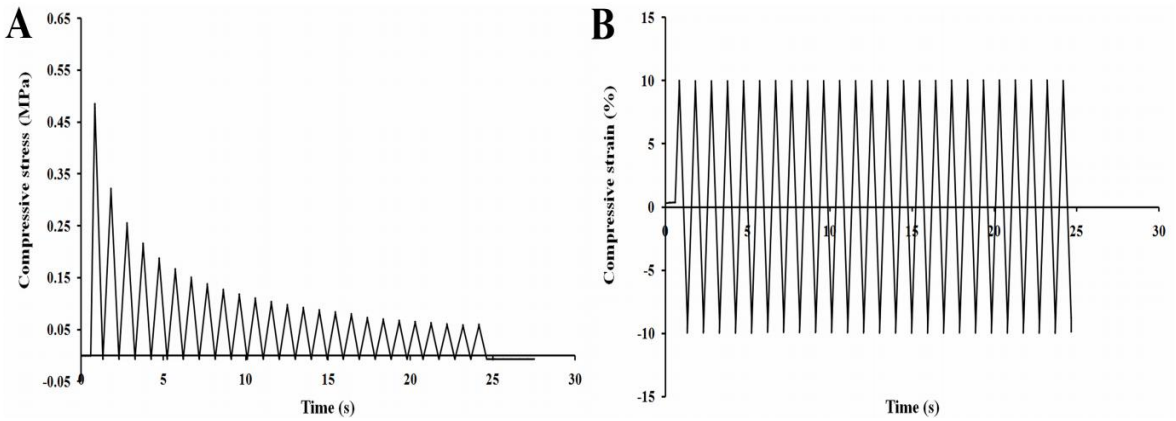

Figure 4.6. A representative graph of compressive stress versus time for the buccal attached gingiva at 10 % strain and 1 Hz frequency, with the first cycle generating the largest peak, after which the peak stress value of each cycle decreased to a steady-state value **(A)**. The percent strain remained constant for the subsequent cycles **(B)**.

The peak stress values, i.e., the maximum compressive values attained during the first compression cycle for tissue regions were displayed in Fig. 4.7. The peak stress exhibited by the buccal attached gingiva (1.17 ± 0.17 MPa) was similar to the peak stress of the lingual attached gingiva, and this peak stress value was significantly higher than all the other regions tested ($p < 0.001$). There was also no significant difference in peak stress values between the lingual and buccal alveolar mucosal tissues**.**

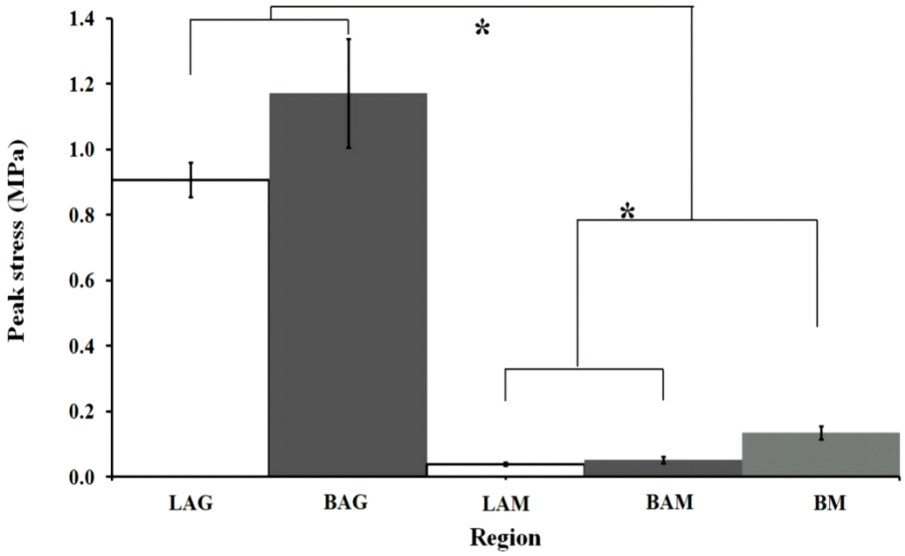

Figure 4.7. Peak stress. Maximum stress values for each tissue section during the initial compression cycle at a frequency of 1 Hz and strain amplitude of 15%. LAG, lingual attached gingiva; BAG, buccal attached gingiva; LAM, lingual alveolar mucosa; BAM, buccal alveolar mucosa; BM, buccal mucosa.Values are means and standard deviations (n = 6). * indicates statistical differences based on pairwise comparisons between regions ($p < 0.001$).

In general, both the instantaneous modulus (E_{int}) and the steady modulus (E_s) increased with strain amplitude and loading frequency (Figs. 4.8 and 4.9). The buccal attached gingiva was shown to have the highest E_{int} and E_s values, 7.81 ± 1.11 MPa and 0.86 ± 0.09 MPa, respectively (1 Hz, 15% strain). Both instantaneous modulus (E_{int}) and steady modulus (E_s) were significantly influenced by region, frequency and strain amplitude (Three-way ANOVA, n = 6, $p < 0.001$).

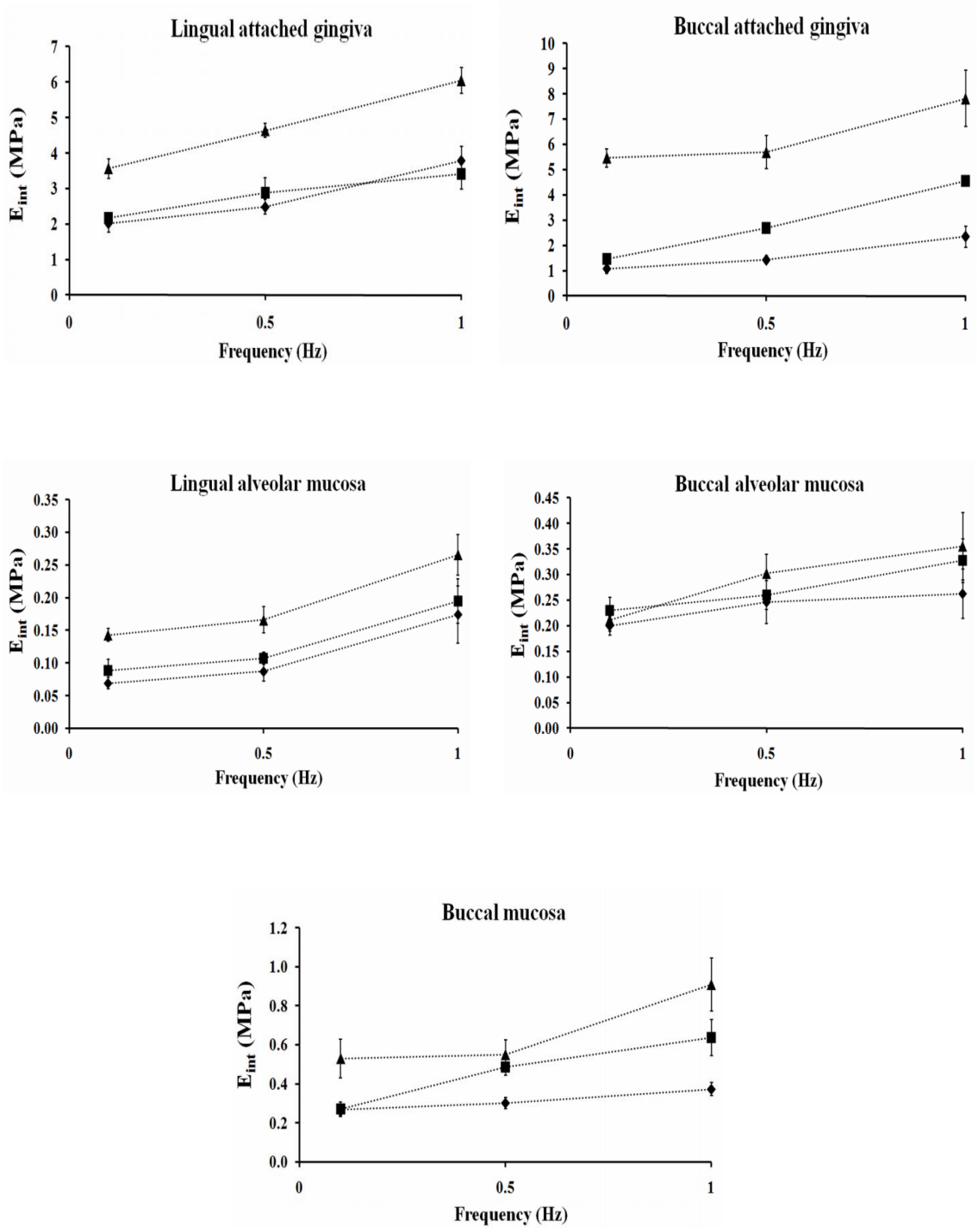

Figure 4.8. Instantaneous modulus (E_{int}), a measure of the contribution of the tissue collagen and proteoglycans to the compressive stiffness at the initial cycle, was dependent on strain amplitude and loading frequency; ♦, 5% compressive strain; ■, 10% compressive strain; ▲, 15% compressive strain. Data are means ± standard deviations, n = 6.

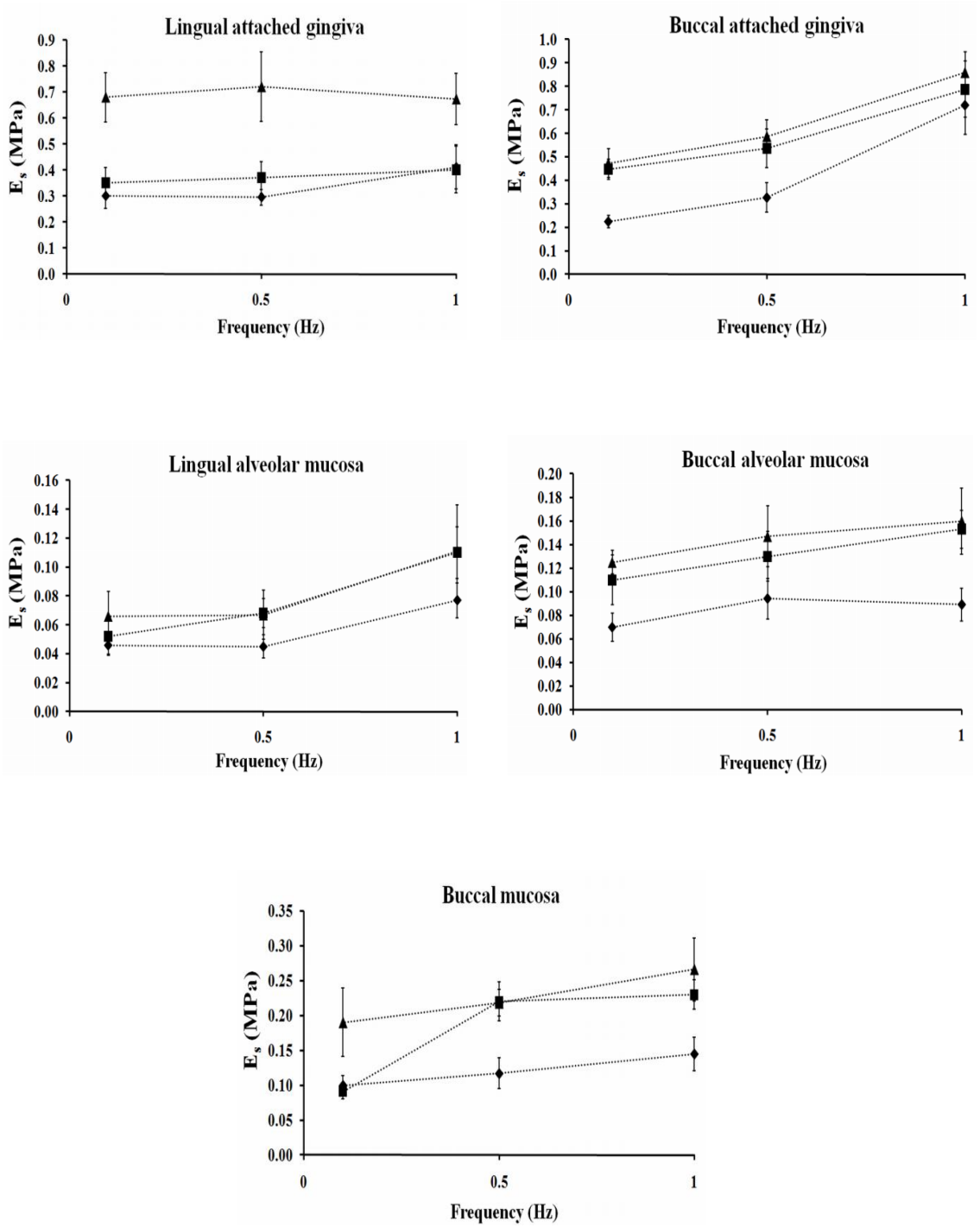

Figure 4.9. Steady modulus (E_s), measure of tissue compressive stiffness at the last cycle when the stress equilibrates, was also influenced by the strain amplitude and loading frequency; ♦, 5% compressive strain; ■, 10% compressive strain; ▲, 15% compressive strain. Data are means ± standard deviations, $n = 6$.

4.3.2. Histological Assessment

The histological analysis showed that the organization of the epithelial and connective tissues varied considerably among different regions. Representative images (n = 6) showed the epithelium of the attached gingiva in both lingual (Fig. 4.10A) and buccal (Fig. 4.10B) aspects to be bound with a clear margin, the stratum corneum (SC), which indicates the keratinization of the tissue. However, such a boundary layer was absent for the epithelium of the buccal mucosa (Fig. 4.10C) and the alveolar mucosa (Figs. 4.10D, 4.10E). The histology also showed the keratinized surface layer, stratum corneum (SC), of the attached gingiva to be orthokeratinized displaying a loss of epithelial cell nuclei, whereas the cells of the non-keratinized regions retained their nuclei. Both lingual and buccal attached gingiva display a well-defined stratum granulosum and basal layer, or stratum basale, with characteristic protrusions intertwined with the underlying connective tissue. As expected the histological analysis shows the buccal mucosal epithelium to be a relatively thick layer (>0.5 mm) compared to the epithelia of the attached gingiva and alveolar mucosa (~ 0.1-0.3 mm).

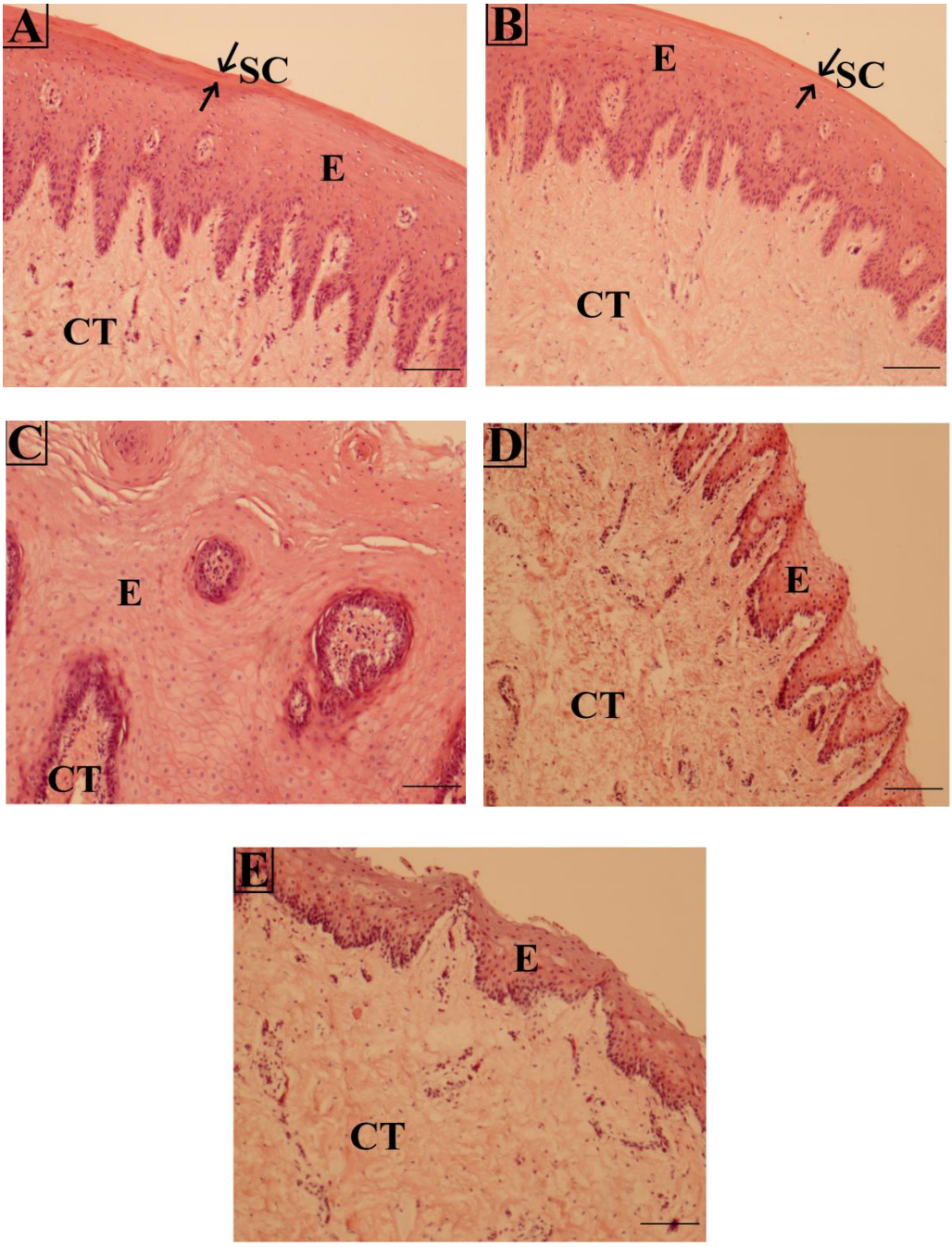

Figure 4.10. Histological analysis (hematoxylin and eosin, original magnification ×10) shows the keratinized epithelium of the lingual **(A)** and buccal **(B)** attached gingiva. The non-keratinizing epithelial layers of the buccal mucosa **(C)**, lingual alveolar mucosa **(D)**, and buccal alveolar mucosa **(E)** were also observed from the histology images. The connective tissue (CT), epithelium (E), and stratum corneum (SC) show the relative thicknesses and ECM structure of each discrete zone. Scale bars indicate 100 μm.

4.4. DISCUSSION

These investigations assessed the biomechanical behavior of oral soft tissues under applied stress conditions, and evaluated mechanical variation as a function of tissue location. A more detailed knowledge of the properties of these tissues, in particular functional and regional variations, will provide an important baseline for the development of improved materials to repair or regenerate these soft tissues. Because of the limited data available on the biomechanical properties of human oral soft tissues and the resemblance of porcine oral tissues to human tissue,[236] porcine tissues were used as a model system in this *ex vivo* study. The biomechanics of the porcine oral soft tissues were examined under compressive and extensional forces. The compressive properties of the tissue were investigated under dynamic compression simulating the forces acting on oral tissue during mastication. Although the chewing frequency of the pig ranges between 2-3 Hz, the compression tests in this study were carried out over a frequency range of 0.1-1 Hz which corresponds to the chewing frequency of humans.[237]

Results from the investigations described herein show that the biomechanical behavior of the porcine oral mucosa displays significant regional variation directly related to unique structural and functional characteristics of these different tissues. The attached gingiva demonstrated the highest tensile and compressive strength amongst all tested regions, and has been assumed to be a consequence of structural adaptations of the ECM.[53] Consistent with the literature, cells in the attached gingiva's keratinized stratum corneum (SC) layer were devoid of nuclei, instead displaying a dense network of keratin filaments. This directly results in the increased tensile stiffness and strength relative to zones more

distant to the tooth/gingiva junction.[238] The higher mechanical strength of the attached gingiva was also attributed to its collagenous fibers within the connective tissue layer. The higher tensile strength of the attached gingiva was also attributed to more abundant collagenous fibers within the connective tissue layer, relative to the buccal mucosa with a higher epithelial tissue content displayed a lower tensile strength. Connective tissue collagenous fibers are also known to be more organized in the attached gingiva.[239] The epithelial tissue layer thickness values obtained for each representative tissue layer are consistent with those reported in the previous studies.[240-242]

Viscoelastic properties of the tissue were detailed using stress relaxation analysis and were found to be consistent with the tissues physiological demands, where repetitive jaw movement and mastication require highly distensible tissue in order to perform appropriately. These results also show the alveolar mucosa to have a relatively high viscoelasticity compared to the other regions. This result can be attributed to several factors, including the abundant and densely arranged elastic fibers,[225] epithelial mucopolysaccharides reducing tissue deformation under load,[243] and the ease of movement of the interstitial fluid within the ECM.[231, 244]

The dynamic compressive properties of these tissues were shown to vary significantly amongst different regions of porcine oral mucosa, in particular the attached gingiva was shown to have higher compressive modulus values relative to the other regions. The attached gingiva is directly affected by compressive forces due to location and thus structural adaptations and composition correlate with the strong compressive forces during mastication.[245] The attached gingiva with its keratinized epithelial layer resists

these compressive stresses more compared to the other regions, and transmits the applied stress to a lesser extent to the underlying connective tissue. The higher compressive strength of the attached gingiva may also be likely due to its higher collagen and proteoglycan content in its ECM.[246] Proteoglycans manage to absorb and release sufficient tissue water for varying compressive strain and frequency values, while the collagen fibers assist the movement of tissue fluid during compression.[231, 247, 248] The collagen fibers of the connective tissue layer were previously reported to realign to a position parallel to the underlying epithelial layer upon compression.[249] Kydd *et al*. (1971) also demonstrated that morphological changes occurred within the connective and epithelial tissue layers of the masticatory mucosa under compressive load.[250]

Although several investigations have shown variation in composition between the lingual and buccal aspects of oral mucosa,[251, 252] the results reported here showed no significant differences in their response to applied *in vitro* stresses. Further, no significant differences in mechanical strength were found between the lingual and buccal aspects of the attached gingiva. The close resemblance in biomechanical properties is primarily driven by the anatomical similarities between the two aspects, as shown in the histological analyses.

Although human and porcine oral tissues are similar in many respects and porcine tissues have been shown to be a useful and a relevant model to draw conclusions about human soft oral tissue function,[253] some variation is observed. Human tissues typically display am increase in collagen and non-collagenous protein content and higher concentrations of DNA relative to the equivalent porcine tissue.[96, 254, 255] As such, caution must be advised

for direct extrapolation of human tissue performance. Variation in animal model data to human oral soft tissues have shown different systems to exhibit higher than expected biological variation and poor reproducibility.[256] In addition, gross anatomy, mastication mechanics, and dietary composition may have a more direct effect on these tissues performance relative to humans.

4.5. CONCLUSIONS

The data reported in this study support our hypothesis that the mechanical properties of oral soft tissues show significant variation in performance as a function of structure and location in the oral cavity. Although it remains to be established what biomechanical properties are minimally necessary to support mastication and other oral functions, the results reported in this study clearly indicate that attached gingiva is significantly stiffer and more resistant to mechanical stresses than regions of non-keratinized oral mucosa. The biomechanical testing results presented herein may have important clinical implications in human systems, where a deeper understanding of periodontal tissue biomechanics may enhance the success of soft tissue graft procedures by improved tissue pairing. By allowing surgeons to better select donor tissue location to be more biomechanically consistent with the implantation site may lead to improved tissue grafting outcomes. Mechanical mismatching has been shown to be predictive of failure of other tissues,[257-259] however further investigation is required to fully assess the effect of mechanical pairing tissues in the oral environment. In addition, a thorough understanding of functional tissue mechanics will set basic targets for biomedical engineers to develop improved materials with appropriate properties that better emulate native tissues.

CHAPTER 5

HUMAN UMBILICAL VEIN (HUV) AS A NOVEL GRAFT FOR PERIODONTAL TISSUE ENGINEERING

5.1. INTRODUCTION

The human umbilical cord (HUC) is a natural tissue complex that is readily available as discarded tissue from birthing centers at an average length of 50-60 cm,[260] and free of valves and branches.[261] The HUC consists of two human umbilical arteries (HUAs), one human umbilical vein (HUV), and the surrounding Wharton's Jelly. The HUA is longer than the HUV, and as the difference becomes larger, it gives the cord a twisted shape.[262] The histological cross-section of the HUC is presented in Fig. 5.1. The HUC also consists of numerous growth factors and various types of cells in its structure, such as autologous cell sources and mast cells involved in immunological and inflammatory reactions.[31, 263-267]

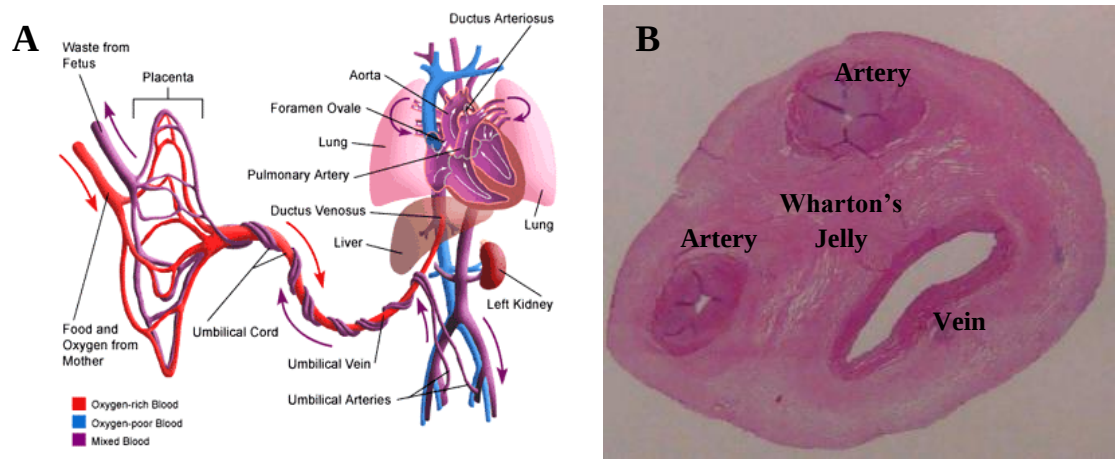

Figure 5.1. (A) Schematic diagram showing the fetal circulatory system. The fetus is connected to the placenta by the umbilical cord. The blood vessels within the umbilical cord provide the transportation of the necessary nutrients and oxygen to the fetus, and the waste products back to the mother's circulation system (www.health.uab.edu). **(B)** Hematoxylin & Eosin (H&E) staining of the human umbilical cord (HUC) showing the two arteries, one vein and the surrounding matrix, Wharton's Jelly.

The human umbilical vein (HUV), having a diameter of approximately 4-6 mm,[268] has been successfully used as a glutaraldehyde-treated graft for reconstructive vascular surgeries showing improved patency rates in small diameter applications.[269-274] The glutaraldehyde-treatment (tanning) process cross-links collagen fibrils to strengthen the material,[275, 276] tends to block the immunogenicity,[273] helps to prevent the degradation of the graft,[277] and completely de-endothelializes the lumenal surface.[278] The major problem with this chemical modification is the aneurysm formation within the graft.[279-281] The complete removal of glutaraldehyde from the grafts prior to implantation is also necessary due to its thrombogenicity and cytotoxicity.[282, 283] However, unmodified or untanned HUV grafts are subject to destruction by host-immune reaction.[284] To improve the HUV grafts against these host-immune reactions, a decellularization process should

be adopted.[285-288] It has been hypothesized that the collagenous tissue structure remained after the decellularization process would retain the tissue characteristic biomechanical properties and provide a suitable background for growing new tissue architecture.[289]

Decellularization alters the scaffold's composition, surface chemistry and ultrastructure, thus influencing cell attachment, viability, proliferation and gene expression for various ECM proteins.[290] Among the decellularization agents, sodium dodecyl sulfate (SDS) is one of the most widely used anionic surfactants because of its efficacy in removing xenogenous cells, solubilizing membrane proteins, and preserving tissue ultrastructure and mechanical integrity.[291-293] Use of SDS, nevertheless, needs some precautions, since the ineffective removal of the surfactant may inhibit the growth of the reseeded cells.

Taking advantage of the HUV's natural structure and composition, a number of other surgical applications are foreseen, particularly as a resorbable (non-crosslinked) material.[227, 294] The HUV is readily dissected from the cord and can be split longitudinally to form a flat sheet, approximately 18-20 mm wide, that may offer a unique approach to periodontal GTR. The HUV is allogenic which potentially reduces immune reactivity compared to xenogenic materials and also the risk of interspecies viral transfer. Its vascular derivation provides a compliant tissue that is conducive to cellular attachment and subsequent remodeling.[295, 296]

The biofunctionality of HUV can be attributed, in part, to its multilayered composite structure, which provides unique composition, architecture, and mechanical properties. This structure is consistent with other blood vessels, having an intima with an endothelial cell layer and basement membrane that separates the medial layer with an internal elastic

lamina composed of longitudinally-oriented elastin fibers.[297, 298] The medial layer is approximately 200-350 μm thick and represents the primary load-bearing layer, that resists pressure induced by blood flow.[30, 222] The medial layer is populated with large numbers of smooth muscle cells dispersed within collagen bundles densely interwoven with a meshwork of thicker elastin fibers, and smooth muscle layers.[26, 299] Collagen fibers are relatively strong and stiff, compared to elastin fibers that are more extensible.[300] The transitional region between the media and adventitia consisted of individual collagen, fibroblasts, fibroblast-like cells and smooth muscle cells sparsely distributed within the tissue.[301] The less structured adventitia contains only a few elastin fibers with most of its collagen I fibrils arranged circumferentially around the vessel.[298, 302, 303] The adventitia layer integrates into a supporting loose connective tissue unique to the HUV, Wharton's Jelly, a mesenchymal matrix consisting of sulphated glycosaminoglycans, and proteoglycans (PG), covalently attached to the sulphated glycosaminoglycans (sGAG).[304] sGAGs mainly contribute to the permeability properties of the connective tissue,[305] while the hyaluronic acid (HA), the most abundant sGAG, helps the Wharton's Jelly maintain its hydrated state.[306] The PGs of Wharton's Jelly form anti-thrombogenic barrier in the vascular lumen.[24] These structures are immobilized in a collagen fibril-glycoprotein microfibril network with dispersed cell populations.[284, 307-309] The loosely arranged collagen fibrils lack a systemic orientation in this layer, whereas their orientation becomes circular for the large umbilical cord vessels.[20, 310]

Given these properties, we envision that in the case of periodontal GTR, the relatively porous ablumenal surface of the tissue-engineered HUV scaffold, composed of collagen types I and III and hyaluronic acid could be implanted against the periodontal defect, and

the gingival flap positioned over the less porous lumenal surface, composed of a type IV collagen basement membrane (Fig. 5.2). Used in this manner, the decellularized HUV matrix may fulfill the requirements for periodontal GTR by providing adequate space for blood clot formation, wound stabilization, and encouraging repopulation of the wound by appropriate progenitor cells.[311] Similar scenarios could be suggested for other surgical procedures that utilize such a barrier. To the author's knowledge, this paper represents the first time the HUV has been investigated as a surgically implantable biomaterial outside vascular applications.

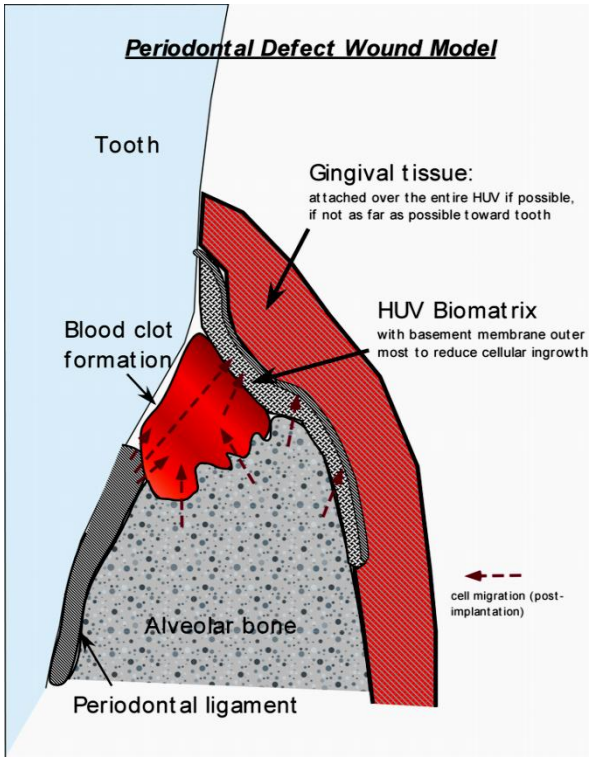

Figure 5.2. A diagram of the proposed surgical application for a periodontal defect, where the human umbilical vein (HUV) matrix is inserted under the existing gingiva.

Any material to be used as a surgical barrier must have sufficient mechanical properties to withstand forces that would be encountered clinically, and also biological properties that allow appropriate interaction with local tissue cells.

These investigations outline the potential of the HUV as a barrier matrix, biomechanical properties and the ability of the matrix to support the growth and proliferation of human gingival fibroblasts (hGFs). These results suggest that the HUV may have potential as a novel biocompatible matrix for use as a barrier in periodontal GTR and other surgical techniques that employ a barrier membrane.

5.2. MATERIALS AND METHODS

5.2.1. Preparation of Human Umbilical Vein (HUV)

Human umbilical cords were obtained from the Delivery Suite of Norman Regional Hospital (Norman, OK) in compliance with a University IRB approved protocol (Fig. 5.3A). Cords were stored at +5°C for no more than 48 h post delivery. Before processing, the cords were washed with double-distilled water to remove the residual blood and cut at an initial length of 100 mm. The cords with an outer diameter of approximately 6 mm were used for the experiments. The cords were stretched on stainless steel mandrels (316 stainless steel tube, 4 mm ID, 6 mm OD× 200 mm L) (MicroGroup, Inc., Medway, MA) and secured at each end with plastic zip ties. Mounted cords were wrapped in paper towels and placed in a polystyrene canister to allow progressive freezing (1°C/min) to -86°C.[227] After a minimum of 48 h, vessels were removed from the -86°C freezer (Fig. 5.3B), mounted into the lathe (Model 23M80D, MicroKinetics Corp., Kennesaw, GA)

(Fig. 5.3C), and machined to wall thicknesses of 0.4 and 0.8 mm with a tungsten carbide cutting tool (Fig. 5.3D). Dimensional control was programmed using TurnMaster Pro for Windows with a spindle speed of 2000 rpm, and ramp speed of 200 steps/sec. Immediately after dissection, tissue sections were stored at -20°C for 1-2 h (Fig. 5.3E), then transferred to a container filled with chilled distilled water at +5°C refrigeration for no more than 24 h to fully thaw. Prior to decellularization, vessels were removed from +5°C storage and maintained at room temperature for 1 h.[227]

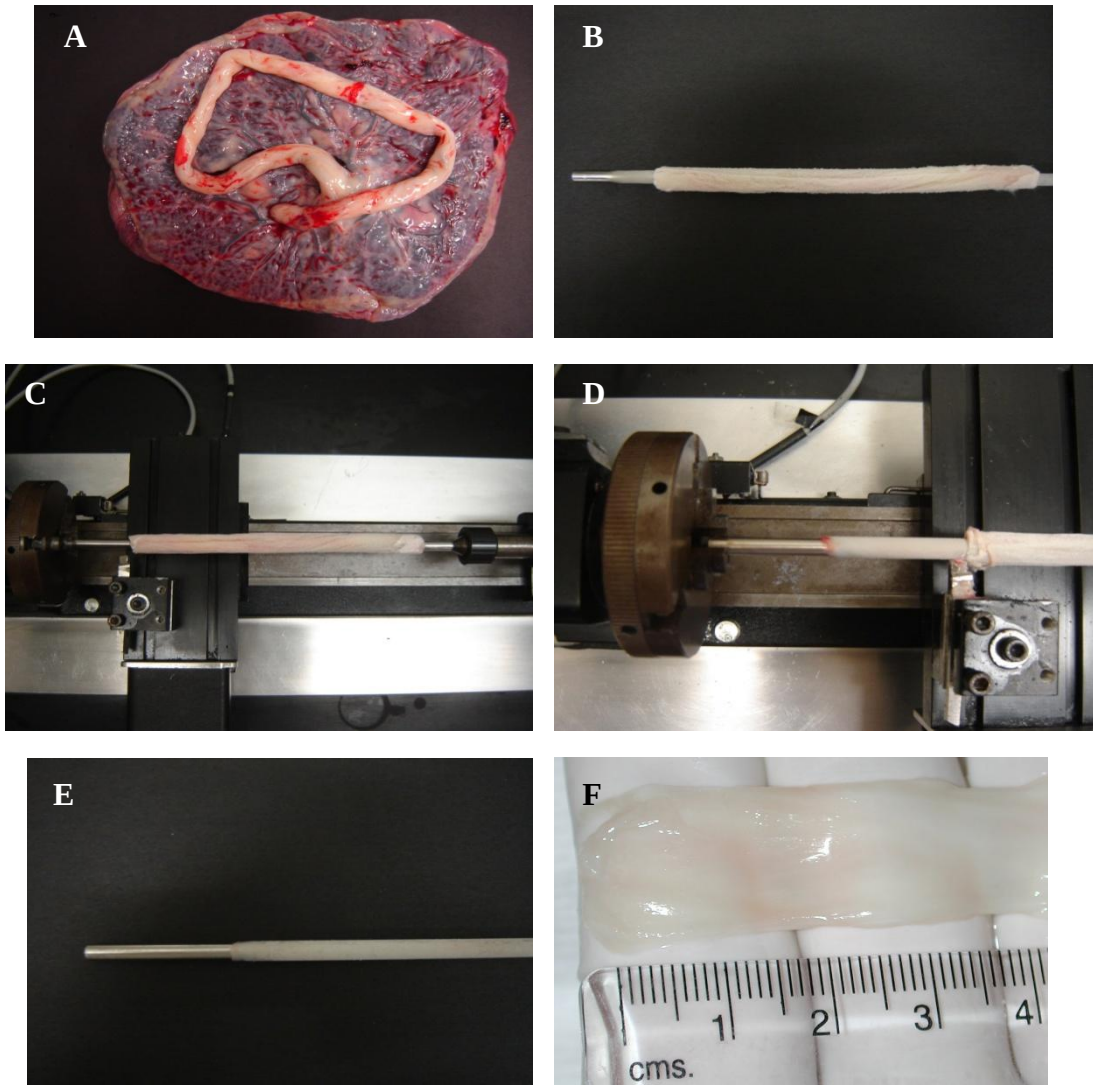

Figure 5.3. Preparation of the HUV scaffold. The human umbilical cords (HUCs) were obtained from the birth center **(A)**, washed thoroughly to remove the blood and mounted on stainless steel mandrels. The cords were then frozen down to -86°C **(B)**. The cord is then placed in a computer-controlled lathe **(C)**, and the lathe is engaged with the cutting tool transversing the section **(D)**. The dissection process yields a smooth surface having the desired tissue wall thickness **(E)**. Thawed human umbilical vein (HUV) segment immediately after longitudinal dissection **(F)**. Image shows the outer 'ablumenal' surface upper most.

5.2.2. Decellularization of HUV Tissue Sections

Thawed HUV sections were cut longitudinally to generate flat sheets (Fig. 5.3F) and placed in glass bottles containing 1% sodium dodecyl sulfate (SDS) (Mallinckrodt Baker, Inc., Phillipsburg, NJ) in distilled water, and agitated under constant shaking (100 rpm) for 24 h. SDS was selected on the basis of being a widely used surfactant for decellularization processes with its ability to preserve scaffold integrity while removing immunogenic cellular components.[288, 291, 292] The decellularization solution was decanted and the tissue samples were washed in distilled water (3x) to remove residual surfactant. Samples were then incubated overnight at room temperature in phosphate buffered saline (PBS) (Gibco Life Technologies, Grand Island, NY) containing 70 U/mL DNase I (Sigma-Aldrich Inc., St. Louis, MO) to digest the DNA. Subsequently tissue sheets were washed in PBS (3x) to remove residual DNase. Samples were terminally sterilized using 0.2% peracetic acid /4% ethanol solution for 2 h, after which samples were pH balanced (pH 7.4) using multiple washes in PBS.[295, 312] Peracetic acid solution was from Sigma Aldrich (St. Louis, MA). All decellularization solutions were sterile and the treatment steps were performed at room temperature (20-25ºC). The tissue/solvent ratio was kept as 1/20 (w/v) for each step, unless otherwise stated.[313]

5.2.3. Biomechanical Analysis

5.2.3.1 ***Uniaxial Tensile Testing.*** A uniaxial tensile testing rig (Instron Corp., Model 5542, Norwood, MA) equipped with a 500 N load cell was used for the stress-strain analysis. Tissue strips (3 × 18 mm) were cut in both longitudinal and circumferential orientations using a template to maintain dimensional consistency. Wall

thickness of the tissue strips (cut at 400 µm and 800 µm initial wall thickness) were measured again with an electronic digital caliper (Starrett Co., Athold, MA) to ± 0.001 mm accuracy after decellularization due to tissue swelling. New dimensions were used for tissue cross-sectional area measurements. Strips were subjected to tensile testing as described in Section 4.2.2.1.

5.2.3.2. *Stress Relaxation.* The viscoelastic tissue response of HUV was assessed by stress relaxation analysis (Please refer to Section 4.2.2.2).

5.2.3.3. *Suture Holding Capacity.* Suture holding capacity was assessed on HUV sections (9 × 18 mm) by applying uniaxial stress. A single sterile 3-0 braided silk suture (Henry Schein, Melville, NY) was passed through the center of one end of the tissue section 3 mm below the edge, with the other glued to sand paper and attached to the grip. Samples were preloaded and preconditioned (as above in tensile testing), and stretched at an extension rate of 5 mm/min until failure.

5.2.4. *In vitro* Culture and Seeding of Human Gingival Fibroblasts (hGFs)

Primary human gingival fibroblasts (hGFs) (American Type Culture Collection (ATCC), Manassas, VA) were cultured in 75-cm^2 culture flasks under a humidified atmosphere of 5% CO_2 and 95% air at 37°C. Cells were maintained with Dulbecco's Modified Eagle's Medium (DMEM) (500 mL) supplemented with 10% animal serum complex (FetalPlex, Gemini Bio-Products, West Sacramento, CA), 1% 200 mM *L*-glutamine, 50 kU penicillin and 50 mg streptomycin (Gibco Life Technologies, Grand Island, NY). Media was replenished every 3 days. The cells were serially passaged when 80-90% confluent by

enzymatic digestion with Accutase (Innovative Cell Technologies, Inc., San Diego, CA) and expanded in the humidified incubator at 37°C with 5% CO_2.

Circular disks (16 mm in diameter) were punched from acellular HUV sheets (0.8 mm-cut) using a stainless-steel hollow punch under sterile conditions. Tissue disks were then placed in 24-well tissue culture plates (BD Falcon, San Jose, CA) and before cell seeding, incubated in DMEM culture media containing 15% FBS overnight to enhance cell attachment.[314] Cells were seeded independently on both the lumenal and ablumenal surfaces of the tissue disks at a density of 1×10^5 cells/cm^2. Before seeding the cells on the scaffolds, the culture media was aspirated from the T75 culture flasks and cells were detached from the surface of T75 culture flasks with 5 mL of accutase for 15 min. Then an equivalent volume of culture media (5 mL) was added to the suspension to inactivate the enzyme. The suspensions were transferred to 15 mL falcon tubes and centrifuged at 1100 rpm for 5 min. The solution was aspirated from the tubes and the cell pellet was resuspended in 10 mL of fresh culture media. Then 0.5 mL of this cell suspension was mixed with 0.5 mL Trypan Blue (Invitrogen Corp., Grand Island, NY) in an eppendorf tube, and the viable cells were counted using a haemocytometer. When the cell clumps appeared, the samples were vortexed to count the cells. The seeded scaffolds were statically cultured for 3, 6, 9, 15, 18, and 21 days, and assayed for metabolic activity and cell proliferation.

5.2.5. DNA Quantification

The DNA content of the cultured HUV scaffolds was evaluated using the Picogreen Assay kit (Molecular Probes, Eugene, OR). PicoGreen methodology was adopted due to

its high sensitivity to low levels of dsDNA, direct correlation with cellular proliferation and highly reproducible nature.[315, 316] PicoGreen reagent effectively binds to ds-DNA, however sample preparation requires enzymatic digestion to release the DNA.[317]

For each culture period (3, 6, 9, 15, 18, and 21 days), the DNA content was assessed to evaluate cell proliferation. Tissue disks were carefully washed with PBS to remove culture media, and then incubated in 1 mL of 200 U/mL DNA-free, sterile-filtered collagenase solution (Sigma-Aldrich Inc., St. Louis, MO) in PBS for approximately 2 hours at 37°C to digest tissue. Cells were then lysed by three consecutive freeze-thaw cycles at -86°C to release DNA. The cell-containing solutions (100 μL) were incubated with an equal volume of (100 μL) diluted PicoGreen reagent (PicoGreen dimethylsulfoxide stock solution diluted ×200 in TE assay buffer) in black bottom, 96-well plates (Greiner).[318] Samples to be assayed were incubated for 5 min protected from light at room temperature. The fluorescence was measured at an excitation wavelength of 480 nm and an emission wavelength of 520 nm using a Synergy HT plate reader (Bio-Tek Instruments, Inc., Winooski, VT). The number of cells per sample was computed using Eqn (1)[319]:

$$\text{Number of cells} = \frac{\text{DNA concentration } (\mu g/mL) \times \text{volume (mL)} \times 10^6 \text{ (pg/}\mu g)}{\text{(DNA content per cell) (pg/cell)}} \quad (1)$$

Where, the DNA concentrations (μg/mL) of the samples with unknown cell densities were calculated by extrapolating the Bacteriophage λ DNA (Invitrogen) standard curve (Appendix A), and the DNA content per hGF was assumed as 6.61 ± 1.2 pg DNA/cell.[320]

5.2.6. Assessment of Cellular Metabolic Activity

Gross metabolic activity of seeded cells on lumenal and ablumenal surfaces of the HUV scaffold was assessed by quantifying the reduction of the non-toxic Alamar Blue (AB) reagent at the end of each culture period. The assay basically yields an oxidation/reduction reaction as the cells grow and lets the experimenter analyze the viability of the cells at the end.[321] The AB assay in concert with direct measures of proliferation (DNA quantification) provides information on the metabolic state of the cells.[322] Briefly, the culture media was aspirated from the wells, and 1 mL of fresh medium supplemented with 10% (v/v) AB reagent (Biosource International, Camarillo, CA) was added to each well. After 6 h of incubation, the 100 µL of solution was sampled from each well and transferred to 96-well plates (Costar). The absorbance was measured at wavelengths of 575 and 600 nm using a Synergy HT plate reader (Bio-Tek Instruments, Inc., Winooski, VT). Acellular tissue discs cultured with media without cells served as negative controls. Percentage AB reduction was calculated according to the manufacturer's protocols by using Eqn (2):

$$\text{Percentage reduction of Alamar Blue} = \frac{(\varepsilon_{OX})^{\lambda 2}A^{\lambda 1} - (\varepsilon_{OX})^{\lambda 1}A^{\lambda 2}}{(\varepsilon_{RED})^{\lambda 1}A'^{\lambda 2} - (\varepsilon_{RED})^{\lambda 2}A'^{\lambda 1}} \times 100 \qquad (2)$$

where, ε_{OX} is the molar extinction coefficient of AB oxidized form (blue), ε_{RED} is the molar extinction coefficient of AB reduced form (red). The molar extinction coefficients for the oxidized form (ε_{OX}) at the wavelengths 570 ($\lambda 1$) and 600 ($\lambda 2$) nm are 80586 and

117216, respectively. On the other hand, the molar extinction coefficients for the reduced form (ε_{RED}) at the wavelengths 570 and 600 nm are 155677 and 14652, respectively. A denotes the absorbance of the test wells, and A' represents the absorbance of the negative control wells.

5.2.7. Scanning Electron Microscopy (SEM) Surface Analysis

SEM analysis was conducted to qualitatively assess the surface morphology of the acellular HUV (for the 0.4 mm- and 0.8 mm-cut sections) and also to demonstrate hGF attachment and visualize cell morphology on the recellularized scaffolds (0.8 mm-cut sections). HUV tissue sheets were fixed in 1% (v/v) glutaraldehyde (Sigma, St. Louis, MO) for 4 h, then washed with PBS 3× for 5 minutes each. The samples were then treated with 1% (v/v) osmium in PBS for 2 h and washed with PBS 3× for 5 minutes each. The samples were then dehydrated in graded ethanol solutions (30%, 50%, 70%, 90%, 95%, 100%, for 10 min each). The final step consisted of critical point-drying (Autosamdri-814, Tousimis, Rockville, MD), and gold sputtering (Model Hummer VI, Anatech Ltd., Hayward, CA) of the samples. Surface images were taken using a JEOL LSM-880 SEM at 15 kV.

5.2.8. Histological Analysis Using Light Microscopy

Histological analysis was performed to evaluate the effectiveness of the decellularization process, and then to observe the attachment and migration of hGF cells reseeded on the acellular HUV scaffolds (0.8 mm-cut). Please refer to Section 4.2.3.

5.2.9. Visualization of the Fixed Cells with 4,6-diamidino-2-phenylindole (DAPI) Fluorescent Dye

The hGFs attached on the ablumenal surface of the HUV scaffold (16 mm-diameter tissue disks) were visualized using a fluorescent nuclear stain that is excited by ultraviolet light, showing blue fluorescence when bound to DNA. Briefly, from a stock solution of 4,6-diamidino-2-phenylindole (DAPI) (Invitrogen, Eugene, OR) (10 mg/ml in distilled water) was diluted 5000-fold in PBS. The culture media was aspirated from the wells of the culture plate containing seeded scaffolds (seeding density = 250,000 cells/disk) and the tissue sections were rinsed three times with PBS (5 minutes each). Due to the light sensitive nature of DAPI dye, the staining should be performed in a dark venue. Samples were then fixed in a 3.7% formaldehyde solution for 20 minutes followed by permeabilization of the cells by immersion in 0.2 % Triton X-100 for 5 minutes. This solution was then aspirated and samples were rinsed in PBS for three times (5 minutes each). Samples were then incubated in the prepared DAPI labeling solution for 1-5 minutes at room temperature. Samples were then rinsed in PBS three times (5 minutes each) and mounted. Observation of DAPI-labeled DNA was carried out with a Nikon Fluorescent microscope (Nikon Eclipse E800) and image analysis with MetaMorph software V6.2 from Molecular Devices. The excitation wavelength maximum is near 359 nm and the emission wavelength maximum is approximately 461 nm when bound to DNA. The cells seeded on the plastic surface of tissue culture plates served as controls.

5.2.10. Statistics

Statistical analyses were performed using the SPSS 15.0 for Windows software (SPSS Inc., Chicago, IL, USA). The Student's *t*-test was used to test for significant differences between two test groups. One-way univariate analysis of variance (ANOVA) was used to test for significant differences among multiple test groups. The Levene's test for homogeneity was used to test for equal variance among samples. When equal variance could be assumed, the Tukey honestly significant difference (HSD) test was applied to perform *post hoc* comparisons among multiple test groups. Otherwise the *post hoc* analysis was done using the Games-Howell method. Statistical significance was set at $p < 0.05$ for all tests. Analysis of cellular interactions with the HUV scaffold used a minimum of three separate cords (from different individuals) with a further three samples taken from each cord (with mean values of each triplicate set used to calculate statistical significance as $n = 3$). Due to increased mechanical variability between cords, a larger data set was used for mechanical analysis with a minimum of nine separate cords used in each set ($n = 9$). All values are expressed as mean ± standard deviation (SD). Results are presented as box plots, representing the mean ± 1 SD, with the dark line within each box representing the median value. Lines extending outside the box represent the data range (minimum/maximum) of recorded values.

5.3. RESULTS

5.3.1. Biomechanical Assessment

5.3.1.1. ***Uniaxial Tensile Testing.*** Irrespective of initial tissue wall thickness (0.4 mm- or 0.8 mm-thick), the longitudinal HUV sections exhibited significantly higher failure loads than circumferential sections ($p < 0.001$, $n = 9$). Representative stress-strain curves derived from the load-displacement data displayed characteristic behavior of soft biological tissues (Fig. 5.4).[323] Data shows an initial toe region demonstrating the alignment of elastin fibers parallel to the stretching axis, followed by a linear region representing the contribution of collagen fibers to the elastic response of the tissue.[324-327]

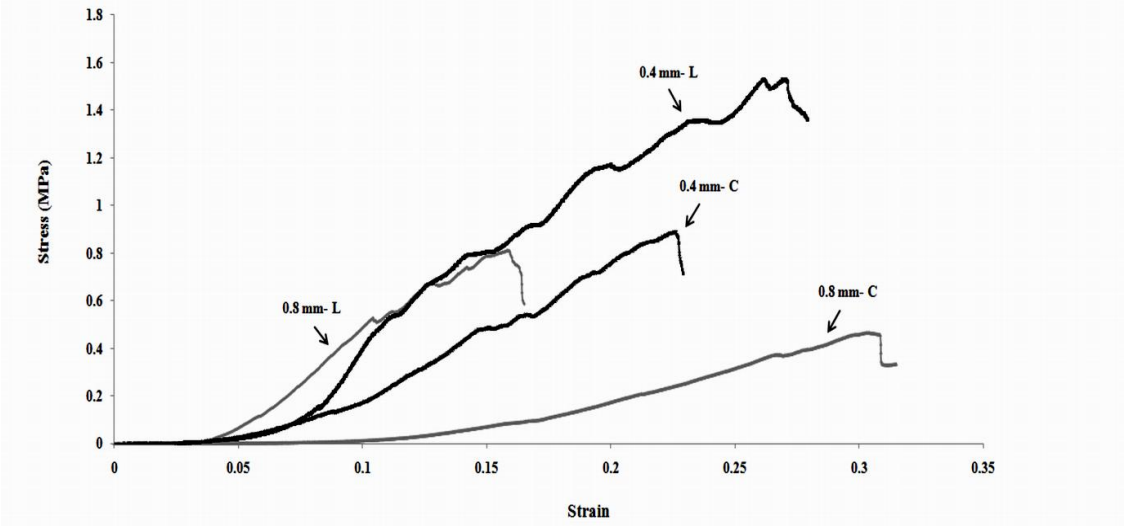

Figure 5.4. Representative stress-strain curves for the HUV samples. The longitudinal (L) strips demonstrated significantly higher stress values compared with the circumferential (C) strips for both 0.4 and 0.8 mm thicknesses.

One-way ANOVA revealed that the longitudinal strips demonstrated a significantly higher tensile strength than circumferential strips ($p < 0.001$). A statistically significant difference in Young's modulus was also detected between the longitudinal and circumferential sections for both thicknesses ($p < 0.005$). Data obtained from tensile testing are summarized in Table 5.1.

TABLE 5.1. TENSILE PROPERTIES OF THE HUMAN UMBILICAL VEIN GRAFTS AFTER DECELLULARIZATION*

Material	Cutting thickness (mm)	Young's modulus (MPa)	Ultimate tensile strength (MPa)	Strain at failure	Failure load (N)
HUV longitudinal (L)	0.4	15.33 ± 0.59 §¥#	1.41 ± 0.07 §¥#	0.30 ± 0.02 ¥	3.75 ± 0.14 ¥#
	0.8	7.94 ± 2.59 ψ#	0.69 ± 0.06 ψ#	0.25 ± 0.06	3.99 ± 0.33 ¥#
HUV circumferential (C)	0.4	6.17 ± 0.80 ψ#	0.61 ± 0.16 ψ#	0.24 ± 0.02 ψ	1.61 ± 0.43 ψ#§
	0.8	3.13 ± 0.56 ψ§¥	0.39 ± 0.03 ψ§¥	0.30 ± 0.05	2.20 ± 0.15 ¥ψ§

* Mean and standard deviation were calculated for each tensile property for a sample size of $n = 9$. Pairwise comparisons (statistical significance set at $p < 0.05$) are reported between the groups: ψ versus 0.4 mm-L; § versus 0.8 mm-L; ¥ versus 0.4 mm-C; # versus 0.8 mm-C.

SEM results showed the ablumenal surface of the 0.4 mm-cut samples (exposing the transitional area between the adventitia and Wharton's Jelly proper) to have a relatively dense three dimensional fibrous network (Fig. 5.5A), compared to the 0.8 mm-cut sections, which was deeper into the Wharton's Jelly, that displayed ECM fibers with a loose, wavy morphology (Fig. 5.5B). The basement membrane on the lumenal surface of the HUV exhibited a relatively compact ECM arrangement as shown in Fig. 5.5C.

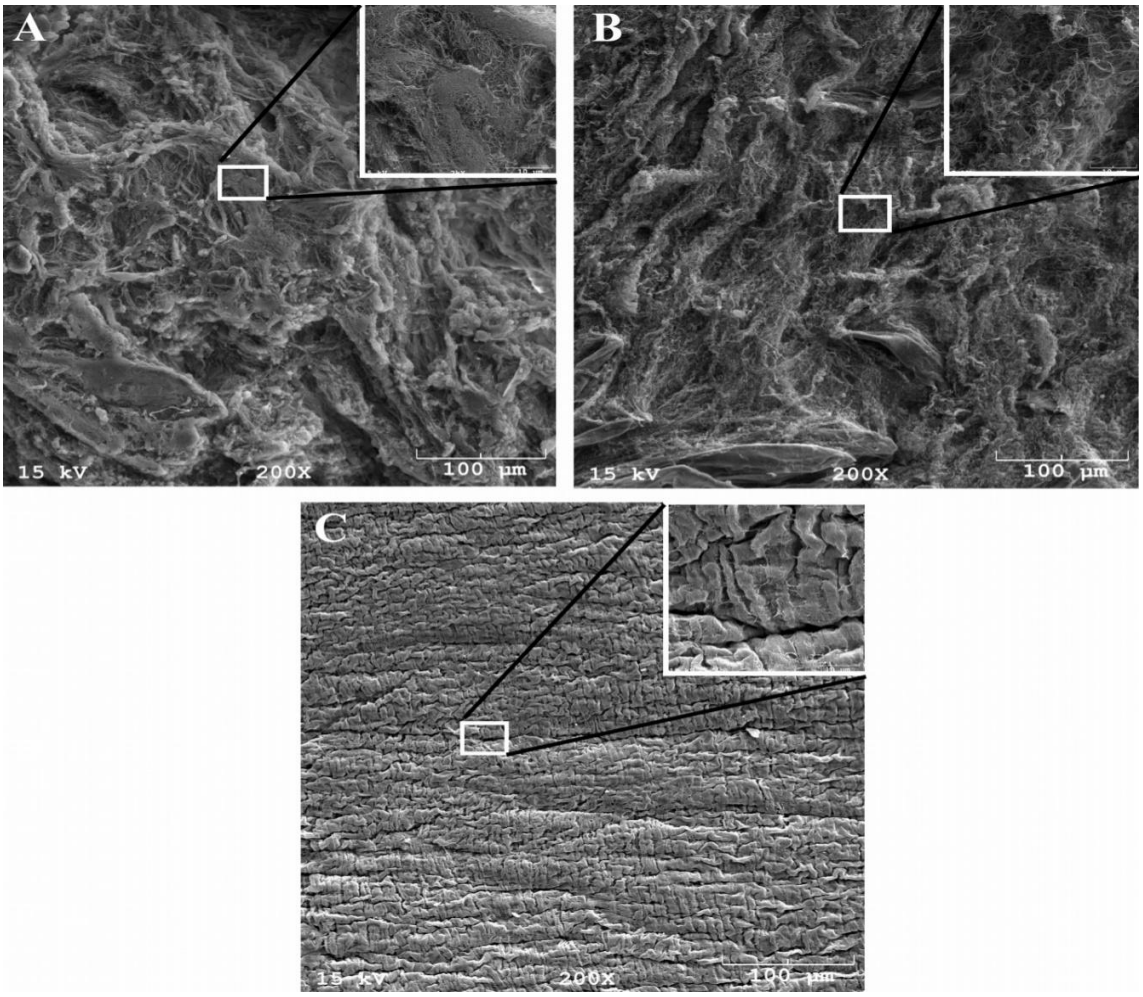

Figure 5.5. Morphological observations of the ablumenal and lumenal surfaces of the acellular HUV scaffold using scanning electron microscopy. Observations show that the ablumenal surface of the HUV cut at 0.4 mm thickness **(A)** (×200) have densely arranged collagen fibers, whereas the 0.8-mm-cut samples **(B)** (×200) have the fibers that are more loosely arranged due to the heterogeneity of the extracellular matrix composition and collagen packing. The lumenal surface **(C)** (×200) shows a tightly packed extracellular matrix structure. The upper insets display a 2000× magnification of the corresponding surface.

5.3.1.2. ***Stress Relaxation Analysis.*** Stress-relaxation curves show an initial rapid stress decay, followed by a gradual decrease over time. Equilibrium stress values, σ_∞, were attained within 180 seconds of relaxation (Fig. 5.6).

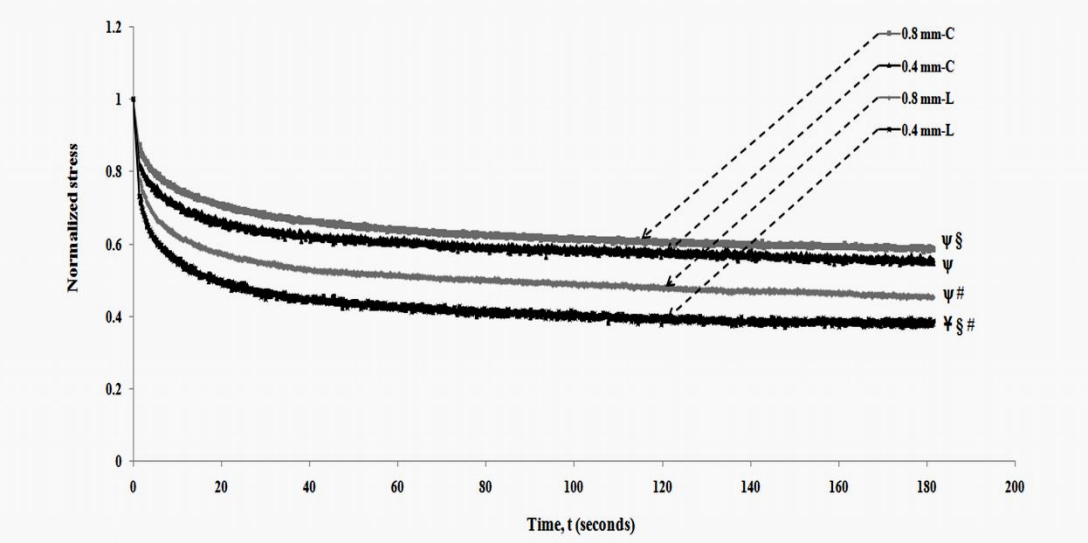

Figure 5.6. Representative normalized stress relaxation curves (n = 9). The initial stress decays to an equilibrium stress over time. The stress-relaxation data showed the viscoelasticity of the longitudinal (L) HUV strips to be significantly higher than the circumferential (C) strips for both thicknesses (Tukey honestly significant difference, $p < 0.05$). Pairwise comparisons for normalized equilibrium stress (t = 180 s) (statistical significance set at $p < 0.05$) are indicated among groups: §, versus 0.8 mm-L; #, versus 0.8 mm-C; ¥, versus 0.4 mm-C; ψ, versus 0.4 mm-L.

The degree of relaxation was greater for tissues in the longitudinal orientation compared with tissues in the circumferential orientation, suggesting the stress contribution of the viscous components (σ_o-σ_∞) to the total stress (σ_o) was higher (Table 5.2) ($p < 0.05$, n = 9). As expected, the relaxation response indicates variation in the composition of the viscoelastic components within the HUV, and demonstrated a time-dependent stress

response. The results for the stress relaxation test on the acellular human umbilical vein (HUV) matrix were summarized in Table 5.2.

TABLE 5.2. STRESS RELAXATION DATA FOR THE ACELLULAR HUMAN UMBILICAL VEIN (HUV)-DERIVED SCAFFOLDS*

Material	Cutting thickness	Initial strain, ε_o	Initial stress, σ_o (MPa)	Equilibrium stress, σ_∞(MPa)	$(\sigma_o-\sigma_\infty)/\sigma_o$*
HUV Longitudinal (L)	0.4 mm	0.08 ± 0.01 §#	0.16 ± 0.01 §#	0.06 ± 0.01 ¥#	0.65 ± 0.09 §¥#
	0.8 mm	0.12 ± 0.01 ψ#	0.14 ± 0.01 ψ¥	0.07 ± 0.01 #	0.54 ± 0.08 ψ#
HUV Circumferential (C)	0.4 mm	0.10 ± 0.01 #	0.16 ± 0.01 §#	0.08 ± 0.01 ψ	0.50 ± 0.08 ψ
	0.8 mm	0.15 ± 0.02 ψ§¥	0.14 ± 0.01 ψ¥	0.08 ± 0.01 ψ§	0.41 ± 0.05 ψ§

* Mean and standard deviation were calculated for each relaxation data for a sample size of $n = 9$. Pairwise comparisons (statistical significance set at $p < 0.05$) are reported between the groups: ψ versus 0.4 mm-L; § versus 0.8 mm-L; ¥ versus 0.4 mm-C; # versus 0.8 mm-C.

5.3.1.3. ***Suture Holding Capacity.*** Suture retention was determined as the maximum load a single sterile 3-0 braided silk suture can withstand under uniaxial tension before failure (Fig. 5.7). The suture holding capacity of the 0.8 mm-cut, circumferential HUV strips (2.20 ± 0.24 N) was significantly higher than the longitudinal strips for the same thickness (1.53 ± 0.16 N) ($p < 0.001$, $n = 9$). However, there was no significant difference in the failure loads between longitudinal (1.38 ± 0.21 N) and circumferential (1.52 ± 0.27 N) orientations of the 0.4 mm-cut sections ($p = 0.59$). The 0.8 mm-cut HUV sections demonstrated significantly higher suture holding capacity than

the 0.4 mm-cut sections in the circumferential direction ($p < 0.001$), whereas there was no significant difference between the two thicknesses in longitudinal orientation ($p = 0.58$).

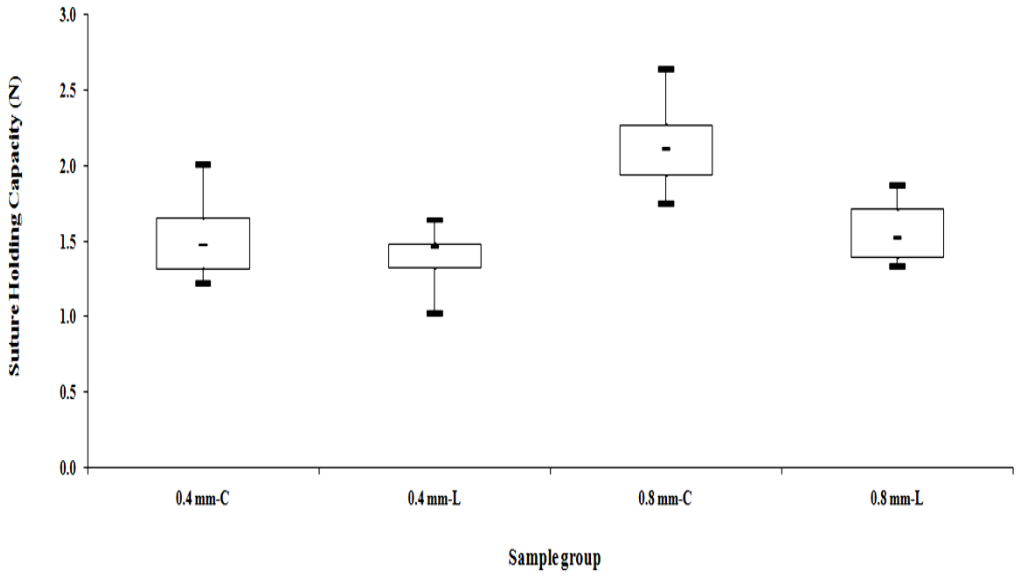

Figure 5.7. Suture holding capacity. The 0.8-mm-cut HUV strips oriented longitudinally (L) showed significantly lower failure rates than the strips oriented in the circumferential (C) direction for the same thickness (after decellularization; Tukey honestly significant difference, $p < 0.0001$, $n = 9$). There was a significant difference in suture holding capacity between the 0.4-mm-cut and 0.8-mm-cut HUV sections in circumferential orientation only ($p < 0.001$); all other data displayed no statistical difference.

5.3.1.4. ***Mechanical Property Comparison Between the HUV Graft and the Porcine Oral Soft Tissues.*** A comparative analysis between the mechanical properties of the HUV and the porcine oral soft tissues was performed to draw a conclusion on the details of HUV's biomechanical properties as a periodontal graft. The mechanical

properties of the longitudinal HUV sections cut at 0.4 mm were considered for the comparative analysis since HUV demonstrated the highest tensile strength and viscoelasticity at this initial wall thickness and orientation. One-way ANOVA indicated the ultimate strength of longitudinal HUV strip (0.4 mm-cut) was significantly higher than the porcine buccal mucosa (Games-Howell, $n = 9$, $p < 0.001$), and significantly lower than the porcine attached gingiva in both lingual and buccal aspects ($p < 0.05$). However, there was no significant difference between the HUV and the lingual and buccal alveolar mucosal sections (Fig. 5.8).

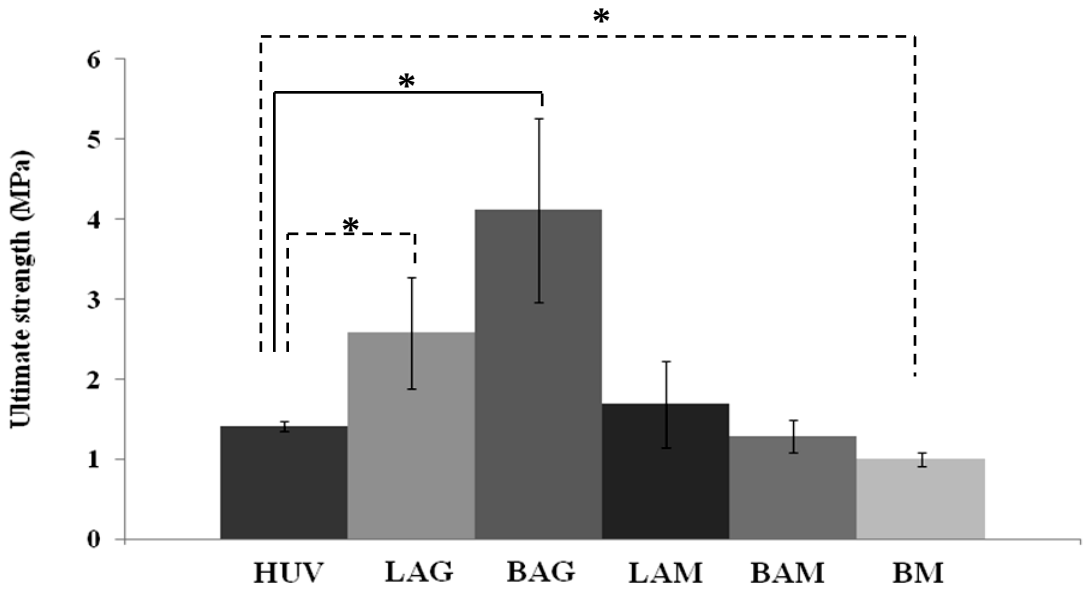

Figure 5.8. Ultimate strength. HUV, human umbilical vein (0.4 mm-L); LAG, lingual attached gingiva; BAG, buccal attached gingiva; LAM, lingual alveolar mucosa; BAM, buccal alveolar mucosa; BM, buccal mucosa. Values indicate mean ± standard deviation ($n = 6$). The symbol * denotes statistically significant difference set at the 0.05 level. Only the comparison between the HUV and different regions of porcine tissue has been made.

One-way ANOVA revealed that the Young's modulus value of the HUV strip (longitudinal, 0.4 mm-cut) was significantly higher than the tissue strips extracted from the porcine lingual and buccal alveolar mucosa and the buccal mucosa (Games-Howell, $n = 9$, $p < 0.001$). However, the stiffness of the HUV was insignificantly different from the lingual and buccal attached gingiva.

The stress relaxation analysis demonstrated the HUV was significantly more viscoelastic than the porcine lingual and buccal attached gingiva and buccal mucosa (Tukey, $n = 9$, $p < 0.005$). The viscoelasticity values of the HUV and the porcine alveolar mucosal tissues were insignificantly different from each other (Fig. 5.9). Viscoelasticity was assessed from the ratio of the stress contribution of the viscous components (σ_o-σ_∞) to the total stress (σ_o) (See Sections 4.2.2.2 and 5.2.3.2).

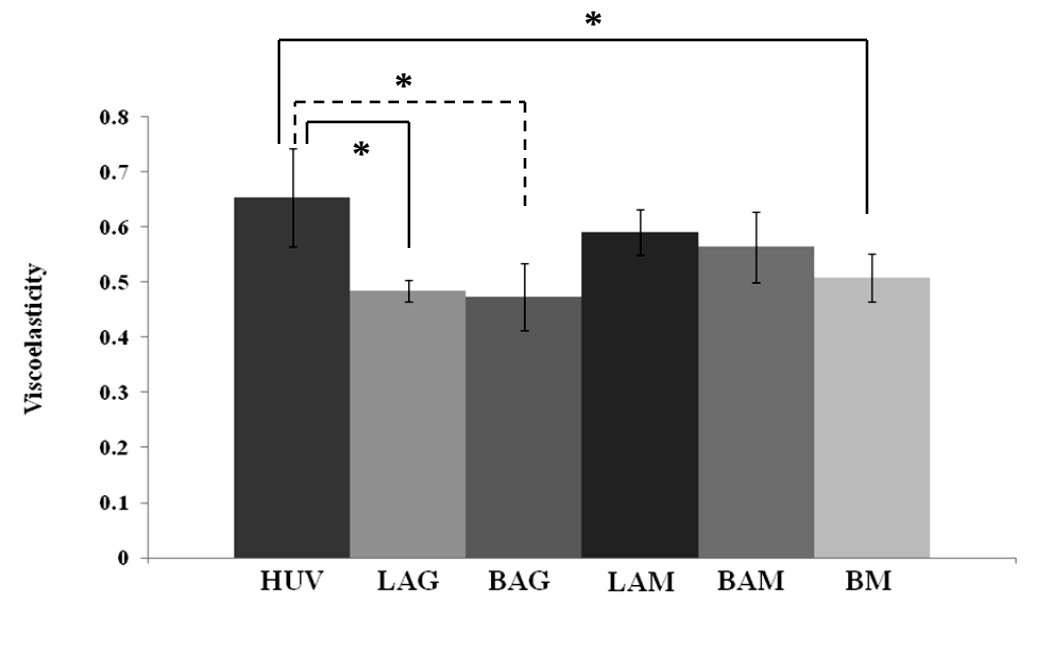

Figure 5.9. Viscoelasticity. HUV, human umbilical vein (0.4 mm-L); LAG, lingual attached gingiva; BAG, buccal attached gingiva; LAM, lingual alveolar mucosa; BAM, buccal alveolar mucosa; BM, buccal mucosa. Values indicate mean ± standard deviation (n = 6). The symbol * denotes statistically significant difference set at the 0.05 level. Only the comparison between the HUV and different regions of porcine tissue has been made.

5.3.2. Cell Growth and Metabolic Activity in Scaffolds

After an initial latency period of 9 days, hGFs started proliferating irrespective of the surface on which they were seeded (Fig. 5.10). However, increased proliferation of cells seeded on the ablumenal surface resulted in a cell density significantly higher (77000 ± 3000 cells/disk) compared to cells cultured on the lumenal surface (42000 ± 4000 cells/disk) by the end of the 21-day culture period ($p < 0.001$, $n = 3$).

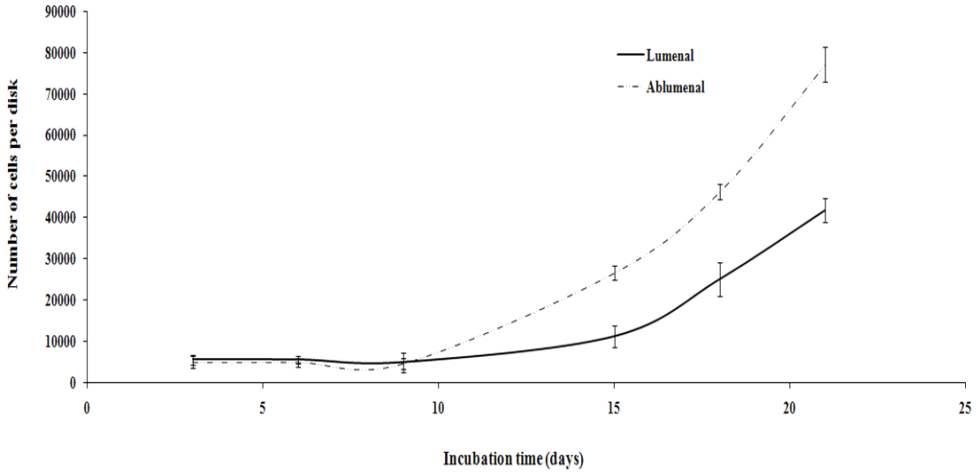

Figure 5.10. Proliferation of human gingival fibroblasts (hGFs) over time. Cell density was significantly higher for the ablumenal surface at days 15, 18, and 21, reflecting a higher cell proliferation on this surface (Student's *t*-test, $p < 0.001$, $n = 3$).

The metabolic activity of cells cultured on the ablumenal surface was significantly higher (per cell) than cells cultured on the lumenal surface, indicating cellular metabolism was influenced by the material's surface structure/composition and higher surface area of the ablumenal surface resulted in a higher proliferative capacity (Fig. 5.11) ($p < 0.05$, $n = 3$).

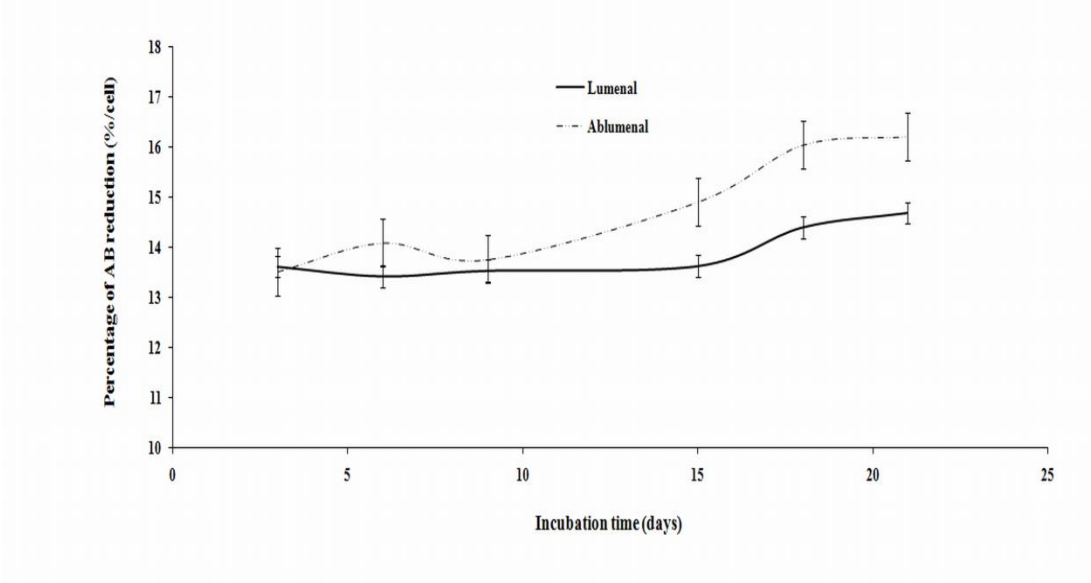

Figure 5.11. Metabolic activity of hGFs seeded on the HUV scaffold. By the end of 21-day culture period, Alamar Blue reduction (%) per cell for the ablumenal surface was significantly higher than cells seeded on the lumenal surface, demonstrating that hGFs metabolic activity was influenced by the material's surface structure/composition (Student's *t*-test, $p < 0.05$, $n = 3$). Penetration into the tissue through the ablumenal surface could account for this difference (see histology, Figs. 5.12B and 5.12C).

The complete removal of cellular material from the HUV matrix after decellularization was confirmed by H&E staining (Fig. 5.12A). Histology verified the adhesion of hGFs on both lumenal and ablumenal surfaces, however cell migration was only observed from the ablumenal surface (Fig. 5.12B). Cells cultured on the lumenal surface did not penetrate the basement membrane and remained on the surface of the scaffold after 21 days in culture (Fig. 5.12C).

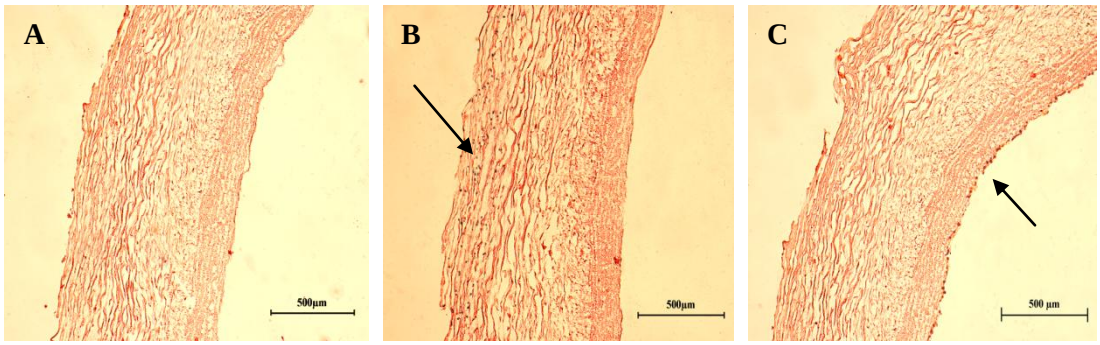

Figure 5.12. Histologic images of hematoxylin and eosin (H&E)-stained HUV sections (0.8 mm-cut) before cell seeding **(A)** and after cell seeding on ablumenal **(B)** and lumenal surface **(C)**. The images show that the decellularization removed all the cellular components, and the hGFs have tendency to adhere both surfaces, but migrate into the scaffold only through the ablumenal side. Arrows indicate the side onto which the cells were seeded.

The DAPI staining also confirmed the attachment of the hGFs on the ablumenal surface of the HUV scaffold (Fig. 5.13A) with the control plastic surface (Fig. 5.13B).

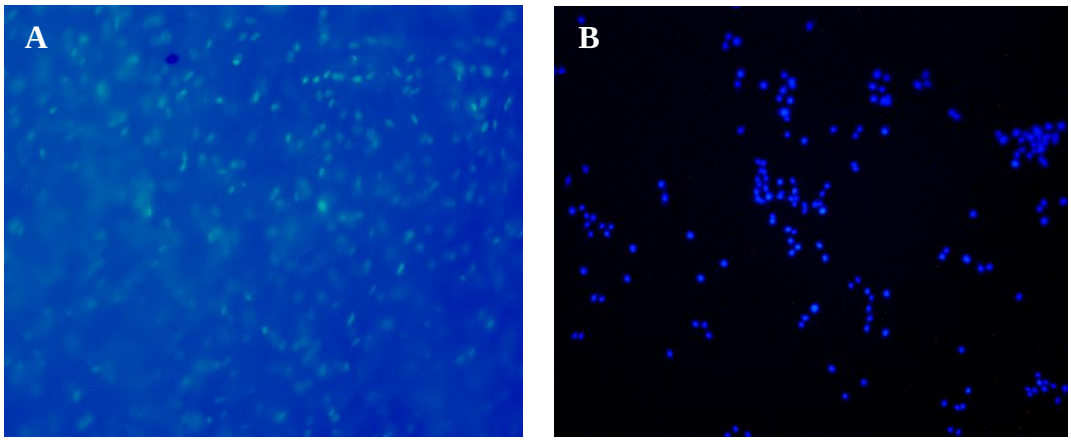

Figure 5.13. Fluorescent microscope images of human gingival fibroblasts (hGFs) seeded on the ablumenal surface of HUV **(A)**, and the plastic control surface **(B)**.

5.4. DISCUSSION

The goal of periodontal tissue engineering is to create a 3D scaffold material that is immunologically compliant, improves cellular integration and remodeling while withstanding physiological loading stresses. While the details of human tissue from the gingival and surrounding tissues are yet to be fully defined, a human derived ECM of similar dimension to the periodontal tissues, such as the HUV, may have these desired properties. It is envisioned that when implanted with its relatively porous ablumenal surface against the wound site, HUV can provide the necessary environmental signals, such as adhesion molecules, and more natural ECM biomechanics, at least compared to rigid synthetic alternatives, for gingival wound healing to occur. The relatively less porous lumenal surface would be implanted facing the oral cavity, with the aim of preventing the penetration of epithelial cells which would inhibit the regenerative healing process. As a potential barrier implant with directional inhibition of cellular migration, the HUV has important implications from a wound healing perspective. Ideally, cells interacting with the ablumenal surface of the HUV (at the wound interface) may have more time to repair damaged tissues before the negative influences of other invading cell types limit repair. Although not assessed in these investigations, the HUV may also mitigate bacterial invasion from the oral cavity through similar mechanisms to eukaryotic cells, and thus limit infection and inflammation at the wound site.

The HUV has potential as a biocompatible material for periodontal tissue regeneration, and as such, it is essential that the material's biomechanical properties and cellular interactions be evaluated prior to *in vivo* testing. However, published data on the

mechanical properties of the HUV is minimal, and requires additional analysis in order to draw appropriate comparisons between the HUV and other surgical barriers. Barriers such as Alloderm and Biomend have been reviewed and their mechanical properties evaluated previously.[328, 329] Hoenicka *et al.*[330] investigated the tensile properties of HUV ringlets with their findings supporting a biphasic and anisotropic behavior. This data was consistent with the findings of Pennati,[222] who reported the anisotropy of HUV while assessing the stress-strain relationship of Wharton's Jelly, longitudinal HUV strips, and circumferential HUV ringlets. An important distinction between this work and previous investigations assessing vessel mechanics has been the use of tissue strips rather than a mixture of ringlets and strips for the circumferential and axial directions. Typically, with smaller vessels, ringlets have been used for analysis of circumferential properties due to limitations in sample size, and strips in the axial direction where sample length is less of an issue. By using strips in both orientations, a more accurate comparative analysis that provides details on fiber structure can be conducted. These investigations have shown the tissues tensile characteristics to have an anisotropic response, with stress-strain behavior differing between longitudinal and circumferential orientations. The greater tensile strength of the longitudinally-oriented samples may be attributed to medial collagen fibers aligned in the axial direction, rendering an orthotropic mechanical behavior. This parallel alignment also increases material stiffness resulting in a higher resistance to tensile loading.[324, 331, 332] The smooth muscle cell alignment within the medial layer was assumed to correlate well with the collagen fiber orientation in this layer.[333] With tissue strips oriented in the circumferential direction, the bulk collagen fibers are aligned perpendicular to the loading axis. As load is applied, the fibers begin to realign parallel to

the stretching axis, and the degree to which this realignment occurs determines the load bearing capacity.[223, 334] When the fiber alignment was perpendicular to the load, these strips demonstrated lower mechanical strength.[335] Similarly, the 0.8 mm-cut tissue sections consisting more of the Wharton's Jelly retained sutures to a higher stress value in the circumferential direction where the fiber orientation was perpendicular to the axial stress.

Tensile properties of the HUV machined to a wall thickness of 0.4 and 0.8 mm demonstrated gradients in stress-strain behavior through the scaffold wall, consistent with a material of heterogeneous composition (Fig. 5.4). The medial layer exhibited higher uniaxial tensile strength and anisotropy and showed a more dense fiber structure predominantly aligned in the axial direction. Conversely, the tissue layer surrounding the media (Wharton's Jelly) was shown to have a lower strength, associated with a randomly organized, less dense fiber structure. Unlike veins, the medial fiber orientation in arteries was reported to be in the circumferential direction.[336]

Stress-relaxation analysis was used to determine the viscoelastic properties of HUV.[334] The initial strain energy is driven by the internal rearrangement of the collagen fiber network, which then gradually diminishes as the stress relaxes.[337] The greater the difference between initial and equilibrium stress values, the lesser the degree of tissue deformation and higher the potential of the tissue to recover toward its initial fiber alignment. Tissue sections with increased decay rates indicate a more viscoelastic material.

Elastin has been reported to have minimal relaxation with a high elasticity, whereas collagen and smooth muscle are relatively stiffer but exhibit greater relaxation.[226] Possible mechanisms responsible for the HUV stress-relaxation properties include, the time-dependent reorientation of the fibrous proteins through the viscous matrix, the relaxation of the non-fibrous ECM components, or the time-dependent interactions between the fibrous and non-fibrous components.[337] The circumferential HUV strips were less viscoelastic, whereas the longitudinal tissue sections showed a more rapid stress-relaxation decay, demonstrating a greater viscoelastic behavior. This result can be attributed to the collagen fibers and smooth muscle layers within the medial layer that are the primary factors influencing the materials viscoelasticity. Material properties of the HUV have demonstrated characteristic features of soft biological connective tissues with a nonlinear stress-strain relationship, a decreasing hysteresis loop in preconditioning (data not shown), and stress relaxation at constant strain.[226] These results show that both the composition and layered architecture of the decellularized HUV plays a significant role in the materials biomechanical and biological properties.

The adhesion, growth, and proliferation of human gingival fibroblasts (hGFs) on the HUV biomatrix were examined to assess characteristics of the lumenal and ablumenal surfaces that may influence cell behavior. Cells adhered on both surfaces of the scaffold, and after a lag phase of 9 days, started proliferating within the scaffold. The penetration of cells into the 3D scaffold was, however, only observed through the ablumenal surface. The extended lag phase is likely a specific response of these human derived primary cells as cultures on tissue culture plastic displayed a similar proliferation profile. The relatively long lag phase, with fewer attached cells than the initial seeding density to modify the

scaffold, may also explain why the total cell density was lower than might have been expected by the end of the 21 day culture period.

The bimodal cell migration characteristics, where cells on the lumenal surface were unable to penetrate the basement membrane maybe attributed to the more densely packed morphology of the extracellular matrix (ECM). In addition, components such as elastin that may inhibit migration by being more resistive to cell secreted matrix remodeling enzymes. By comparison, ECM components on the ablumenal surface are more loosely arranged with large void spaces. These results were supported by assays quantifying cellular metabolic activity and proliferation rates where the more porous structure of the ablumenal surface, composed predominantly of Wharton's Jelly, enhanced the migration of hGFs into the matrix. However, a quantitative analysis of the porosity of the HUV-derived scaffold as well as studies that assess cell migration and ECM remodeling over longer time frames are yet to be done.

5.5. CONCLUSIONS

In these investigations, we have developed a unique scaffold that may have promise as a biofunctional matrix for periodontal and other regenerative surgical procedures. Results have shown the potential of the HUV bioscaffold to serve as a strong, elastic tissue matrix. We have demonstrated the processed HUV-derived ECM graft to have *in vitro* biocompatibility, with desired natural tissue matrix characteristics that acts as a selective barrier while enhancing cell growth, as well as having favorable mechanical characteristics. As such, the HUV bioscaffold offers a promising approach that utilizes the natural structure of the vascular wall to modulate cellular interactions. By allowing

cells to adhere to the lumenal surface (at the oral cavity interface), but limit their apical migration, an extended period for natural wound healing responses will be available to regenerate these underlying tissues. In addition, the material's bimodal cell migration characteristics may be taken advantage of in a number of surgical applications that require cell barriers. Further analysis of these interactions may improve our understanding of the mechanisms that drive cell migration and wound healing responses. In addition, the unique features of a vascular-derived material that functions as a resorbable barrier scaffold may have a number of reconstructive and regenerative applications from cosmetic repair and enhancement to the treatment of ulcers.

CHAPTER 6

BIOREACTOR DESIGN CONSIDERATIONS FOR INVESTIGATING THE CELL BEHAVIOR IN A PERIODONTAL WOUND ENVIRONMENT

6.1. INTRODUCTION

Tissue engineering aims to develop scaffolding materials under the mechanical (shear, tension, compression, etc.), biological and physicochemical (pO_2, pH, pCO_2, glucose, etc.) conditions that are similar to *in vivo* conditions. Bioreactors are therefore important tools for achieving this specific goal. The operating parameters within the bioreactor system should be controllable in order to manufacture tissue constructs that could meet the market demand in terms of performance, uniformity, reproducibility and scalability.[338] Therefore, emerging technologies, such as biosensors, are utilized to control the varying composition of these vital components.[339] Mass transport of the nutrient supply, gases and waste products should also be considered while designing a bioreactor system. The above-mentioned factors are closely interconnected and should be considered together to design a bioreactor system that simulates the physiological conditions during periodontal wound healing.

6.1.1. Mechanical Stresses

Perfusion culture systems are used for the cultivation of engineered constructs due to their superior effects on the scaffolds compared to the static cultures.[340] While perfusing media through the bioreactor system, the nature and magnitude of the mechanical stresses applied have a direct and profound influence on the biomaterial. The tissue constructs under mechanical stimulation demonstrate changes in their biological responses, mechanical properties, and matrix composition.[341-343] Therefore, the role of the mechanical forces within a bioreactor system is very important as it determines the final tissue characteristics by the end of culture period.

The nature of the applied mechanical force on human gingival fibroblasts (hGFs) has a tremendous effect on cellular attachment, proliferation and expression of specific regulatory genes.[344-346] Theilig *et al*. (2001) studied the influence of gravitational force on cultured hGFs and reported an enhanced tenascin expression by the hGFs due to applied stresses.[347] In another study, it has been concluded that the expression levels for the mRNAs encoding for the matrix metalloproteinase-2 (MMP-2) and tissue inhibitor of metalloproteinases-2 (TIMP-2) were higher in human gingival fibroblasts (hGFs) subjected to continuous stretching.[348]

However, a few studies have been reported in literature regarding the culture of hGFs in dynamic flow conditions.[349, 350] One of the leading reasons behind this is that the current literature is deplete of studies regarding the quantification of the mechanical stresses acting in the oral environment. Jozef Kokini and co-workers estimated the shear stress on the tip of the tonque using the transport phenomena principles for the fluids in the mouth.[351-353] Shama and Sherman (1973), estimated the range of shear rates acting in the mouth as 10-1000 s^{-1} depending on the type of fluid/food.[202]

6.1.2. Gas Concentrations

Variation in oxygen concentration has a significant influence on the development of tissue-engineered constructs.[354] The *hyperoxic conditions* (high O_2 tension) are known to stimulate the synthesis of tissue inhibitors against collagenase activity, induce the production of collagen, and thus increase the wound tensile strength, and cause an increase in glucose consumption rate by the wound cells.[355, 356] On the other hand, hypoxia, i.e., low O_2 tension, regulates the synthesis of specific genes by different cell types.[357-359] The hypoxic conditions have been previously reported to have a stimulatory effect on various types of cells to synthesize vascular endothelial growth factor (VEGF), an important modulator for vascularization during wound healing.[360] Hypoxia is also known to have an inhibitory action on angiogenesis.[361]

While operation of the bioreactor systems for the cultivation of the tissue constructs, the rate of oxygen consumption of the cells within the scaffolds should periodically be monitored, as oxygen is usually the limiting factor in a bioreactor system due to its low solubility in culture media.[362]

In a periodontal wound healing environment, the defect site experiences low oxygen tensions due to the poor vasculature carrying 0_2 to the wound tissue, and the supply of oxygen towards this region promotes soft tissue wound healing processes.[354, 363] Therefore, in designing such systems mimicking the periodontal wound healing environment, one should consider keeping the oxygen concentration on the healing side relatively low (hypoxic).

The carbon dioxide (CO_2) concentration has been reported to vary during the periodontal wound healing processes, and this change in the CO_2 tension also creates changes in the pH values.[364, 365] The pH of the circulating media within the bioreactor system needs to be kept around ~7-7.4, as the acidic culture conditions prevent the synthesis of newly-formed ECM structures.[366] Continuous replacement of the culture media with the perfusion flow helps maintaining the pH at its desired level, as due to the cellular metabolism, pH decreases.

6.1.3. Fluid Composition

The literature is scarce with regard to the fluid compositions in a periodontal wound healing environment. Similar to the gas concentrations, the periodontal wound fluid composition is also prone to change continuously through the healing cascade. Especially during the early stages of wound healing, blood clot formation occurs on the wound site. The blot clot mainly consists of cellular components, particularly red and white blood cells and platelets, in a matrix of fibrin, vitronectin, plasma fibronectin, and so forth.[367] Wilkes *et al*. (2007) previously constructed the blood clot in their bioreactor system using a fibrin matrix.[368]

6.2. MATERIALS AND METHODS

6.2.1. Scaffold Preparation

Human umbilical cords collected from the Delivery Suite of the Norman Regional Hospital were washed thoroughly with tap water to remove residual blood and cut at an initial length of 160 mm. The twisted cords were excluded from the study. Vessels were dissected according to an automated dissection protocol to 0.5 mm initial wall-thickness. The 0.5 mm initial wall thickness was the smallest attainable thickness which demonstrated the least variation in tissue thickness after thawing process. Relatively small tissue thickness was also preferred to minimize the variation in diffusion resistance values for the O_2, nutrient and waste through the HUV scaffold during culture. The thinner scaffold also gives a lower rate of O_2 consumption rate per unit volume of tissue construct depending on the density of the hGFs repopulating the scaffold. Please refer to Section 5.2.1 for the details of the scaffold preparation process.

6.2.2. Decellularization of the HUV Scaffold

After refrigeration in chilled distilled water, HUV's were cut longitudinally to generate flat sheets (~18 × 160 mm) and decellularized according to our optimized protocol (Please refer to Section 5.2.2) with the exception of DNAse I treatment for 4 h.

6.2.3. Culture of Human Gingival Fibroblasts (hGFs)

Primary human gingival fibroblasts (hGFs) were obtained from a patient and cultured as explained in Section 5.2.4. When the cells grown on 75 cm^2 culture flasks reached to

approximately 70% confluency, they were recovered by acutase and subcultured. The gingival fibroblast cells used in this study were between their 4^{th} and 10^{th}.

6.2.4. Bioreactor Design Considerations

The bioreactor system was designed while considering the physiological conditions during periodontal wound healing. In surgical practice, the HUV graft is implanted between the overlying gingival flap and the wound space. The graft is in contact with three different zones (regions) on the wound site, namely, the tooth surface (Region 1), wound space including the blood clot (Region 2), and the alveolar bone interface (Region 3) (Fig. 6.1). The HUV graft is simply sandwiched between these three different regions and the gingival flap interacting with the oral cavity. Therefore, we designed and fabricated a modified parallel-plate flow bioreactor, where the HUV graft is placed between two flow compartments simulating the conditions in the oral cavity and wound site.

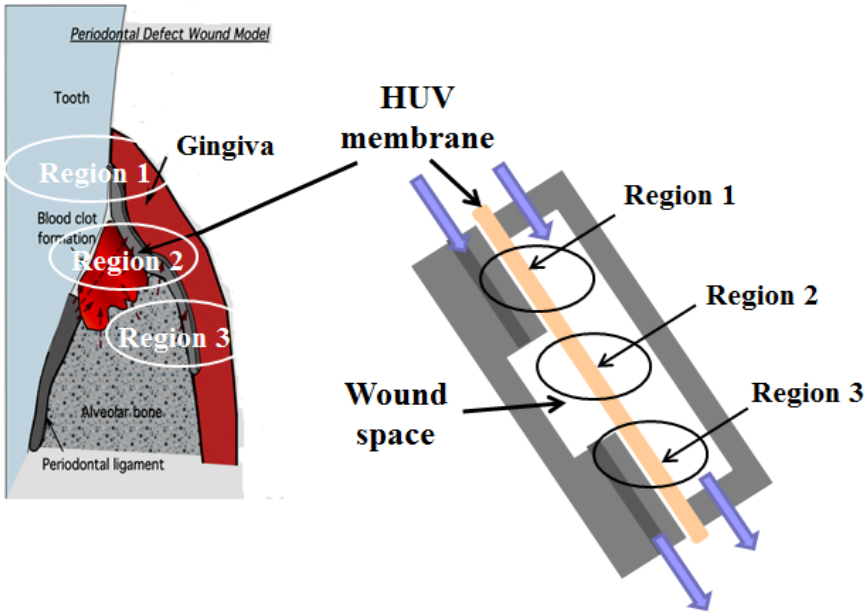

Figure 6.1. Bioreactor design mimicking the periodontal wound healing environment. Region 1 (Entrance): Tooth interface, Region 2 (Central): Blood clot zone, Region 3 (Exit): Alveolar bone interface.

Each bioreactor assembly was made of acrylic plastic. The two flow compartments of the bioreactor were attached together with stainless-steel screws and silicone closed cell foam gasket (1.57 mm thick, Rogers Corp., Carol Stream, IL) was placed between the two parts. The assembly was connected to the perfusion flow with three-way stopcocks (Baxter Healthcare Corp., Deerfield, IL) (Fig. 6.2).

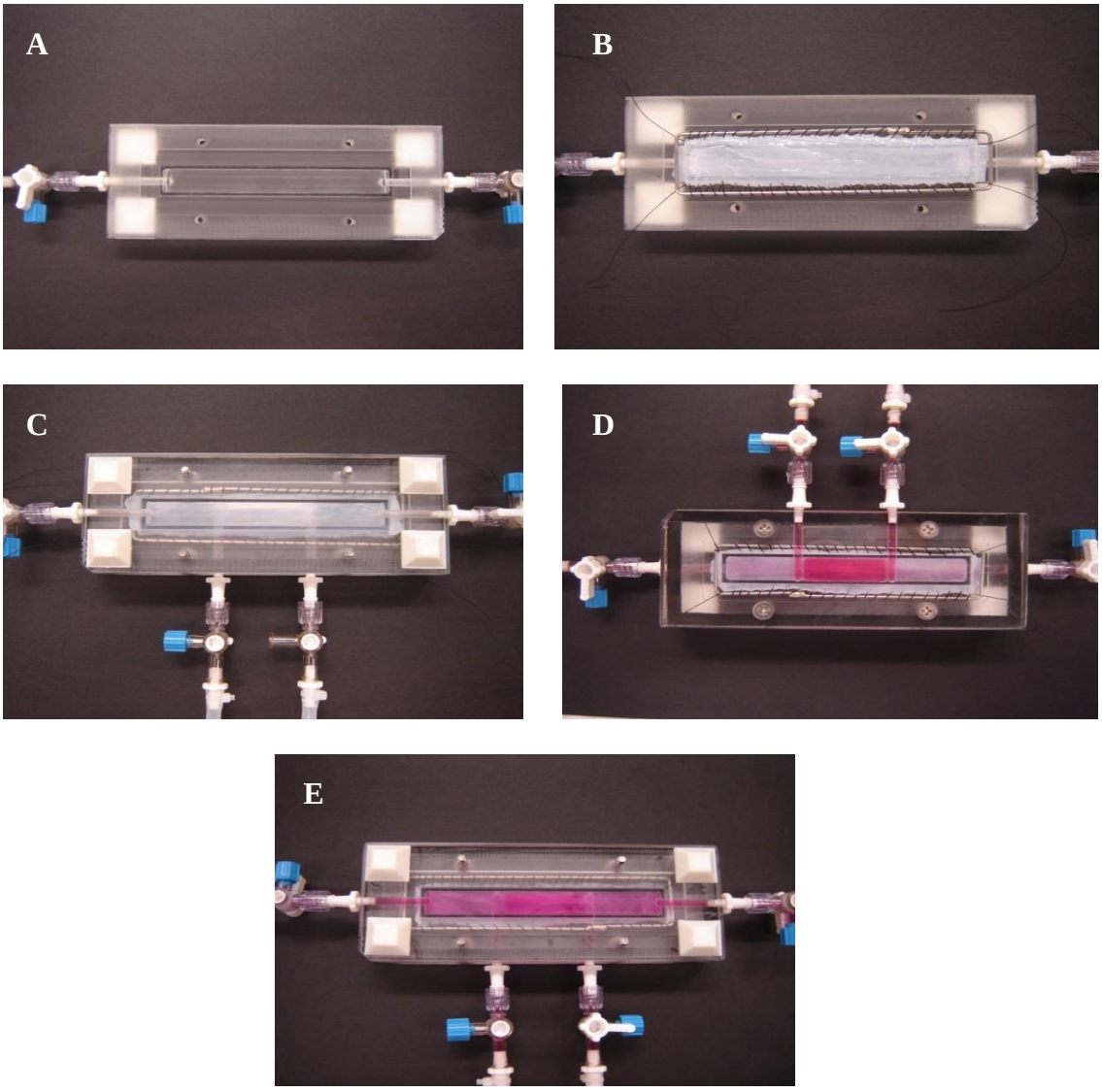

Figure 6.2. The top view for the top chamber of the bioreactor assembly **(A)**, with the HUV membrane inserted in its place **(B)**. The two flow compartments were attached with stainless steel screws **(C)**, and the flow is maintained on both sides of the bioreactor; view for the bottom chamber **(D)** and the top chamber **(E)**.

The pulsatile flow bioreactor system consisted of bioreactor assemblies, 2 peristaltic pumps (Masterflex L/S digital standard drive (model 7523-70) with L/S 4-channel pump head (model 7519-06, Cole-Parmer Ins. Co., Vernon Hills, IL), glass culture medium

reservoirs (diameter = 4.5 cm, height = 12 cm, 125 mL capacity each), silicon tubing, air filters (for the oxygenation of the medium reservoirs), polypropylene-based PharMed tubing (Cole-Parmer) and luer connectors (Value Plastics, Inc., Fort Collins, CO) (Figs. 6.3 and 6.4). Zip ties were used to tighten the connections between the tubing and the luer connector. The whole bioreactor system was situated in an incubator at 37°C and 5% carbon dioxide (CO_2).

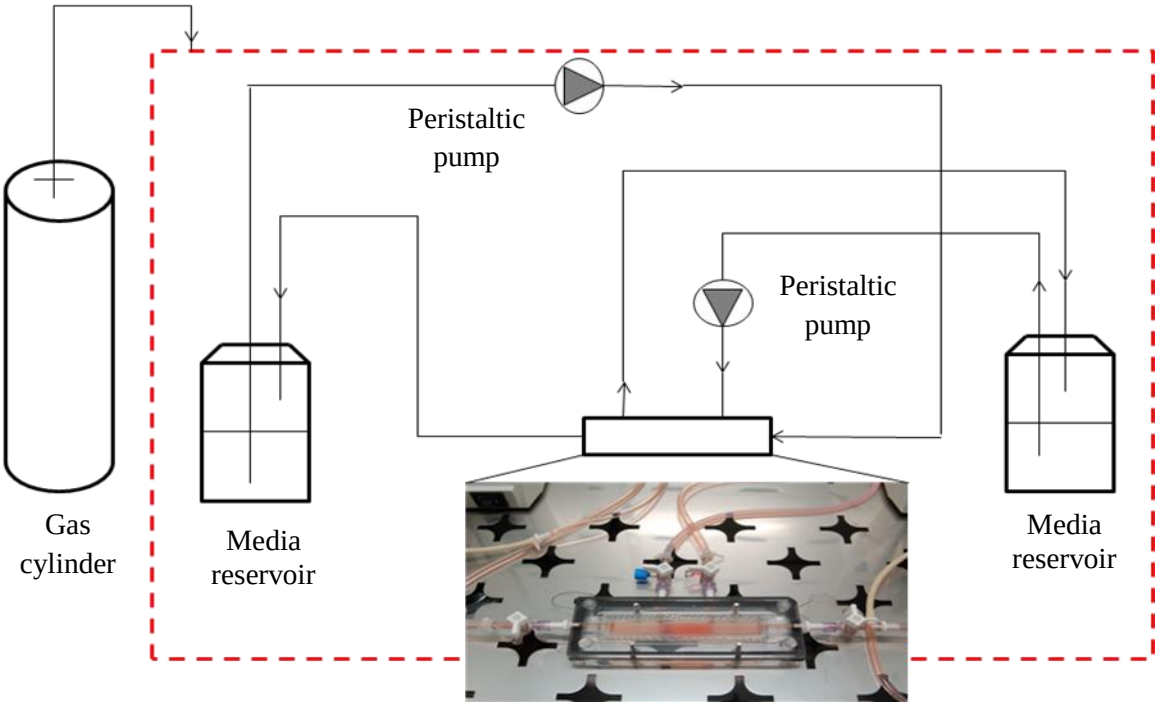

Figure 6.3. Schematic representation for the perfusion bioreactor system. Two peristaltic pumps circulate fluid through both sides of the bioreactors.

The bioreactor system is presented in Fig. 6.4, where the three bioreactors maintain dynamic continuous flow conditions whereas the fourth bioreactor (top) serves as the quasi-static culture bioreactor. For the quasi-static conditions (i.e., low flow), the bioreactor was subjected to the same dynamic flow conditions for 3 hours every day, and the flow was stopped for this bioreactor. The three-way stopcock valves were used to control the flow to the bioreactors.

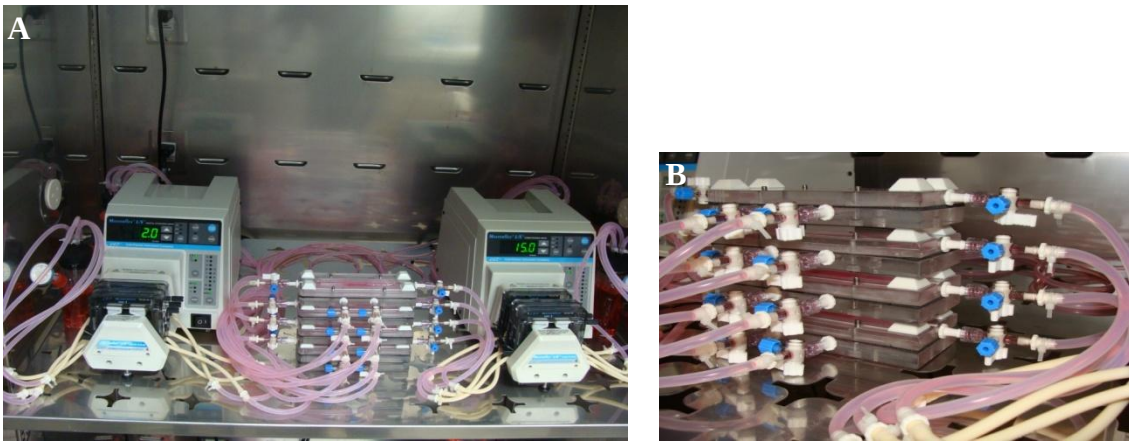

Figure 6.4. (A) The perfusion bioreactor system used for the cultivation of the HUV bioscaffolds. The whole bioreactor system consists of four bioreactors connected in parallel arrangement. The top bioreactor maintains the quasi-static culture of the grafts. The media was changed every three days for all bioreactors. **(B)** Close-up view of the modified parallel plate flow bioreactors.

6.2.4.1. *Flow Conditions*

Literature is still scarce regarding the quantification of the mechanical forces acting on the periodontal soft tissues and the wound site. In the case of flow, the effective forces acting in the oral cavity are shear and extensional forces.[369] However, prediction of the

mechanical forces that could act on the HUV-derived membrane for periodontal GTR applications is difficult. In a surgical application, ideally, the HUV membrane will be completely covered with the gingival flap and the direct exposure of the graft to the oral environment conditions will be eliminated (See Fig. 6.1).

The flow rate of saliva in the oral cavity is subjected to continuous change due to the type of stimulation.[370] The unpredictability of the saliva flow rates in the oral environment, and the indirect contact of the HUV membrane with the oral environment due to its complete insertion beneath the flap, presented a challenge to predict the mechanical stresses that could be exerted on the implanted HUV scaffold from the oral cavity. To emulate the nearly stagnant fluid conditions within the wound space, fluid flow within the bioreactor section mimicking the wound space was kept very low as ~ 0.9 mL/min = 0.015 mL/sec, which is the corresponding speed of the pumps lowest attainable pulsating rate of 2 rpm (pulsating frequency of 0.13 Hz).

Different pump settings were selected for the two sides of the bioreactor to adjust the flow rate. The tubing size was kept the same for the two chamber flow as 3.175 mm inside diameter (VWR, Suwanee, GA). The total medium volume circulating through the bioreactor system is 268.37 mL and 270.35 mL for the top and bottom chambers, respectively.

A photograph and a schematic drawing for the bioreactor assembly are shown in Fig. 6.5. The height of the flowing fluid in the top chamber was denoted as h, the length of the flow with L, the width as b. The human umbilical vein (HUV)-derived scaffold is placed in between the two flow compartments.

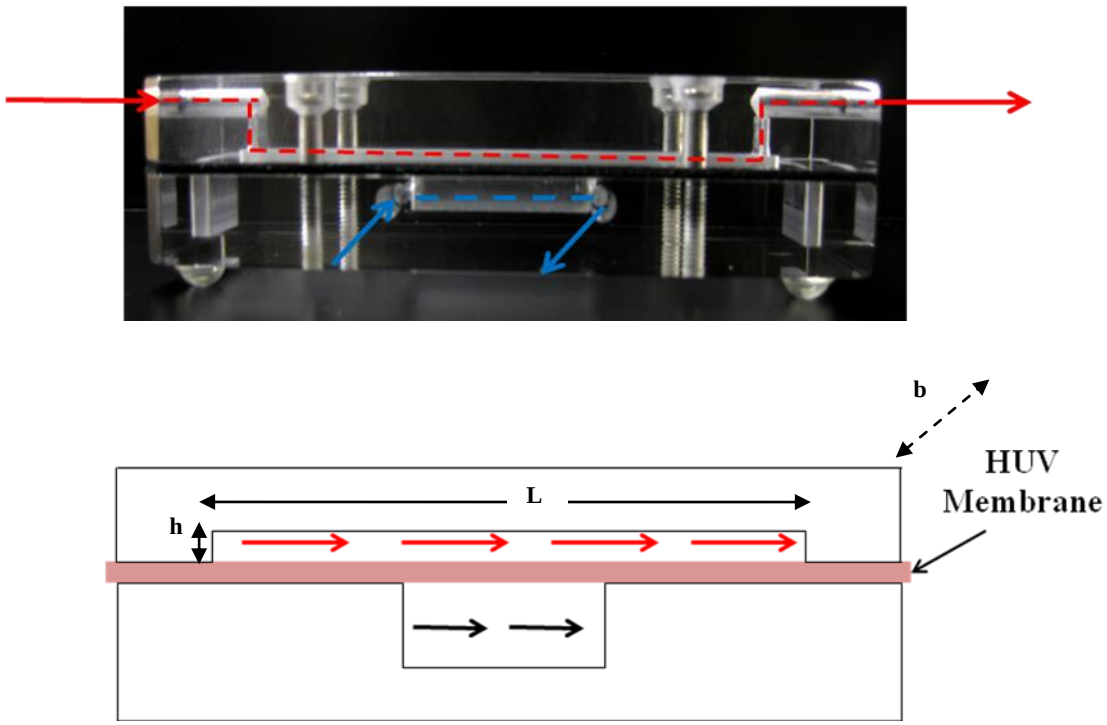

Figure 6.5. Photograph and schematic drawing of the bioreactor assembly used in the study. The bioreactor consisted of two flow compartments mimicking the periodontal wound environment. The top chamber has a fluid flow length of 105 mm, whereas the bottom chamber has the length of 35 mm. The fluid height for the top and bottom sides of the bioreactor are 1 and 6 mm, respectively. The arrows within the two compartments represent the direction of flow.

The wall shear stress, τ_w (dyne/cm^2) in the top chamber (Fig. 6.5) was calculated according to Eqn (3):

$$\tau_w = \frac{6\mu Q}{bh^2} \quad (3)$$

where μ represents the dynamic viscosity of the culture media in dyne-s/cm^2, Q is the fluid flow rate expressed in mL/s, b is the width of the flow chamber in cm, and h is the

height of the fluid flowing in the top chamber, in cm. The dynamic viscosity of the culture media was 1.4×10^{-2} dyne-s/cm^2.[371] The width, b, and the height, h, of the top chamber were 12 and 1 mm, respectively. The width-to-height ratio (b/h) for the top chamber of the bioreactor assembly was 12, which was greater than 1 demonstrating that the flow at the top side of the bioreactor remained parabolic and two-dimensional, i.e., fully-developed.[372, 373]

The flow regime on the top chamber was examined by calculating the Reynolds Number (Re) by using Eqn (4) having the wall shear stress (τ_w); density of the culture media, ρ, of 1 g/cm^3 [374]; height of the fluid gap, h, of 1 mm; dynamic viscosity of the culture media, μ, of 1.4×10^{-2} dyne-s/cm^2 [371]:

$$Re = \frac{\tau_w \rho h^2}{6 \mu^2} \quad (4)$$

In the case of fully-developed flow, the entry length for the top chamber was calculated using Eqn (5):

$$L_e \approx 0.05 (h) (Re) \quad (5)$$

Table 6.1 tabulates the wall shear stress, Reynolds Number (Re) and entry length (L_e) values for different fluid flow rates within the top chamber.

TABLE 6.1. WALL SHEAR STRESS (τ_w), REYNOLDS NUMBER (RE) AND ENTRY LENGTH (L_e) VALUES FOR DIFFERENT PUMP SETTINGS OF THE TOP FLOW CHAMBER

Pump rate (rpm)	Flow rate, Q (mL/s)	Wall shear stress, τ_w (dyne/cm^2)	Reynolds Number, Re	Entry Length, L_e (mm)
5	0.03	0.21	1.786	0.089
7.5	0.047	0.329	2.798	0.139
10	0.062	0.434	3.690	0.184
12.5	0.075	0.525	4.464	0.223
15	0.088	0.616	5.238	0.262
17.5	0.103	0.721	6.131	0.306
20	0.12	0.84	7.143	0.357

* average of triplicate measurements (n = 3).

The calculated Reynolds numbers for different flow rates within the top chamber of the bioreactor were very low indicative of laminar flow. Due to the pulsating nature of the pumps, the flow was unsteady.[372] The fluid flow rate for the top chamber was chosen as 0.088 mL/s, driven by the four-roller pump at a rate of 15 rpm and a pulse repetition frequency of 1 Hz which was consistent with the chewing frequency of human.[375, 376] The entry length for this flow rate was 0.262 mm, or 0.25% of the total length. The tissue within the entry length was excluded from the analyses.

6.2.4.2. Permeability of HUV Membrane

The permeability of the oral mucosal tissues has been investigated in literature due to their potential use in drug absorption studies.[377, 378] *In vitro* methods revealed that the keratinized oral tissue demonstrated less permeability compared to the non-keratinized tissues.[379]

In our modified parallel plate flow bioreactor system, the culture medium flows along and across the HUV membrane, thus creating both shear stresses and transmural pressure.[380] Transmural pressure has been reported to tangentially strain the vessel walls and alter the tissue permeability, therefore different transmural pressures were tested on the HUV membrane.[381] The fluid pressures on both sides of the bioreactor were measured using the Edwards TruWave Disposable Pressure Transducers (Edwards Lifesciences, Irvine, CA) connected to the four-channel biopotential amplifier of a sonomicrometry system (Sonometrics Corporation, Ontario, Canada) (Fig. 6.6). The instrument was calibrated before recording any pressure readings using the transducers. The system consisted of the Sonometrics' Data Acquisition Computer and Sonometrics 4 Channel BioPotential Amplifier. SonoSoft v.3.4.45 software was used for the data acquisition and to analysis.

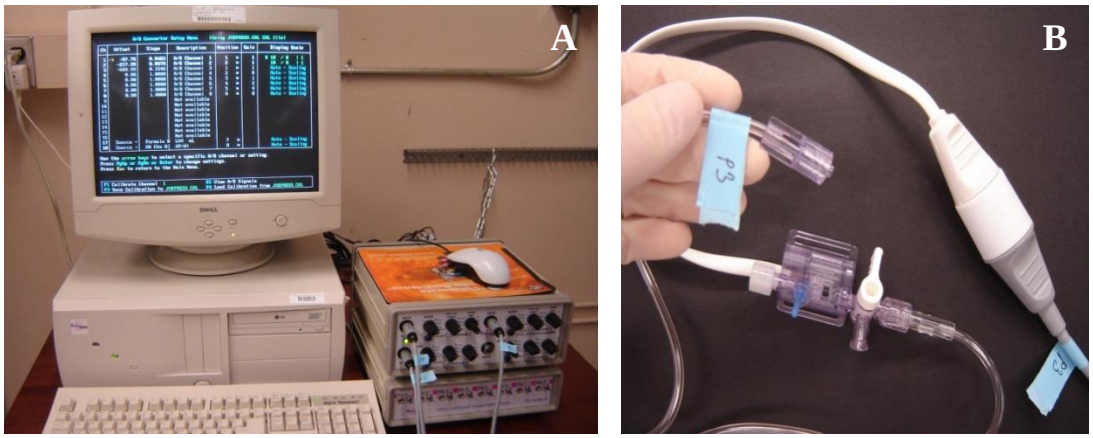

Figure 6.6. Sonomicrometry system **(A)**. Pressure transducers **(B)** were connected to the flow through the luer connectors of the bioreactor assembly to monitor the pressure within the top and bottom chambers.

The pressure readings for the inlets and outlets of the top and bottom chambers were recorded after 25-30 min when the steady-state was reached for each pump pulsating rate, and the average transmural pressure (mmHg) across the membrane within the bioreactor was calculated using Eqn (6):

$$\text{Average Transmural Pressure} = \frac{(P_{\text{Top, inlet}} - P_{\text{Bottom, inlet}}) + (P_{\text{Top, outlet}} - P_{\text{Bottom, outlet}})}{2} \quad (6)$$

The transmural flow rate (Q_f) for the tested top flow chamber flow rates were calculated by simply measuring the decrease in fluid amount (mL) in the media reservoirs feeding the top chamber with time. The average transmural pressure (TMP_a) values and the corresponding Q_f values for different pump speeds were listed in Table 6.2.

TABLE 6.2. AVERAGE TRANSMURAL PRESSURE (TMP_a) AND TRANSMURAL FLOW RATE (Q_f) VALUES FOR DIFFERENT PUMP SPEEDS OF THE TOP FLOW CHAMBER*

Pump pulsating rate (rpm)	Average Transmural Pressure, TMP_a (mmHg)	Transmural flow rate, Q_f (mL/min)
5	5.038 ± 0.126	0.032 ± 0.013
7.5	6.103 ± 0.388	0.055 ± 0.009
10	7.934 ± 0.403	0.066 ± 0.011
12.5	8.713 ± 0.665	0.088 ± 0.006
15	9.845 ± 0.419	0.111 ± 0.012
17.5	11.327 ± 0.481	0.122 ± 0.011
20	12.396 ± 0.206	0.153 ± 0.009

* values expressed as mean ± standard deviation of triplicate measurements (n = 3).

In order to calculate the permeability of the HUV membrane, the Q_f values were plotted against the TPM_a values. Fig 6.7 depicts the interaction between the transmural flow rates and the transmural pressures across the HUV membrane.

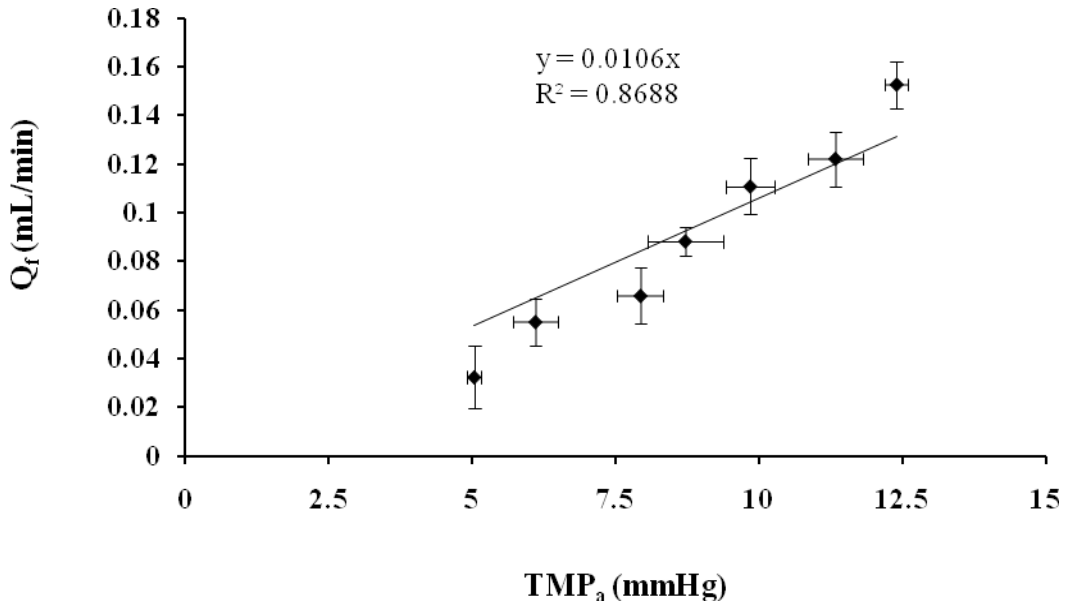

Figure 6.7. Transmural flow rate (Q_f) as a function of average transmural pressure (TMP_a) across the HUV membrane.

The flow across the membrane could be calculated by Darcy's Law presented with Eqn (7) [380]:

$$Q = L_p\,(bL)\,TMP \tag{7}$$

where L_p is the hydraulic permeability of the porous lower ablumenal side of the HUV membrane; b is the width of the flow channel, 12 mm; L is the length of the flow channel, 35 mm. The L_p was calculated from the simultaneous measurements of the Q and TMP (Fig. 6.7) as 1.514×10^3 mL/(mmHg.h.m^2).

6.2.4.3. *Fluid Composition*

During wound healing, the wound space of the periodontal defect contains the blood clot and the growth factors accumulated in that region. The blood clot residing within the wound site will provide the necessary proteins to initiate and accelerate the healing processes. Therefore, the bottom chamber mimicking the protein concentrated wound site was circulated with culture media having relatively high serum (FBS) content (10%), whereas the top chamber mimicking the oral environment was perfused with media containing 1% FBS (serum). Izumi *et al*.[382] studied the behavior of keratinocytes within oral mucosal substitutes with media having variable serum content and, interestingly, showed the cellular growth was not affected by the absence of serum in the media. In situations where the gingival flap is not sufficient to completely cover the GTR membrane placed underneath, the membrane could be in contact with saliva in the oral environment. The saliva protein concentration is known to be very low as 0.5 g/dL,[383] however, the protein concentration in saliva has been reported to increase for the periodontitis subjects.[384]

Glucose concentrations on both sides of the bioreactor were also kept different. Culture media without glucose was circulated on the side of the bioreactor mimicking the wound site, whereas the side of the bioreactor mimicking the oral cavity side was fed with media having low glucose concentration (1 g/L). As a result, a gradient in glucose concentration (driving stimulus) was created to further facilitate the migration of the hGFs seeded on the ablumenal side (facing the wound site) toward the lumenal surface.

6.2.5. Seeding of Tissue Constructs and Culture of Human Gingival Fibroblasts (hGFs)

Decellularized HUV flat tissue sheets were fixed with sterile 3-0 silk black braided suture (Ethicon, Inc., Somerville, NJ) around a stainless-steel frame and cultured in sterile 150-mm diameter petri dishes (VWR International, Sugar Land, TX). The scaffolds were incubated with the ablumenal surface facing up in culture media containing 15% FBS overnight to facilitate the initial attachment of the human gingival fibroblasts (hGFs) onto the scaffold. The potential of HUV as a GTR membrane has been reported in our previous study, where the results revealed that the hGF penetration was only observed through the ablumenal surface of the HUV membrane.[29] This finding was probably due to the presence of Wharton's Jelly on the ablumenal surface of the scaffold which has a relatively more porous, less-densely arranged fibrous structure and consists of the essential molecules, i.e., growth factors, signaling factors, etc. facilitating the attachment, growth, and proliferation of the hGFs.[294] Therefore, in this study, the repopulation of the HUV graft by the human gingival fibroblasts (hGFs), and the subsequent healing via tissue ingrowth was expected to occur predominantly within the tissue region closer to the ablumenal surface of the HUV graft.[385] A lamina propria-like tissue layer formation is high likely to be created on this side of the scaffold for prolonged culture times.[386, 387]

Fibroblasts were then seeded on the ablumenal surface of HUV matrices at a seeding density of 1×10^6 cells/cm², a relatively high seeding density to ensure there are enough matrix-secreting cells in the scaffolds. First, 7 mL of the cell suspension was dripped on each membrane and after 4 h of incubation, 30 mL medium was added to each petri dish.

The seeded scaffolds were incubated statically under a humidified atmosphere of 5% CO_2 and 95% air (Model Hera Cell 150, Thermo Scientific Heraeus, Waltham, MA) at 37°C. The media was changed 24 h after seeding to remove the debris, and then static culture was performed for 7 days to ensure adequate cell attachment prior to dynamic culture. The media was replenished every 3 days. By the end of the 7 day static culture period (t = 0), the scaffolds in petri-dishes were transferred to the bioreactor assemblies situated in another incubator (Shel Lab Incubator Systems, Sheldon Manufacturing, Inc., Cornelius, OR). The HUV scaffolds were cultured under dynamic (flow) conditions within the perfusion bioreactor system for 7 days (t = 7) and 28 days (t = 28). No glucose media and low glucose media were circulated through the bottom (wound site) and top chambers (oral environment), respectively. Static cultures, including the control (acellular) and seeded scaffolds, were performed with the standard culture medium, and the media was replenished every 3 days (40 mL culture media per petri-dish).

The bioreactor system components were sterilized with ethylene oxide while the medium reservoirs were autoclaved. Prior to ethylene oxide sterilization, silicone and PharMed tubing were cleaned in a solution of hot water and mild surgical soap, and then rinsed thoroughly in running distilled water. The tubing was sterilized after the interior surface becomes dry. The Petri dishes were wrapped with micropore tape (3M Company, St. Paul, MN). Contact surface areas between the flow and the HUV scaffold were 105 × 12 mm and 35 × 12 mm for the top and bottom chambers, respectively.

6.2.6. Metabolic Activity of Cultured hGFs

Metabolic activity of hGFs cultured on the HUV scaffold was assessed by the end of each culture period (t = 0, t = 7 days, and t = 28 days) using the Alamar Blue assay. At each time point, 5-mm diameter tissue disks (n = 3) were cut from the three different zones of the HUV scaffold and placed in white/clear bottom 24-well plates (BD Biosciences, Franklin Lakes, NJ) after washing with PBS (1 mL) to remove the loosely-attached cells from the scaffold surface. 1 mL of culture medium supplemented with 10% (v/v) Alamar Blue reactant (Biosource International, Camarillo, CA) was added to each well with the tissue disks. The serum content of the culture medium for the assay was kept constant for all samples as 10% v/v due to the interaction of Alamar Blue reagent with serum concentration.[315] 1 mL AB/DMEM mixture was placed into each of three empty wells as a negative control. Triplicate absorbance readings for each disc (n = 3) were averaged and the cellular metabolic activity (expressed as percentage Alamar Blue reduction) was calculated. Please refer to Section 5.2.6 for the details of the assay.

6.2.7. Quantification of double stranded (ds)-DNA

Briefly, HUV tissue disks (5 mm diameter) were extracted from the cultured scaffolds and washed with 1 mL PBS three times. Three constructs per dynamic (flow) culture duration and one construct per quasi-static (low flow) culture duration were tested for cellularity from the bioreactor study, with duplicate tissue disks tested from each region (Regions 1, 2 and 3). The disks were placed in cryovials, weighed wet and kept in liquid nitrogen over night. The samples were then lyophilized using an FD 2.5 freeze dryer (Heto-Holten, Gydevang, Denmark). Freeze-dried samples were stored at -20°C or

immediately prepared for DNA extraction. Tissue disks were then digested in papain buffer (papain 125 µg/ml [EMD Biosciences, Inc., La Jolla, CA], 5 mM cysteine-HCl [Thermo Scientific, Rockford, IL], and 5 mM di-sodium EDTA [Fair Lawn, NJ] in sterile PBS) (10-200 mg tissue/mL) at 60°C overnight.[285, 388] The papain sample solution was diluted to 0-25 mg/mL with TE buffer (10 mM Tris-HCl and 1 mM EDTA) (EMD, Gibbstown, NJ) in 50 mL NALGENE® Oak Ridge centrifuge tubes (Thermo Fisher Scientific, Rochester, NY) and centrifuged at 21,000 g (Sorvall RC-5C centrifuge, Kendro Laboratory Products, Asheville, NC) for 5 min at room temperature.[389] The supernatant was transferred to a new tube and samples were assayed for the quantification of hGFs (Please refer to Section 5.2.5). The standard dilutions were also prepared in papain digestion solution for accurate DNA quantitation. Three replicate fluorescence readings were taken from each sample and averaged.

6.2.8. Gene Expression Profiling Using Quantitative Real-time Polymerase Chain Reaction (RT-PCR)

To quantify the expression of specific genes in cultured hGFs, the RNA extracted from HUV scaffolds was first reverse transcribed to cDNA with reverse transcriptase and then the quantitative Real-time Polymerase Chain Reaction (qRT-PCR) was used to amplify the DNA.

6.2.8.1. *RNA Extraction*

Tissue samples were cut into 5 mm-diameter tissue disks using a stainless-steel puncher (each tissue disk weighs ~20 mg). Then, each tissue disk was put into RNase-free

microfuge tubes and incubated in RNAlater (Ambion, Austin, TX) to preserve Ribonucleic acid (RNA) at 4°C overnight. The tissue-to-RNAlater solution ratio was kept as 1:10 (v/v) to ensure that the solution thoroughly penetrates the tissue. The supernatant was then removed, and the samples were retrieved from RNAlater solution with sterile forceps, and the excess RNAlater solution was blotted away with an adsorbent paper towel. Then, the tissue disks were kept at -80°C until the analysis.

Prior to analysis, the eppendorf tubes having the tissue samples were placed in liquid nitrogen for at least 24 hr. Just before the analysis, the eppendorf tubes with the tissues were transferred to a Styrofoam container filled with liquid N_2. On the other hand, the tissue pulverizer was first washed well with detergent, cleaned with ethanol, then RNAse decontamination solution and DNAse-free solutions. The pulverizer was then placed in a shallow container and pre-chilled with liquid nitrogen. The frozen tissues were then taken out of the eppendorf tubes and placed in the well of the pulverizer (Fig. 6.8). The pulverizer was then removed from the shallow container filled with liquid N_2, placed on the lab bench and hammered on top to powder the tissue samples. The powdered-tissue was recovered quickly and put in eppendorf tubes and filled with 600 µl lysis/binding solution to homogenize the tissue promptly (lysis/binding solution was 10-12 volumes of tissue mass).

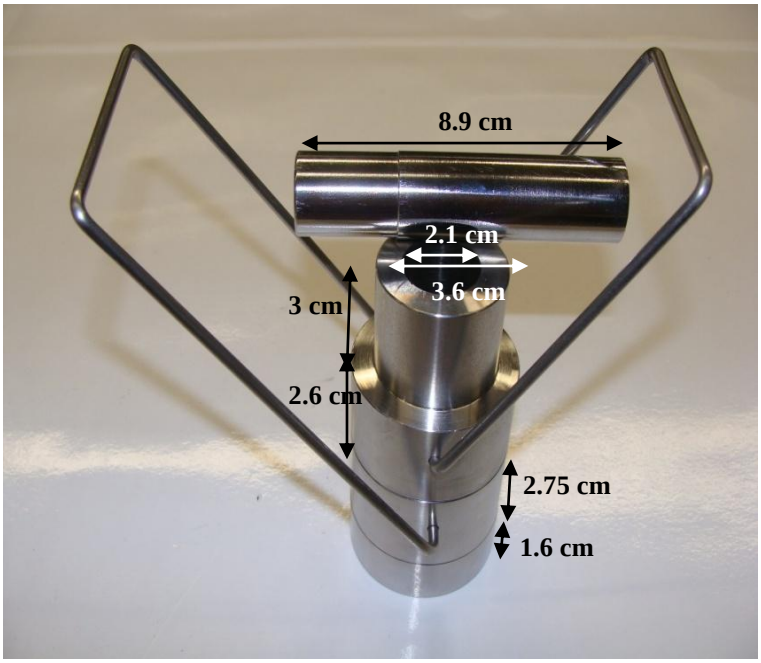

Figure 6.8. Tissue pulverizer (crusher) used to digest the frozen tissue for RNA extraction.

Total RNAs were extracted from the scaffolds using the RNAqueous® -4PCR Kit (Ambion Inc., Austin, TX) according to the manufacturer's protocol. This RNA extraction method on tissue samples is mainly based on lysing the cell membrane and rapidly inactivating the cellular ribonucleases.[390, 391]

Briefly, 64% ethanol solution and wash solution #2/3 were prepared. At the same time, elution solutions (220 μL) in RNase-free PCR 8-strip tubes (Eppendorf, Hamburg, Germany) were heated in a water bath set to 70-80°C. An equal volume of 64% ethanol (600 μL) was added to the lysate-tissue mixture and mixed gently but thoroughly by inverting the tube several times. Then, the lysate/ethanol mixture was drawn through a filter cartridge (Ambion) inserted in a collection tube (Ambion) and centrifuged at 10,000

rpm for 1 min (National Labnet Co., Woodbridge, NJ). The solution is discarded and 700 μL of Wash Solution #1 was applied to the filter cartridges and centrifuged at 10,000 rpm for 1 min. Then, 1 mL of Wash Solution #2/3 added onto the cartridges and centrifuged for 1 min at 10,000 rpm. After that, a final centrifuge without putting any solution (10,000 rpm for 1 min) was performed to make sure all the wash solution is discarded from the cartridges. Then, elution solutions were taken out of the water bath and sequential aliquots of Elution Solution were pipetted to the center of the cartridges and centrifuged at 10,000 rpm. At the end, a total of 100 μL RNA solution was collected in the collection tubes.

In order to effectively remove trace DNA contamination, first 0.1 volume of 10X DNase 1 Buffer (10 μL) and then 1 μL of DNase I was added to each tube containing RNA solution. The tubes were shaken well with finger tips, and incubated for 25 min at 37°C. Then, 0.1 volume DNase Inactivation Reagent (10 μL) was added to the sample to remove the DNase I from RNA and the divalent cations introduced by the DNase I Buffer. The tube was flicked gently to disperse the DNase Inactivation Reagent in the reaction and incubated for 2 min at room temperature. The sample was then centrifuged for 1 min at 10,000 rpm. The liquid phase containing the RNA was recovered, and used for cDNA synthesis and RT-PCR. The extracted RNA was stored at -80°C until the analysis (the freeze-thaw cycle was applied only once for the RNA extracts). During the whole RNA extraction process, RNase-free pipette tips were used to handle the kit reagents and samples.

The concentration of the RNA solution was determined using a traditional spectrophotometer after a dilution in TE (10 mM Tris-HCl pH 8, 1 mM EDTA) (1:50 to 1:100 dilution). The RNA concentration in μg/ mL was calculated according to Eqn (8) while assuming an A_{260} of 1 was equivalent to 40 μg RNA/ mL:

$$A_{260} \times \text{dilution factor} \times 40 = \mu g\ RNA/mL \quad (8)$$

The RNA purity of the RNA solution was calculated by just taking the ratio of the absorbance values, A_{260} to A_{280} (the ratio should fall in the range of 1.8 to 2.1).

6.2.8.2. *Reverse Transcription (RT)*

The mRNA extracted from the tissue samples was reverse transcribed to complementary DNA (cDNA) using TaqMan Reverse Transcription Reagents (Applied Biosystems, Austin, TX). A 100-μL RT reaction efficiently converts a maximum of 2 μg total RNA to cDNA, so it is important that the starting RNA solution is diluted (if necessary) with RNase free water to adjust the final RNA concentration to a maximum of 2 μg total RNA in 100 μL RT reaction mixture (0.02 g/L).

Briefly, for a total of 100 μL RT reaction mixture, the nonenzymatic components (10 μL of 10X RT Buffer, 22 μL $MgCl_2$ (25 mM), 20 μL deoxyNTPs Mixture (2.5 mM), 2.5 μL Oligo $d(T)_{16}$ (50 μM) and 2.5 μL Random Hexamers (50 μM) were combined in an RNA-free microcentrifuge tube and vortexed briefly. Then, the enzymatic components- 2 μL RNase Inhibitor (20 U/L), 2.5 μL MultiScribe Reverse Transcriptase (50 U/μL) and

the RNA solution (38.5 μL) were added and the RT reaction mixture was mixed by inverting the tube gently a couple of times. By using a thermal cycler (Mastercycler ep *realplex*, Eppendorf, Westbury, NY), reaction mixture was incubated at 25°C for 10 min, then RT reaction was performed at 48°C for 30 min, after which the reaction was stopped by heating of the mixture at 95°C for 5 min. The instrument was warmed up for at least 15 min before starting the reverse transcription. The cDNA concentration was determined by measuring the absorbance at 260 nm in a spectrophotometer.[392] The cDNA was stored at -20°C until required.

6.2.8.3. Quantitative Real-time Polymerase Chain Reaction (qRT-PCR)

The cDNA aliquots were then subjected to quantitative reverse transcription-polymerase chain reaction (qRT-PCR) to investigate the ability of the cultured hGFs to synthesize the extracellular matrix (ECM) components. A Power SYBR Green PCR Master Mix kit (Applied Biosystems, Foster City, CA) was used for the RT-PCR reaction. SYBR Green I is an asymmetric cyanine dye that has a strong affinity to dsDNA.[393] The assay is based on measuring the increase in the fluorescent dye's signal that is proportional to the amount of DNA produced in each cycle.[394]

Amplification of cDNA was performed in a 25 μL RT-PCR reaction containing 3 μL forward primer (3 μM), 3 μL reverse primer (3 μM), 7 μL cDNA as template and 12 μL SYBR Green Master Mix. The reaction mixture was added to the RT-PCR 96- well plate (Eppendorf AG, Hamburg, Germany) and sealed with cap strips (Eppendorf AG, Hamburg, Germany).

The forward and reverse primer sequences for collagen (COL) (COL-I and COL-III), matrix metalloproteinases (MMP) (MMP-1 and MMP-2), MMP tissue inhibitor (TIMP) (TIMP-1) and decorin were listed in Table 6.3. Glyceraldehyde-3-phosphate dehydrogenase (GAPDH; a housekeeping gene) was used to normalize marker gene expression in each sample.

TABLE 6.3. PRIMER SEQUENCES USED IN THE STUDY

Gene	***Primer***	***Amplicon Size (bp)***
Col-I [395]	Forward : GTGGGCTTCCTGGTGA Reverse : CTT TGGAGCCAGCTGGA	400
Col-III[395]	Forward : GGTACTCCTGGTCTGCA Reverse : GAAGCCAGCAGCACCA	449
MMP-1[396]	Forward : GGT GAT GAA GCA GCC CAG Reverse : CAG TAG AAT GGG AGA GTC	437
MMP-2[396]	Forward : CCT CTC CAC TGC CTT CGA TAC ACC Reverse : AGC ATC TAT TCT TGG GCA CCG	162
TIMP-1[396]	Forward: AGT CAA CCA GAC CAC CTT ATA CCA Reverse : TTT CAG AGC CTT GGA GGA GCT GGT C	386
Decorin[395]	Forward: GATCACCAAAGTGCGAA Reverse : CCAGAGAGCCATTGTCA	297
GAPDH[397, 398]	Forward: ATGCAACGGATTTGGTCGTAT Reverse : TCTCGCTCCTGGAAGATGGTG	220

RT-PCR amplification was performed in a thermal cycler and the amplification conditions for each primer were listed in Table 6.4.

TABLE 6.4. RT-PCR AMPLIFICATION CONDITIONS FOR THE PRIMERS

Primers	***RT-PCR Cycles***	***Denaturation temperature and time***	***Annealing temperature and time***	***Elongation temperature and time***
Col-I	40	94°C for 1 min	55°C for 2 min	72°C for 3 min
Col-III	45	94°C for 1 min	55°C for 2 min	72°C for 3 min
MMP-1*	40	94°C for 30 sec	53°C for 1 min	72°C for 1 min
MMP-2	40	94°C for 1 min	60°C for 2 min	72°C for 3 min
TIMP-1	40	94°C for 1 min	60°C for 2 min	72°C for 3 min
Decorin	40	94°C for 1 min	50°C for 30 sec	72°C for 1 min
GAPDH	40	95°C for 15 sec	56°C for 15 sec	72°C for 30 sec

*+ 72 °C 10 min to finalize extension.

At the end of the RT-PCR reaction, melting curves were analyzed. Melting curves were obtained by heating at a 10 min ramp time from 60 to 95°C. The quantification of the RT-PCR results was achieved using the comparative threshold method. Basically, the threshold cycle (C_T) of each gene of interest was normalized to the housekeeping gene yielding the relative expressions.[399, 400] The number of required cycles for RT-PCR response curves to reach a specific threshold fluorescence signal level is called the C_T.[401] Fig. 6.9 illustrates the C_T values obtained from the RT-PCR response curves.

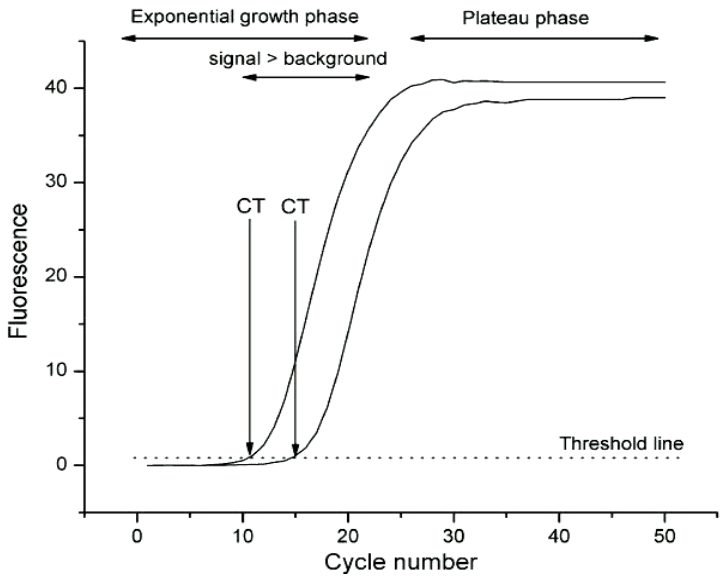

Figure 6.9. Schematic illustration of RT-PCR response curve, where a threshold level sufficiently above the background signal, and C_T depicts the number of PCR cycles required to reach that level.[401]

The relative expression ratios for a target gene were computed using Eqn (9)[402]:

$$\text{Ratio} = \frac{E_{target}^{\Delta C_{T,\,target}}}{E_{ref.}^{\Delta C_{T,\,ref.}}} \qquad (9)$$

E_{target} and $E_{ref.}$ represent the RT-PCR efficiencies for the target and reference (GAPDH) genes, respectively. The RT-PCR efficiencies (E) were calculated using the Relative Expression Software Tool-XL (REST-XL).[403, 404] The C_T values were determined by the

instrument software, and $\Delta C_{T,\ target}$ and $\Delta C_{T,\ ref.}$ were calculated by subtracting the C_T value of the sample from the C_T value of the control [$\Delta C_T = \Delta C_T$ (control) - ΔC_T (sample)] for the target and reference genes, respectively. Thus, the fold increase (upregulation) or decrease (downregulation) of the target gene in the sample was calculated relative to the control sample. The seeded and statically cultured HUV tissue at t = 0 was used as control.

6.2.9. Histological Analysis Using Light Microscopy

Histological analysis was conducted to visualize the cellular attachment and migration into the acellular tissue. Briefly, tissue samples from different zones (n = 6) were fixed and dehydrated with graded ethanol solutions before embedding in paraffin, as described in Section 5.2.8. Paraffin-embedded blocks were serially sectioned at 7 μm thickness. Tissue mounting, deparaffinization and rehydration steps were also performed as described in Section 5.2.8. Hematoxylin and eosin (H&E) staining was used to investigate the tissue architecture. The slides were first deparaffinized in Clearite (3×, 3 min each), and dehydrated in 100 EtOH (2×, 3 min each) and 95% EtOH (2×, 1 min each). After dehydration in tap water, the slides were stained with hematoxylin for 5 min and rinsed with tap water. Then the slides were kept in 0.2% Ammonia-water solution for 1 min and placed in running water for 5 min. The sections were stained with eosin for 1 min followed by changes of 95% EtOH (2×, 1 min each), 100% EtOH (3×, 3 min each) and clearite (3×, 3 min each).[405] Finally, the slides were mounted and histologic images were obtained utilizing the Nikon 80i microscope and DXM1200C camera for brightfield

microscopy. The histology images were captured with NIS-Elements software (Nikon Instruments, Melville, NY).

6.2.10. Immunohistochemistry

The immunohistochemistry technique was used to identify the location and distribution of a target antigen in the hGFs by staining with a specific antibody.[406] Antibodies are immunoglobulins that bind to different natural and synthetic antigen proteins that stimulate the production of and react specifically with antibodies.[407]

The immunohistochemical analysis was conducted for the formalin-fixed paraffin-embedded sections according to the protocol developed by May *et al*.[408] The formalin fixation forms inter- and intramolecular cross-linkages in antigen proteins that may preclude their recognition by a specific antibody.[409] Therefore, heat-induced epitope retrieval technique was applied to cleave these cross-links by utilizing a pressurized decloaking chamber (Biocare Medical, Concord, CA) in citrate buffer (pH 6.0) at 99°C for 18 min.[410] Then, slides were incubated in 3% hydrogen peroxide at room temperature for 20 min to quench any endogenous peroxidase activity and thus block non-specific staining.[411, 412] The slides were incubated with primary antibody [anti-vimentin 1:300 (rabbit), (Santa Cruz Biotechnology, Santa Cruz, CA)] at 4°C overnight.[413] Anti-vimentin antibody has been reported to recognize a large number of cell types, including fibroblasts, macrophages, mesenchymal cells, and so forth.[414, 415] Anti-vimentin antibody has also been used as a marker to detect the vimentin filaments within the human gingival fibroblast (hGF) cytoskeleton.[416, 417] After incubation with primary antibody, the slides were labeled with rabbit polymer-horseradish peroxidase (HRP) secondary (Biocare

Medical) for 25 min at room temperature. The secondary antibody links to the bound primary antibody for detection purposes.[418] Then, the visualization of the bound immune complex was obtained developing the slides with the chromogen diaminobenzidine (DAB) (Sigma, St. Louis, MO) that initiates a colorimetric reaction and causes the immunopositive cells appear brown.[419] The immunohistochemistry images were obtained utilizing the Nikon 80i microscope and DXM1200C camera for brightfield microscopy. Images were captured with NIS-Elements software (Nikon Instruments, Melville, NY). Immunohistochemical staining was conducted for all the samples and the control at the same time.

6.2.11. Sample Analysis and Statistical Data Interpretation

Regarding the assays, tissue constructs to be tested were divided into four groups: (1) *Static Control (SC)* - Static cultures of acellular HUV membranes in petri dishes; (2) *Static Sample (SS)* - Static cultures of HUV scaffolds reseeded with hGFs in petri dishes; (3) *Low Flow Sample (LFS)* – Quasi-static cultures of reseeded HUVs within the bioreactor assembly; (4) *Flow Sample (FS)* - Continuous flow cultures of reseeded HUVs within the bioreactor assemblies. The description and the coding of the samples were tabulated in Table 6.5.

TABLE 6.5. SAMPLE DESCRIPTION AND CODING USED IN DATA ANALYSIS

Sample Description	Sample Coding
Flow Sample from Bioreactor Region 1 (Entrance)	FS1
Flow Sample from Bioreactor Region 2 (Central)	FS2
Flow Sample from Bioreactor Region 3 (Exit)	FS3
Low Flow Sample from Bioreactor Region 1 (Entrance)	LFS1
Low Flow Sample from Bioreactor Region 2 (Central)	LFS2
Low Flow Sample from Bioreactor Region 3 (Exit)	LFS3
Static Sample	SS
Static Control	SC

The 7- and 28-day flow experiments were repeated three times with three flow and one low flow control per group, resulting $n = 9$ experimental flow and $n = 3$ low flow control samples. The sample size was three ($n = 3$) for the static seeded and static acellular samples for each culture period (t = 0, 7 and 28 days).

The statistical software PASW 18 for Windows (SPSS, Chicago, IL) was used to perform the statistical analysis for cellular metabolic activity and proliferation assays. Independent samples *t*-test was used to test for significant differences between 2 test groups. One-way analysis of variance (ANOVA) was used to test for significant differences among multiple test groups. One-way ANOVA was followed by Tukey or

Games-Howell *post hoc* tests depending on if the equal variance assumption was valid. To assess for differences in gene expression profiles, REST-XL was used.[402, 420] Statistical significance was set at $p < 0.05$ for all tests. All values are expressed as mean ± standard deviation.

6.3. RESULTS

6.3.1. Cellular Proliferation and Metabolic Activity within the HUV Bioscaffolds

Proliferation of hGFs, related to the DNA content within the HUV scaffolds, was assessed using the Picogreen assay and the change in DNA content over time was presented in Fig. 6.10. The concentration of DNA in HUV tissue (micrograms per mg wet tissue) varied amongst different samples and changed with culture time.

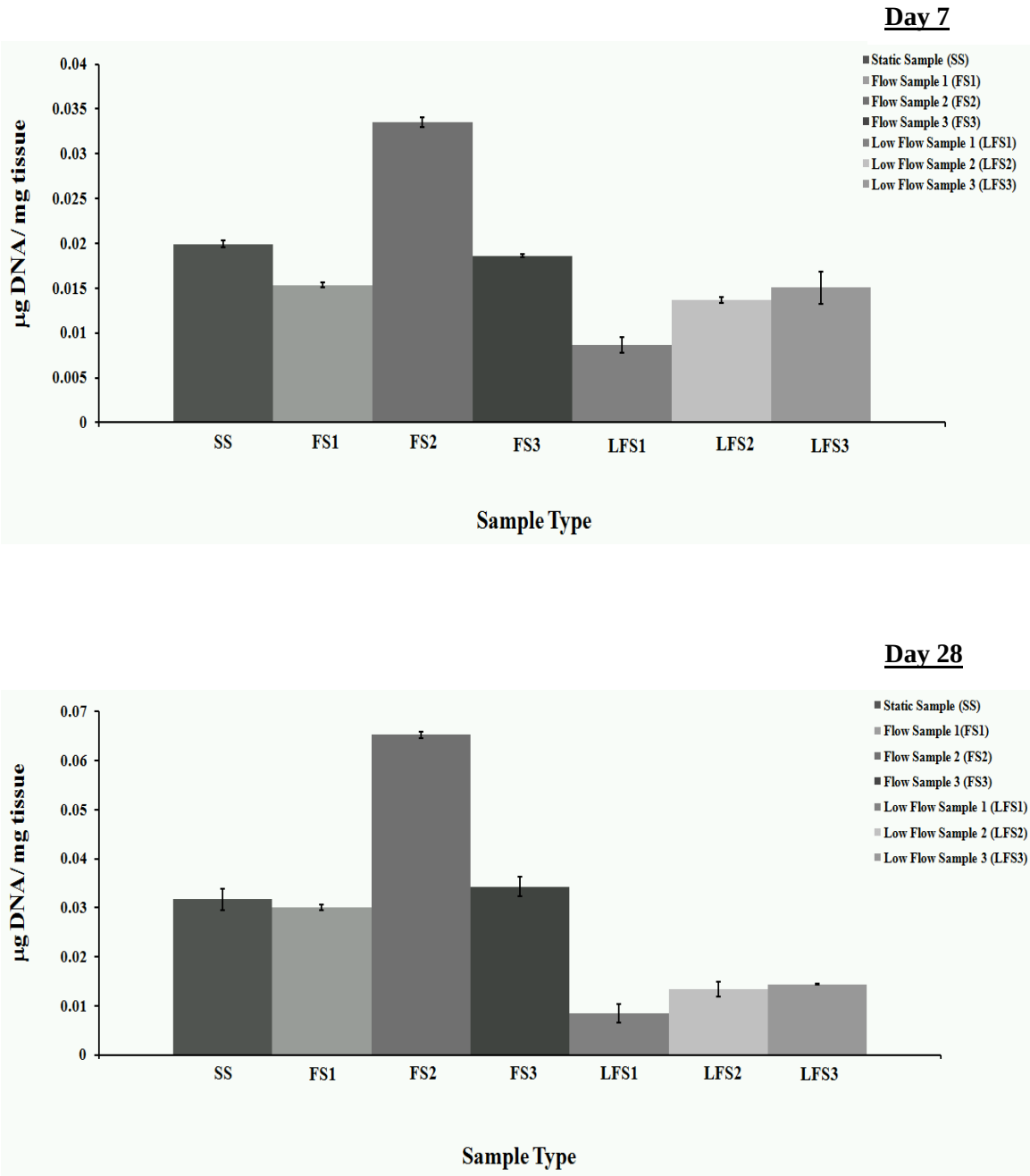

Figure 6.10. DNA content within the HUV tissue was quantified using the Picogreen assay and expressed in µg DNA per mg tissue. DNA content was found to vary with sample type and culture duration. Values are expressed as mean±SD (*n* = 3-9).

Significant differences in tissue DNA content were observed amongst different test samples (One-way ANOVA, Games-Howell *post hoc*, $p < 0.05$) and listed in Tables 6.6 and 6.7 for 7 day- and 27 day-cultures, respectively. The DNA concentration (μg DNA per mg wet tissue) increased significantly from day 7 to day 28 (Independent samples *t*-test, $p < 0.05$) for the samples coded – SS, FS1, FS2, and FS3 (See Table 6.5).

TABLE 6.6. DIFFERENCES IN TISSUE DNA CONCENTRATION AMONG SAMPLES AT DAY 7. SYMBOL √ REPRESENTS THE STATISTICALLY SIGNIFICANT DIFFERENCES SET AT 0.05 LEVEL

Sample Type	SS	FS1	FS2	FS3	LFS1	LFS2	LFS3
SS		√	√		√	√	
FS1	√		√	√	√	√	
FS2	√	√		√	√	√	√
FS3		√	√		√	√	
LFS1	√	√	√	√		√	
LFS2	√	√	√	√	√		
LFS3	√		√				

TABLE 6.7. DIFFERENCES IN TISSUE DNA CONCENTRATION AMONG SAMPLES AT DAY 28. SYMBOL √ REPRESENTS THE STATISTICALLY SIGNIFICANT DIFFERENCES SET AT 0.05 LEVEL

Sample Type	SS	FS1	FS2	FS3	LFS1	LFS2	LFS3
SS			√		√	√	√
FS1			√		√	√	√
FS2	√	√		√	√	√	√
FS3			√		√	√	√
LFS1	√	√	√	√			
LFS2	√	√	√	√			
LFS3	√	√	√	√			

The number of human gingival fibroblasts (hGFs) within HUV tissue disks was computed using Eqn. 7 and found to vary with culture time and sample type (Fig. 6.11). Significant differences were observed amongst the test samples (One-way ANOVA, Games-Howell *post hoc*, $p < 0.05$) and listed in Tables 6.8 and 6.9 for 7 day- and 27 day-cultures, respectively. The hGF content of HUV disks increased significantly from day 7 to day 28 (Independent samples *t*-test, $p < 0.05$) for all the samples tested.

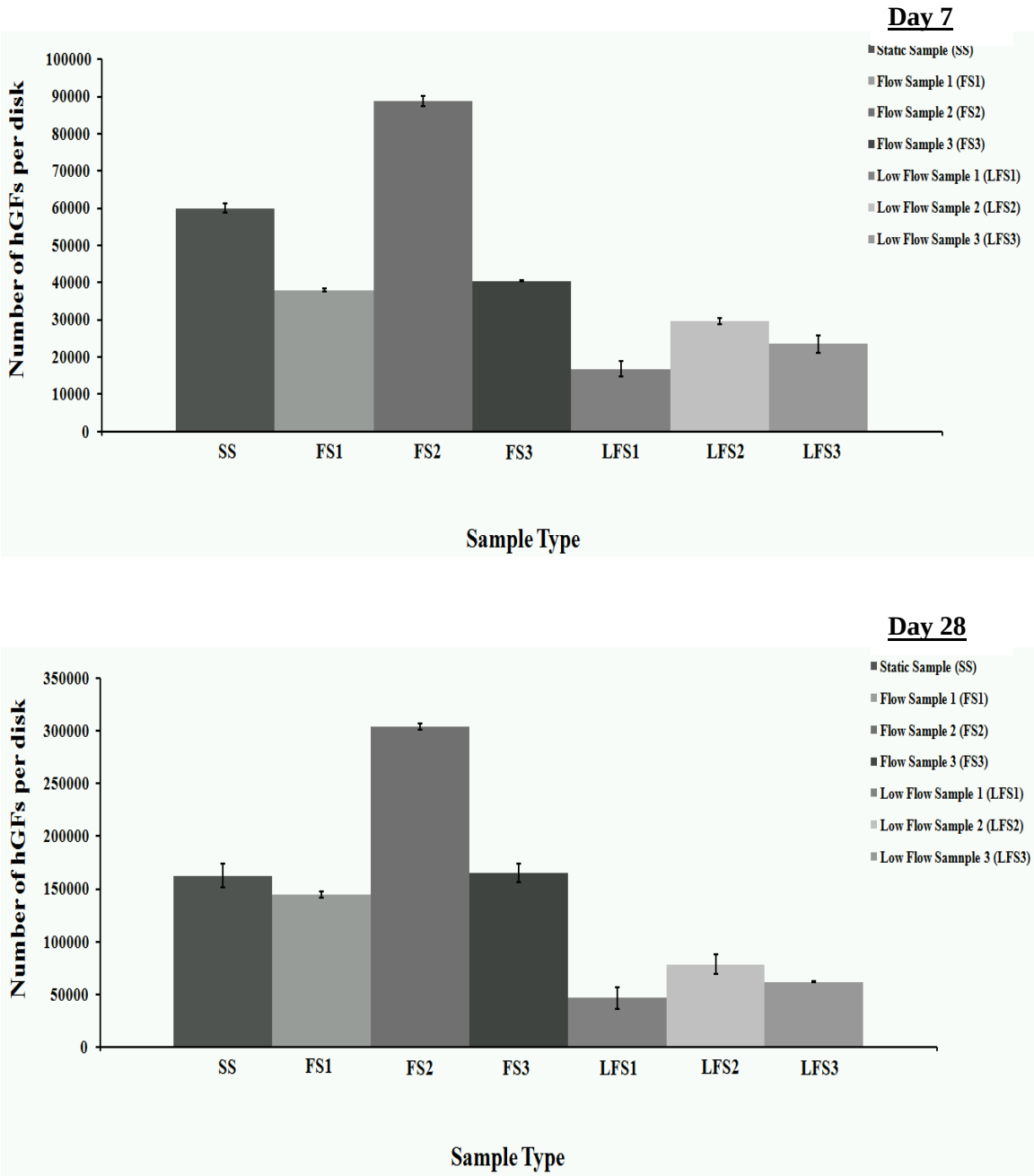

Figure 6.11. Proliferation of hGFs cultured within the HUV scaffolds was found to vary with sample type and culture time. Values are expressed as mean±SD (*n* = 3-9).

TABLE 6.8. VARIATION IN HGF POPULATION FOR DIFFERENT SAMPLE TYPES AT DAY 7. SYMBOL √ REPRESENTS THE STATISTICALLY SIGNIFICANT DIFFERENCES SET AT 0.05 LEVEL

Sample Type	SS	FS1	FS2	FS3	LFS1	LFS2	LFS3
SS		√	√	√	√	√	√
FS1	√		√	√	√	√	√
FS2	√	√		√	√	√	√
FS3	√	√	√		√	√	√
LFS1	√	√	√	√		√	
LFS2	√	√	√	√	√		
LFS3	√	√	√	√			

TABLE 6.9. VARIATION IN HGF POPULATION FOR DIFFERENT SAMPLE TYPES AT DAY 28. SYMBOL √ REPRESENTS THE STATISTICALLY SIGNIFICANT DIFFERENCES SET AT 0.05 LEVEL

Sample Type	SS	FS1	FS2	FS3	LFS1	LFS2	LFS3
SS			√		√	√	√
FS1			√		√	√	√
FS2	√	√		√	√	√	√
FS3			√		√	√	√
LFS1	√	√	√	√			
LFS2	√	√	√	√			
LFS3	√	√	√	√			

The metabolic activity of hGFs seeded on HUV scaffold was assessed and the differences between the experimental groups and control group were evaluated (See Table 6.5 for the detailed description of the sample types). The percent (%) Alamar blue (AB) reduction per tissue disk data showed that static samples (SS) demonstrated higher metabolic activity than the static controls (SC) (Independent samples *t*-test, $p < 0.05$) at day 0 (Fig 6.12). Statistically significant differences in metabolic activity were observed amongst different sample types at day 7 and day 28 ($p < 0.05$; Tukey's *post-hoc* test with one-way ANOVA), and indicated on Fig. 6.12.

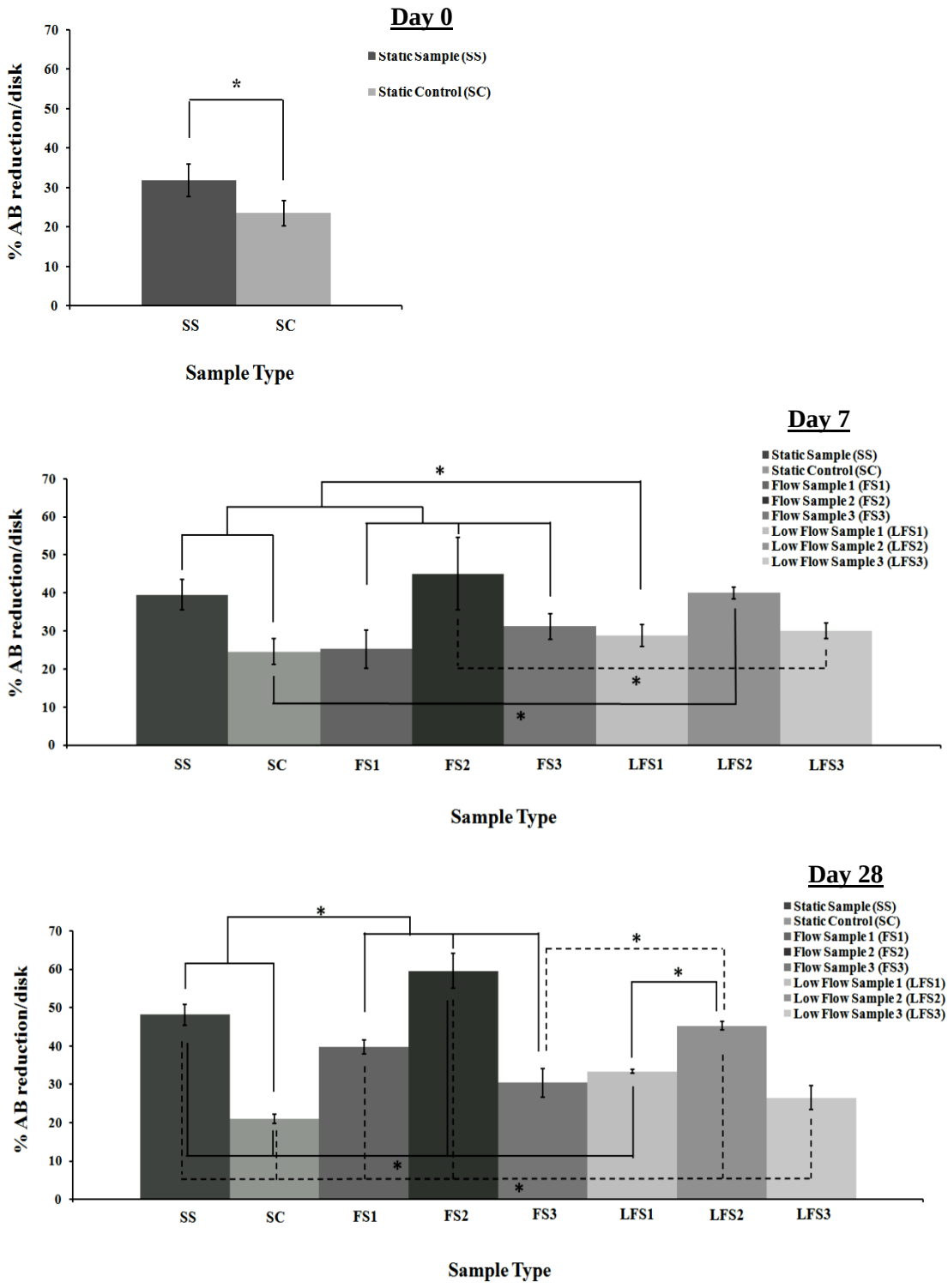

Figure 6.12. Percent (%) Alamar blue (AB) reduction per tissue disk versus sample type. Viability of the cultured hGFs in the HUV scaffolds (n = 3-9) was assessed with AB and was found to vary with culture time. Values are expressed as mean±SD. * denotes statistically significant difference set at the 0.05 level.

The percentage (%) AB reduction per tissue disk for the static sample (SS) at day 7 was significantly greater than at day 0, and at day 28 was significantly greater than day 7 (One-way ANOVA, Tukey's *post hoc* test, $p < 0.05$). The % AB reduction per tissue disk increased significantly from day 7 to day 28 (Independent samples *t*-test, $p < 0.05$) for the samples coded – FS1, FS2, and LFS3 (see Table 6.5), indicating the continuity of cellular metabolic activity over culture period. However, there was no statistically significant change in cellular metabolic activity for the samples coded FS3, LFS1, and LFS3 between days 7 and 28.

The statistical differences in %AB reduction among different sample types at days 7 and 28 were also tabulated in Tables 6.10 and 6.11, respectively.

TABLE 6.10. DIFFERENCES IN PERCENT (%) ALAMAR BLUE (AB) REDUCTION PER TISSUE DISK AMONG SAMPLES AT DAY 7. SYMBOL √ REPRESENTS THE STATISTICALLY SIGNIFICANT DIFFERENCES SET AT 0.05 LEVEL

Sample Type	SS	SC	FS1	FS2	FS3	LFS1	LFS2	LFS3
SS		√	√		√	√		
SC	√			√			√	
FS1	√			√			√	
FS2		√	√		√	√		√
FS3	√			√				
LFS1	√			√				
LFS2		√	√					
LFS3				√				

TABLE 6.11. DIFFERENCES IN PERCENT (%) ALAMAR BLUE (AB) REDUCTION PER TISSUE DISK AMONG SAMPLES AT DAY 28. SYMBOL √ REPRESENTS THE STATISTICALLY SIGNIFICANT DIFFERENCES SET AT 0.05 LEVEL

Sample Type	SS	SC	FS1	FS2	FS3	LFS1	LFS2	LFS3
SS		√	√	√	√	√		√
SC	√		√	√	√	√	√	
FS1	√	√		√	√			√
FS2	√	√	√		√	√	√	√
FS3	√	√	√	√			√	
LFS1	√	√		√			√	
LFS2		√		√	√	√		√
LFS3	√		√	√			√	

By combining the hGF number assessed by the Picogreen Assay (cells per tissue disk) (Fig. 6.11), and the % Alamar blue (AB) reduction per tissue disk data (Fig. 6.12), we obtained the cellular metabolic activity (%AB reduction per cell) as shown in Figure 6.13. The % AB reduction per cell decreased significantly from day 7 to day 28 (Independent samples *t*-test, $p < 0.05$) for all the samples tested.

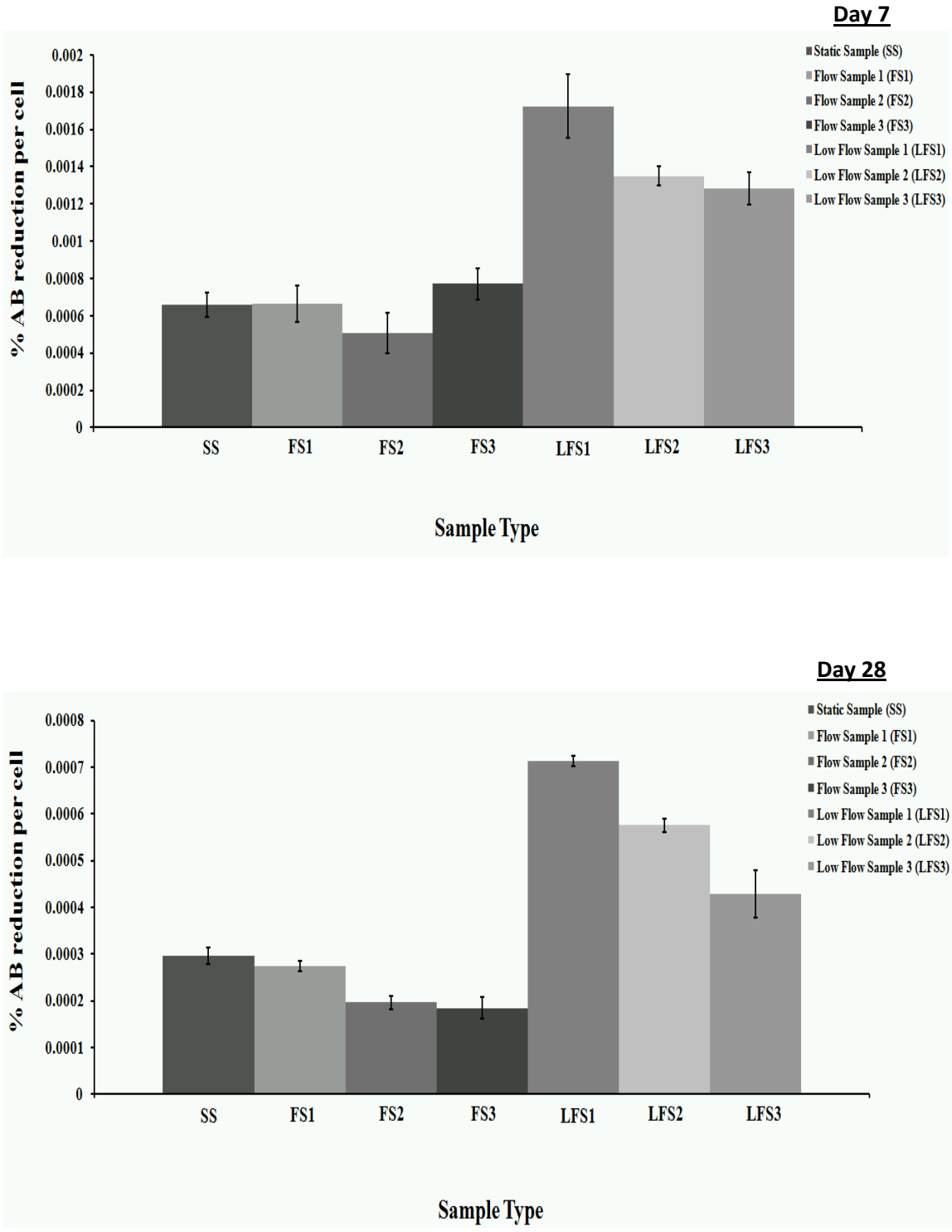

Figure 6.13. The Alamar blue (AB) reduction per cell within HUV disks after 7 days and 28 days in culture. Values are expressed as mean±SD (n = 3-9).

The statistically significant differences among different tissue types (One-way ANOVA, Tukey's test, $p < 0.05$) were indicated in Tables 6.12 and 6.13, respectively.

TABLE 6.12. DIFFERENCES IN PERCENT (%) ALAMAR BLUE (AB) REDUCTION PER CELL VALUES AMONG SAMPLES AT DAY 7. SYMBOL √ REPRESENTS THE STATISTICALLY SIGNIFICANT DIFFERENCES SET AT 0.05 LEVEL

Sample Type	SS	FS1	FS2	FS3	LFS1	LFS2	LFS3
SS					√	√	√
FS1					√	√	√
FS2				√	√	√	√
FS3			√		√	√	√
LFS1	√	√	√	√		√	√
LFS2	√	√	√	√	√		
LFS3	√	√	√	√	√		

TABLE 6.13. DIFFERENCES IN PERCENT (%) ALAMAR BLUE (AB) REDUCTION PER CELL VALUES AMONG SAMPLES AT DAY 28. SYMBOL √ REPRESENTS THE STATISTICALLY SIGNIFICANT DIFFERENCES SET AT 0.05 LEVEL

Sample Type	SS	FS1	FS2	FS3	LFS1	LFS2	LFS3
SS			√	√	√	√	√
FS1			√	√	√	√	√
FS2	√	√			√	√	√
FS3	√	√			√	√	√
LFS1	√	√	√	√		√	√
LFS2	√	√	√	√	√		√
LFS3	√	√	√	√	√	√	

6.3.2. Assessment of Gene Expression Profiles for the Cultured hGFs

The purity of total RNA extracted from the cultured HUV scaffolds was checked by a spectrophotometer and the wavelength absorption ratio (260/280 nm) was between 1.8 and 2.0 in all preparations.

The mRNA levels of COL-I, COL-III, MMP-1, MMP-2, TIMP-1 and decorin (Table 6.3) were analyzed in the hGFs cultured samples for 7 and 28 days by reverse-transcription polymerase chain reaction (RT-PCR). The relative expression levels (upregulation or downregulation) for the genes COL-I, COL-III, MMP-1, MMP-2, TIMP-1 and decorin compared to the control samples, were graphically illustrated in Figs. 6.14-6.20. Expression of these genes, however, remained below the detection level for the samples that were not shown on the graphs. The seeded static samples (SS) at t = 0 served as control.

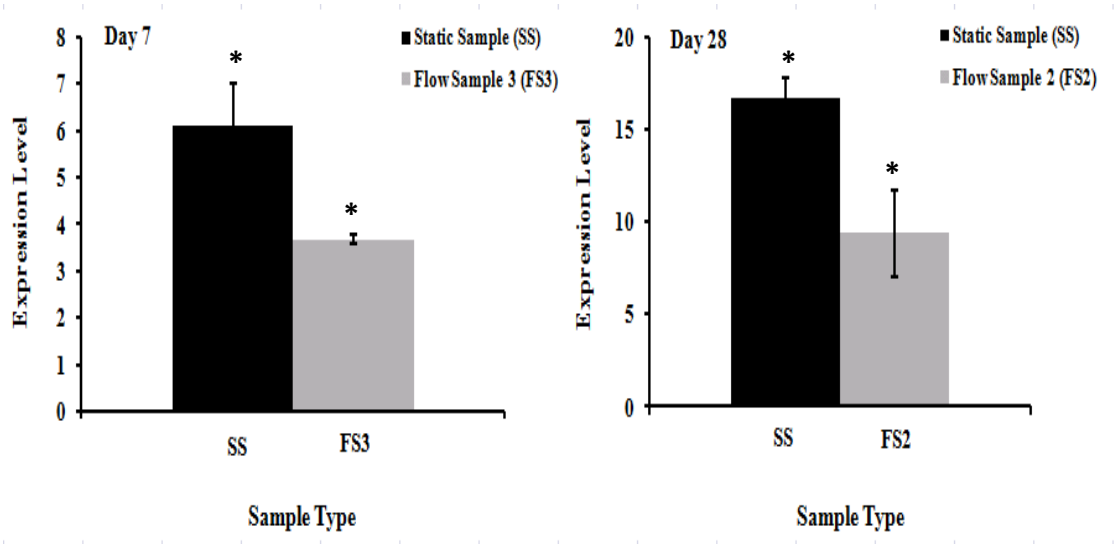

Figure 6.14. mRNA levels of COL-I in hGFs in culture at day 7 and day 28. Seeded HUV samples under static culture (t = 0) served as controls. Fold changes were obtained by normalizing to the housekeeping gene GAPDH and expressed as mean±SD. * denotes significant upregulation and ** denotes significant downregulation compared to control ($p < 0.05$, n = 3-9).

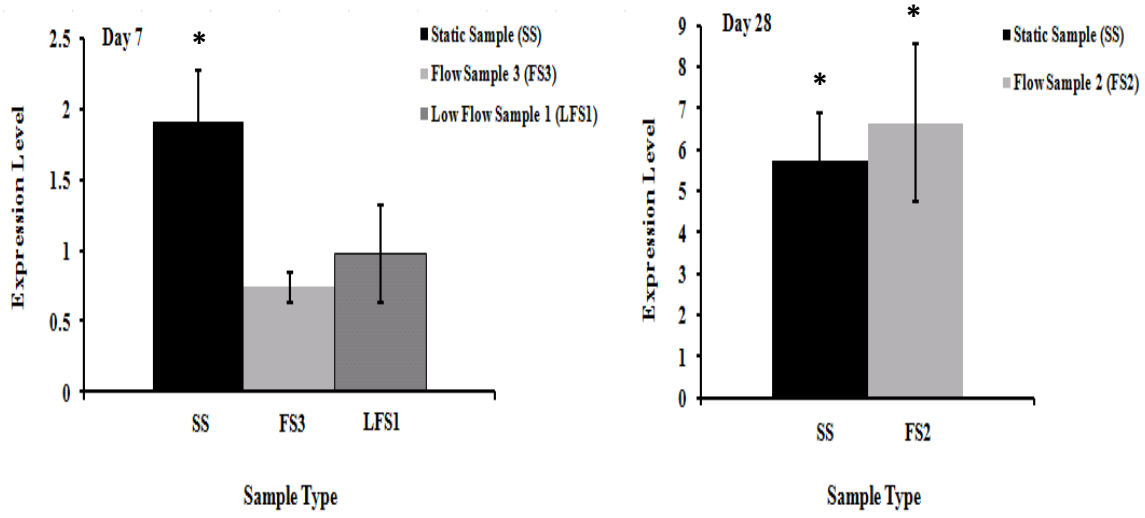

Figure 6.15. mRNA levels of COL-III in hGFs in culture at day 7 and day 28. Seeded HUV samples under static culture (t = 0) served as controls. Fold changes were obtained by normalizing to the housekeeping gene GAPDH and expressed as mean±SD. * denotes significant up-regulation and ** denotes significant down-regulation compared to control ($p < 0.05$, n = 3-9).

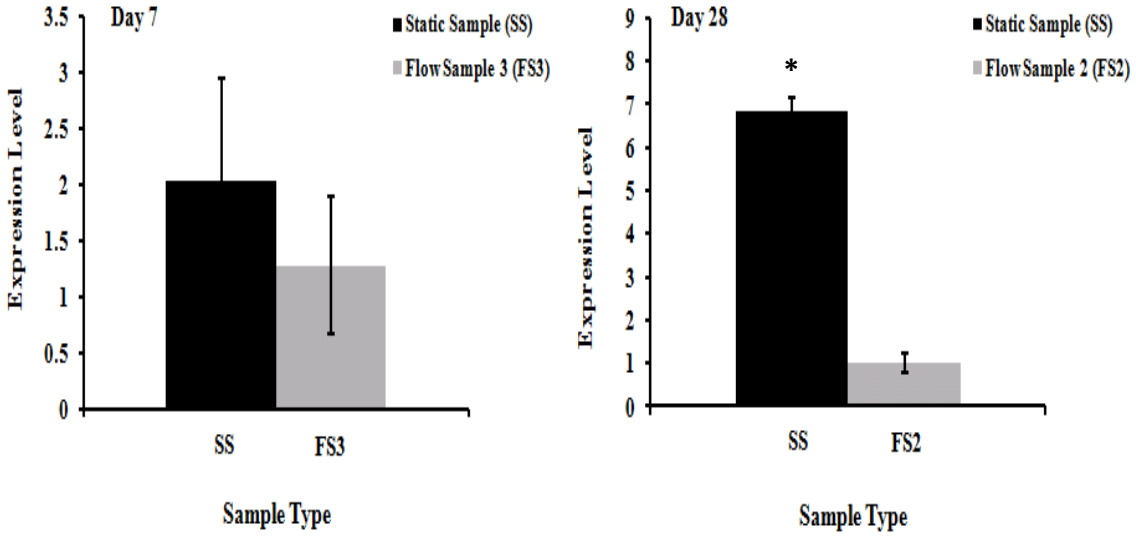

Figure 6.16. mRNA levels of MMP-1 in hGFs in culture at day 7 and day 28. Seeded HUV samples under static culture (t = 0) served as controls. Fold changes were obtained by normalizing to the housekeeping gene GAPDH and expressed as mean±SD. * denotes significant up-regulation and ** denotes significant down-regulation compared to control ($p < 0.05$, n = 3-9).

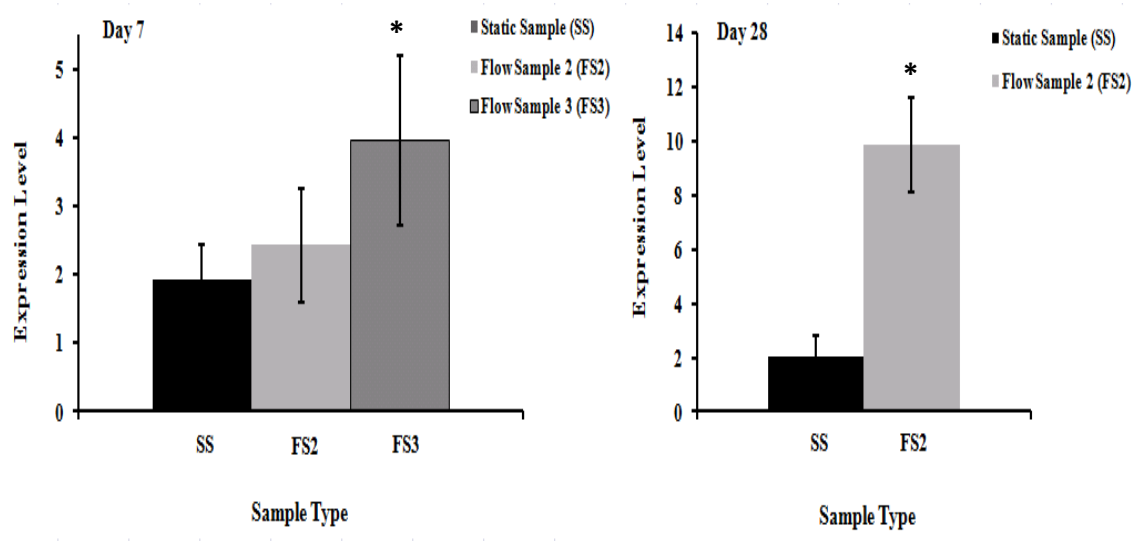

Figure 6.17. mRNA levels of MMP-2 in hGFs in culture at day 7 and day 28. Seeded HUV samples under static culture (t = 0) served as controls. Fold changes were obtained by normalizing to the housekeeping gene GAPDH and expressed as mean±SD. * denotes significant up-regulation and ** denotes significant down-regulation compared to control ($p < 0.05$, n = 3-9).

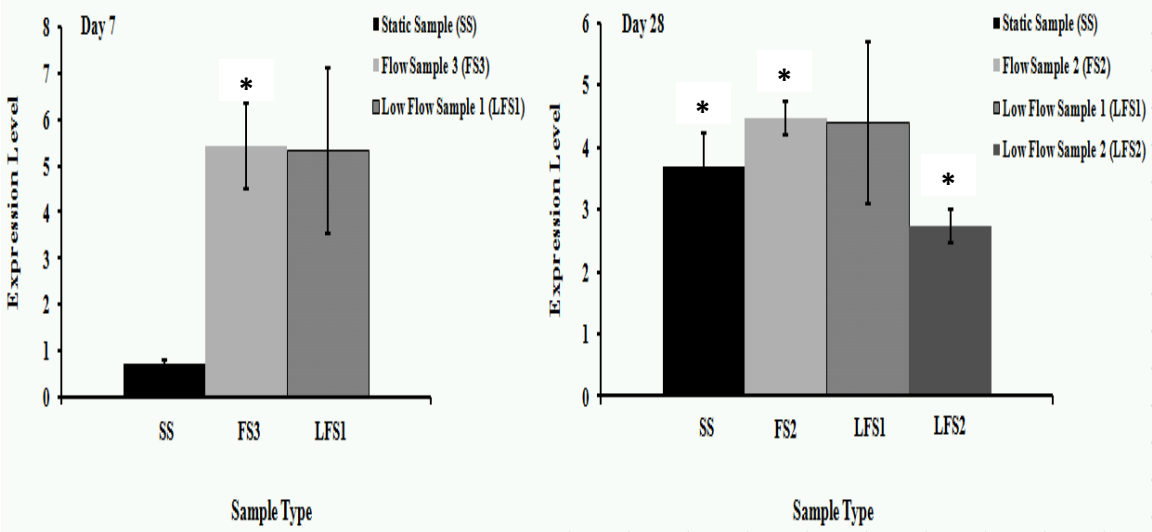

Figure 6.18. mRNA levels of TIMP-1 in hGFs in culture at day 7 and day 28. Seeded HUV samples under static culture (t = 0) served as controls. Fold changes were obtained by normalizing to the housekeeping gene GAPDH and expressed as mean±SD. * denotes significant up-regulation and ** denotes significant down-regulation compared to control ($p < 0.05$, $n = 3$-9).

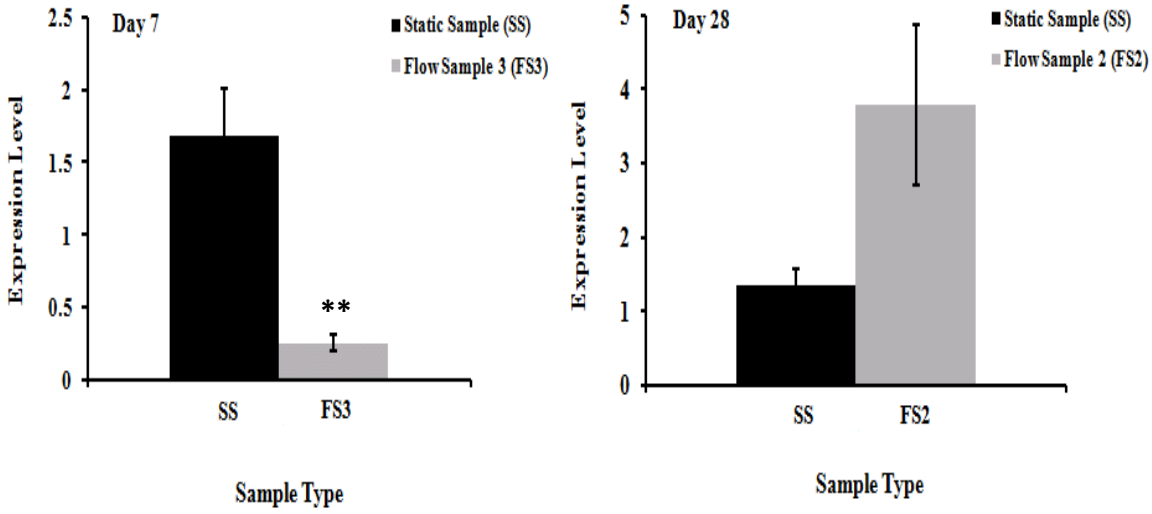

Figure 6.19. mRNA levels of decorin in hGFs in culture at day 7 and day 28. Seeded HUV samples under static culture (t = 0) served as controls. Fold changes were obtained by normalizing to the housekeeping gene GAPDH and expressed as mean±SD. * denotes significant up-regulation and ** denotes significant down-regulation compared to control ($p < 0.05$, $n = 3$-9).

6.3.3. Histological Assessment of HUV Scaffolds

Hematoxylin & Eosin (H&E) staining technique was used to visualize the cellular components within the human umbilical vein (HUV) scaffolds. The histological analysis demonstrated the native cells of the HUV before decellularization (Figs. 6.20A and 6.20B), and confirmed a complete removal of smooth muscle cells and endothelial cells from the vessel wall of the HUV treated with SDS buffer for 24 h (Figs. 6.20C and 6.20D).

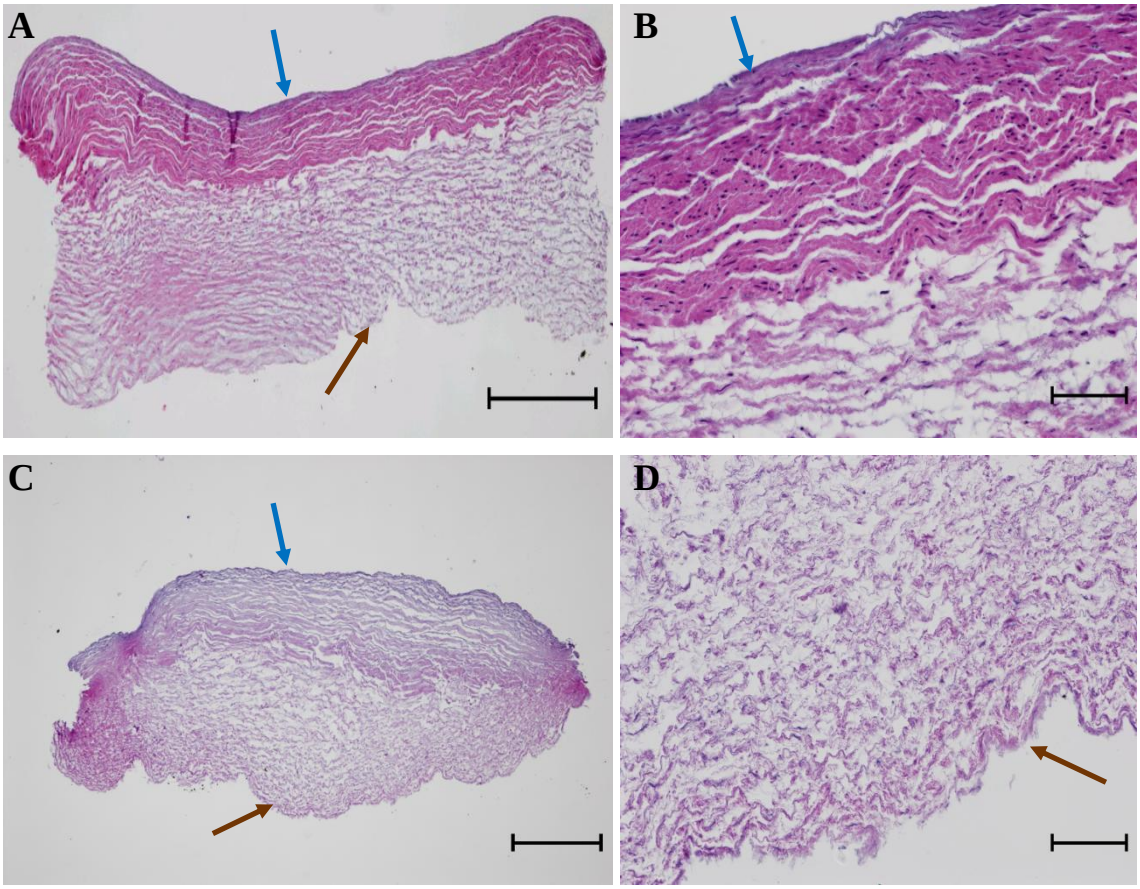

Figure 6.20. H&E-stained HUV scaffolds before decellularization (**(A)**- 4X magnification, **(B)**- 20X magnification), and after decellularization (**(C)**- 4X magnification, **(D)**- 20X magnification) with SDS surfactant for 24 h. The blue arrow indicates the lumenal surface; the brown arrow indicates the ablumenal surface. The scale bars for the 4X magnification indicate 500 μm, and scale bars for the 20X magnification images indicate 100 μm.

The histological analysis at t = 0 revealed that the control samples (Fig. 6.21A) were devoid of hGFs, whereas the cells adhered on the scaffold surface and migrated further through the tissue for the static samples (SS) (Fig. 6.21B).

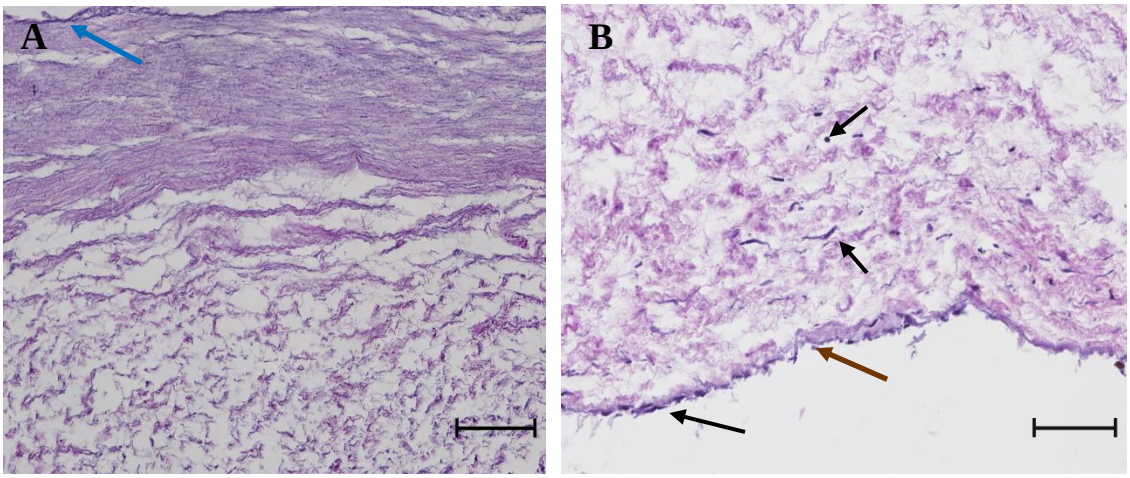

Figure 6.21. Histological analysis for the sample control (SC) **(A)** and static sample (SS) **(B)** at t = 0. The sample control was observed to be devoid of cellular components, whereas the cells were visualized (indicated by arrows) within static samples. The black arrows indicate hGFs on the surface and interior parts of the re-cellularized human umbilical vein. The blue arrow indicates the lumenal surface; the brown arrow indicates the ablumenal surface. Cells were round and spindle-shaped throughout the scaffolds. Original magnification: 20X. Scale bars indicate 100 μm.

Hematoxylin and Eosin (H&E) staining of the control and test samples at day 7 and day 28 are presented in Figs. 6.22 and 6.23, respectively. The staining demonstrated variation among the samples for both culture times.

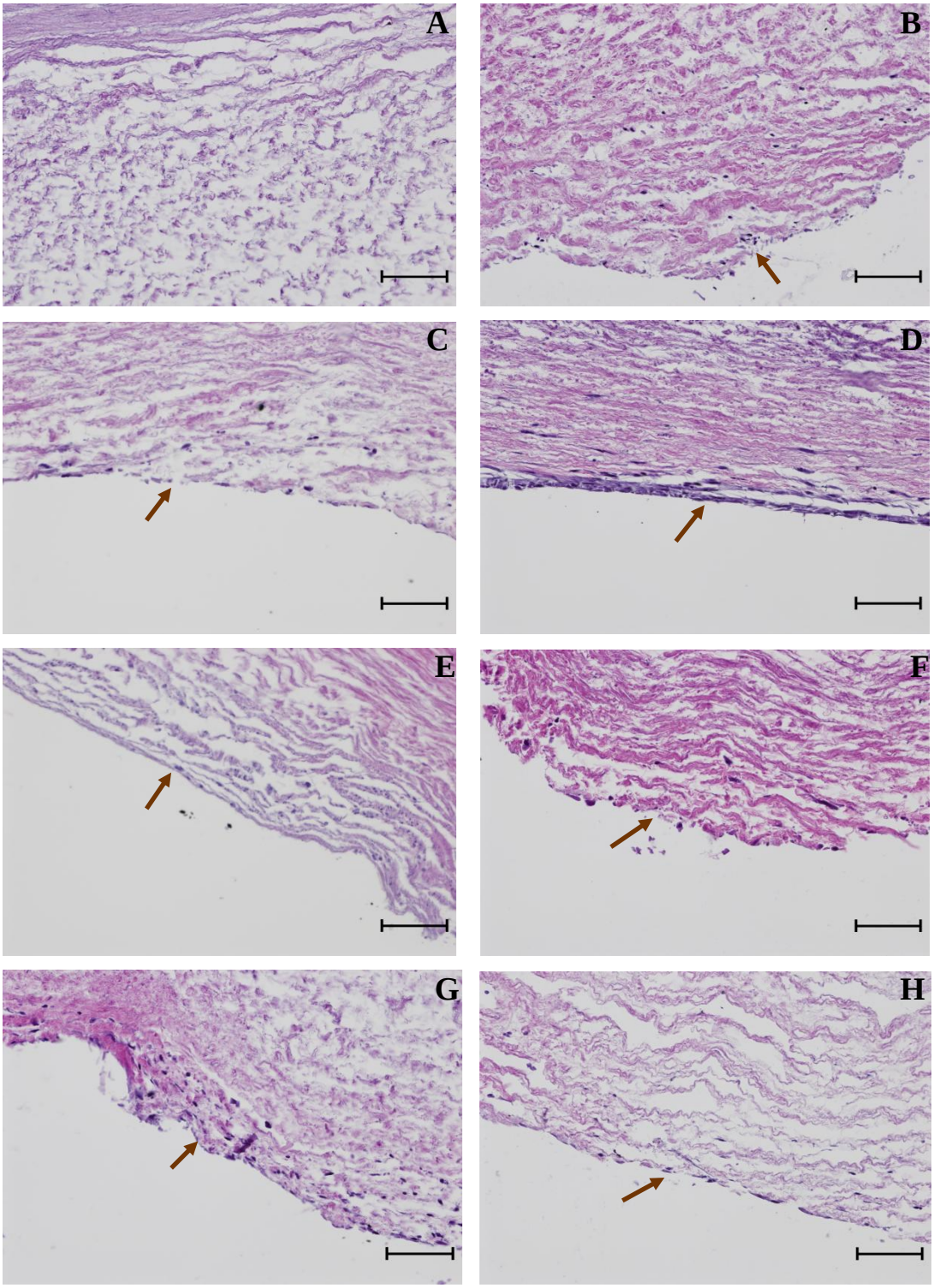

Figure 6.22. Histology for the sample control (SC) **(A)**, static sample (SS) **(B),** flow sample 1 (FS1) **(C)**, flow sample 2 (FS2) **(D)**, flow sample 3 (FS3) **(E)**, low flow sample 1 (LFS1) **(F)**, low flow sample 2 (LFS2) **(G)**, and low flow sample 3 (LFS3) **(H)** at day 7. Original magnification: 20X. Purple stain shows the cellular components, and the brown arrow indicates the ablumenal surface. Scale bars indicate 100 μm.

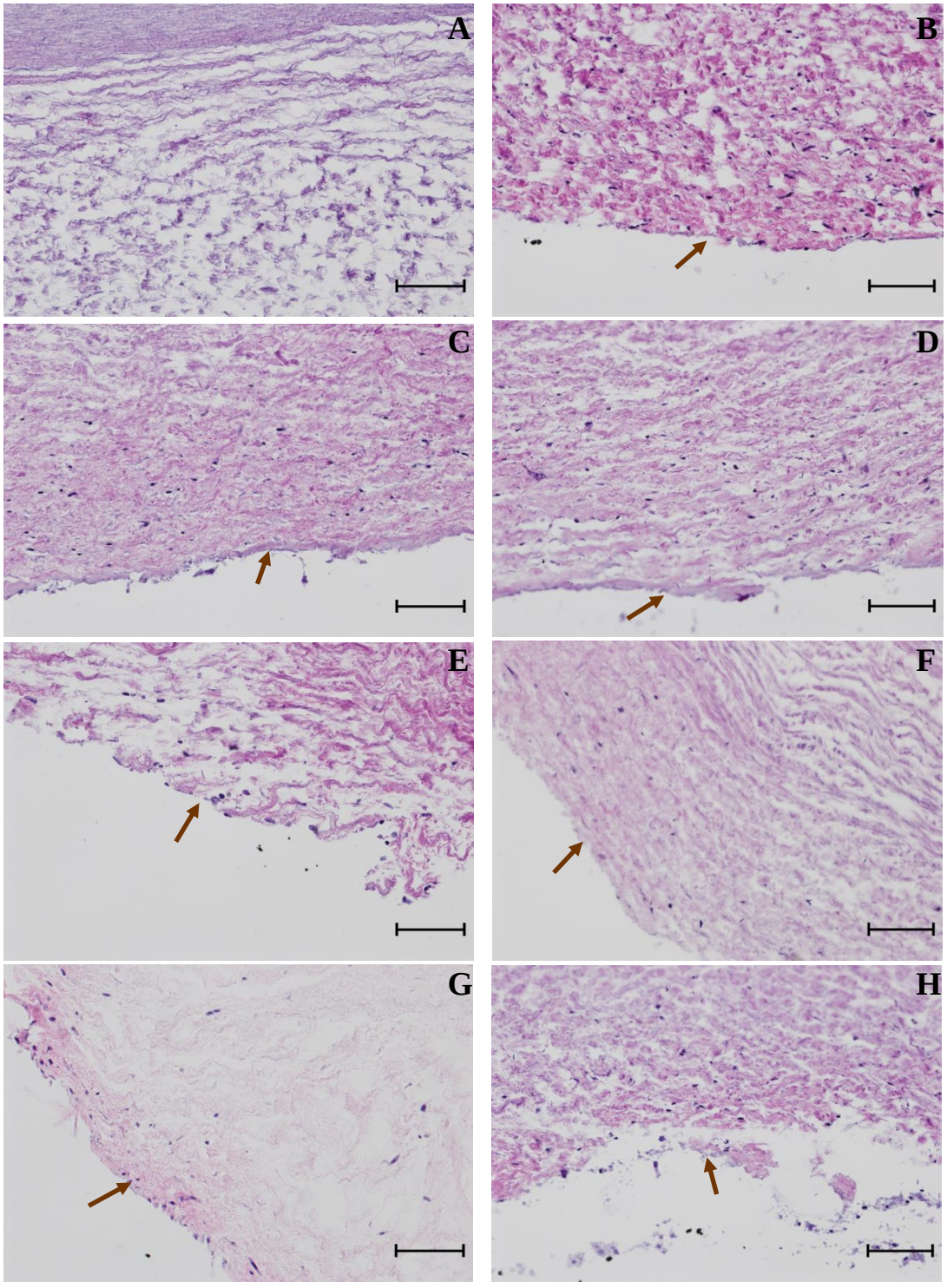

Figure 6.23. H&E staining for sample control (SC) **(A)**, static sample (SS) **(B),** flow sample 1 (FS1) **(C)**, flow sample 2 (FS2) **(D)**, flow sample 3 (FS3) **(E)**, low flow sample 1 (LFS1) **(F)**, low flow sample 2 (LFS2) **(G)**, and low flow sample 3 (LFS3) **(H)** at day 28. Purple stain shows the cellular components, and the brown arrow indicates the ablumenal surface. Scale bars indicate 100 μm (at 20X magnification).

6.3.4. Immunohistochemical Analysis of HUV Scaffolds

Immunostaining technique adopted in this study required the binding of the primary antibody vimentin to cultured hGFs, and then the detection and visualization of bound vimentin with rabbit polymer-horseradish peroxidase (HRP). The immunohistochemical micrographs show that the antibody to vimentin stained the hGFs (brown stains). The negative staining for vimentin in the decellularized tissue revealed the complete removal of the cellular components from the scaffold (Figs. 6.24A and 6.24B). The attachment and migration of the hGFs within the HUV scaffold at t = 0 was demonstrated in Figs. 6.24C and 6.24D.

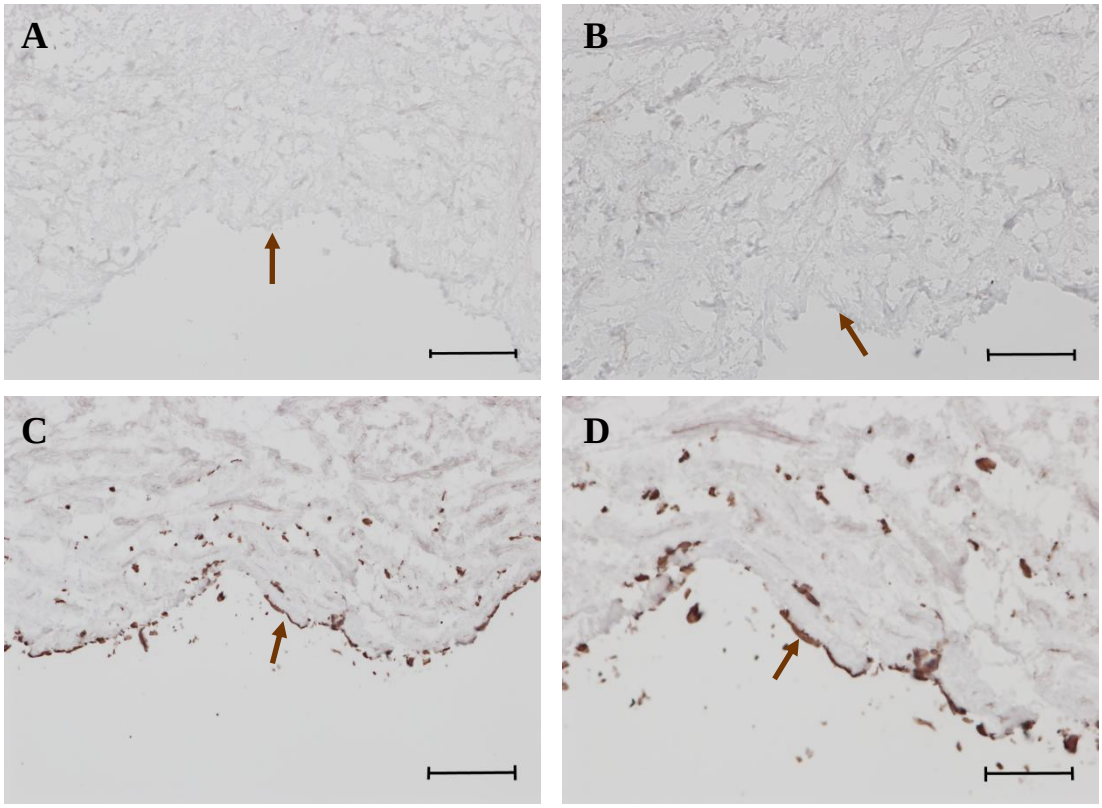

Figure 6.24. The immunohistochemical staining of the HUV scaffolds at t = 0. The static control (SC) samples (**(A)**- 20X magnification, **(B)**- 40X magnification) demonstrate no fibroblastic component, whereas fibroblasts are clearly visualized (brown stains) for the static samples (SS) (**(C)**- 20X magnification, **(D)**- 40X magnification). The brown arrow indicates the ablumenal surface. Scale bars for the 20X magnification images indicate 100 μm, and scale bars for the 40X magnification indicate 50 μm.

Immunostaining of the cultured HUV samples for 7 and 28 days are presented in Figs. 6.25 and 6.26, respectively. The acellular HUV sections showed negative staining for vimentin (Figs. 6.25A and 6.26A), whereas the cells showed strong positive staining for all the other test samples (Figs. 6.25B-H and 6.26B-H). Variation in hGF migration and distribution was observed among the recellularized test samples for both culture times.

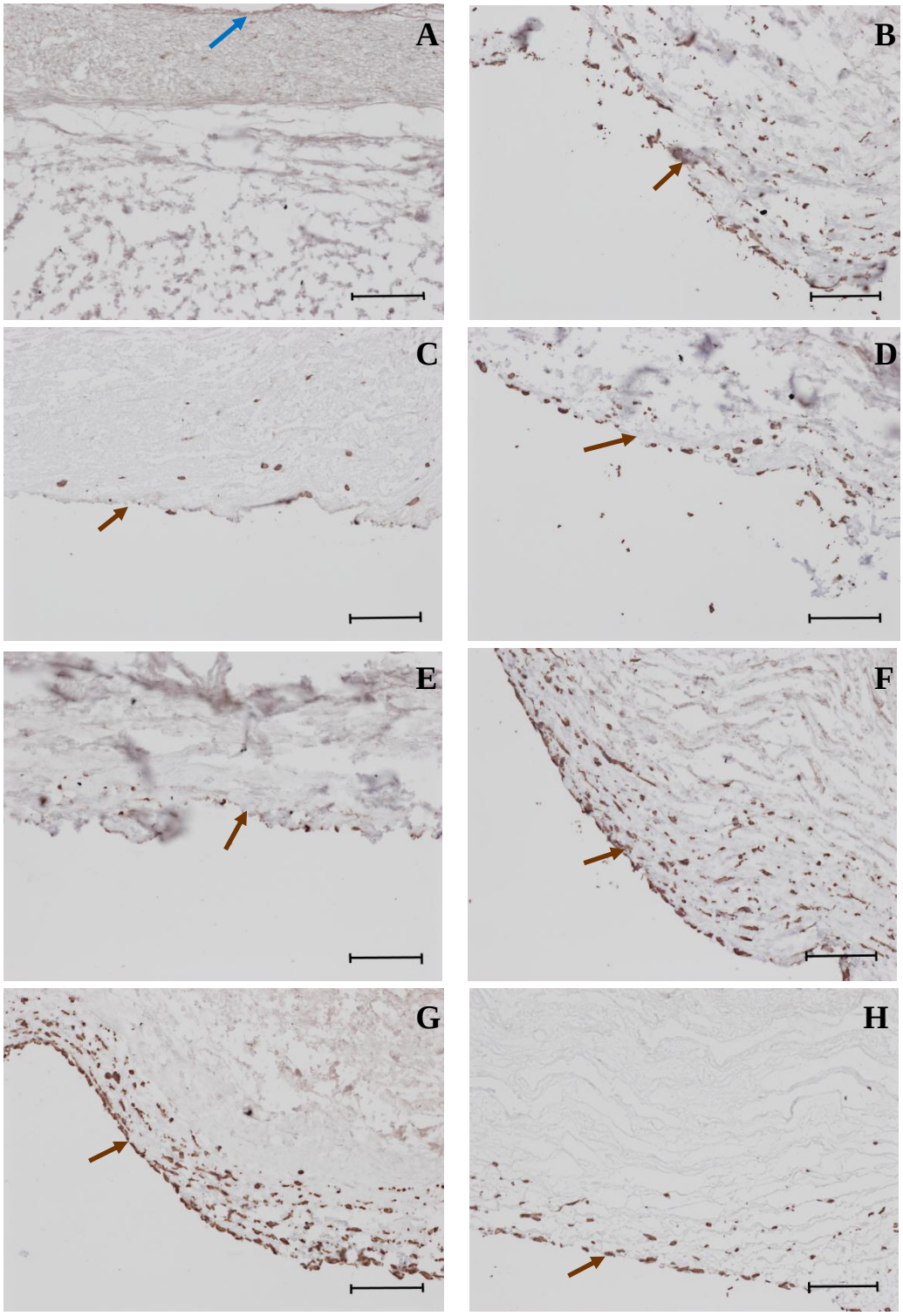

Figure 6.25. Immunohistochemistry of the HUV scaffolds at day 7 - sample control (SC) **(A)**, static sample (SS) **(B),** flow sample 1 (FS1) **(C)**, flow sample 2 (FS2) **(D)**, flow sample 3 (FS3) **(E)**, low flow sample 1 (LFS1) **(F)**, low flow sample 2 (LFS2) **(G)**, and low flow sample 3 (LFS3) **(H)** at day 7. The blue and brown arrows indicate the lumenal and ablumenal surfaces, respectively. Scale bars indicate 100 μm at 20X magnification.

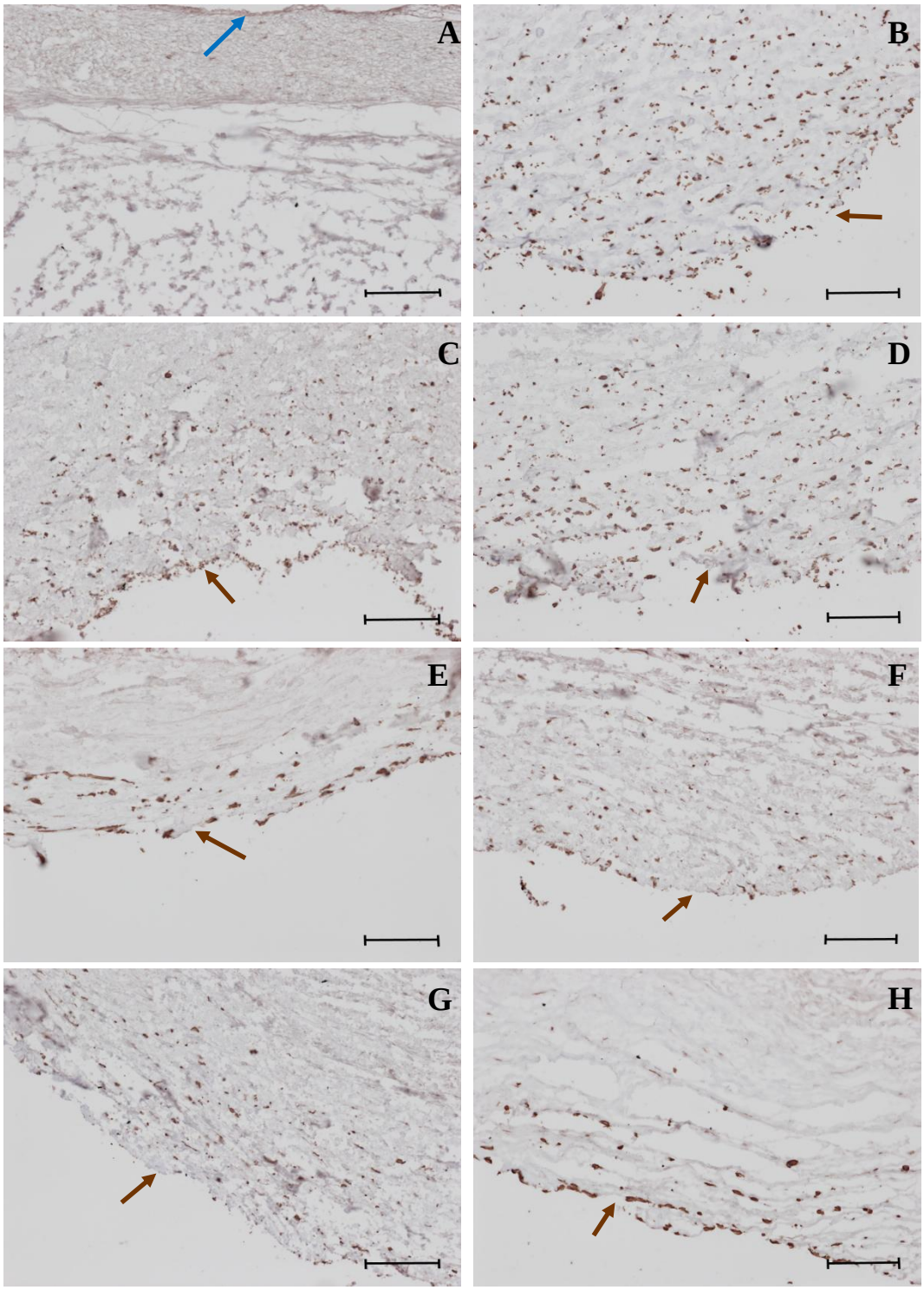

Figure 6.26. Immunohistochemical photomicrographs of the HUV scaffolds at day 28 - sample control (SC) **(A)**, static sample (SS) **(B),** flow sample 1 (FS1) **(C)**, flow sample 2 (FS2) **(D)**, flow sample 3 (FS3) **(E)**, low flow sample 1 (LFS1) **(F)**, low flow sample 2 (LFS2) **(G)**, and low flow sample 3 (LFS3) **(H)** at day 28. The blue arrow indicates the lumenal surface; brown arrow indicates the ablumenal surface. Original magnification: 20X. Scale bars indicate 100 μm.

6.4. DISCUSSION

Guided tissue regeneration (GTR) technique has been an effective strategy to treat diseased periodontal tissues while employing space-maintaining barriers that coordinate the healing processes. Numerous GTR membranes have been proposed for use in periodontal wound healing and regeneration.[421-423] In this study, we assessed the ability of the human umbilical vein (HUV) to function as a periodontal GTR membrane.

The human umbilical vein (HUV) has been well documented for its use as a vascular conduit in numerous studies,[424-426] as a mesenchymal stromal cell (MSC) reservoir for several tissue engineering applications,[427-430] and as a scaffolding material in tissue replacement for various defects.[431, 432] We have previously introduced the HUV as a surgical barrier for periodontal GTR applications. With this scaffold, the ablumenal surface enabled cells to penetrate into the extracellular matrix (ECM), whereas the lumenal surface acted as a barrier and inhibited cell migration.[29] Upon decellularization, the HUV graft possessed larger void spaces compared to the native tissue that may be advantageous by increasing the mass transfer of nutrients and gases.[433] While these *in vitro* assessments show significant promise, further development of these systems using bioreactors to precisely control perfusion conditions may improve the biological interactions and tissue functionality.

The aim of this study was to design a modified parallel-plate bioreactor system that broadly mimics conditions during periodontal wound healing and then to understand the role these conditions have on the biological function of the hGFs. The HUV membrane was inserted between the two flow compartments of the bioreactor with the HUV's

lumenal side facing the top compartment perfused at low shear rates to actively reorganize and remodel the ECM.[434, 435] The ablumenal side of the scaffold was placed in contact with the lower flow compartment resembling the wound space (Fig. 6.1). The upper flow compartment was circulated with culture media having no glucose in order to create a chemotactic gradient that may drive hGF migration from the ablumenal side through the scaffold toward the lumenal surface. In addition, flow was perfused through both compartments of the bioreactor simulating the physiological pulsating frequency.[436, 437] We hypothesized that several factors including the pulsation rates through the scaffold, the central region (region 2) of the scaffold being in direct contact with the flow and the change in the gas, nutrient and waste concentration of the media through the bioreactor (from region 1 to region 3) might lead to zonal variations in the biological response of the cultured hGFs. Our second hypothesis was that the continuous flow conditions would improve the functional activity of the cells relative to static and quasi-static conditions.

The DNA-quantification tests revealed that the DNA concentration was higher for the continuous flow samples (FS) compared to the low flow (quasi-static) samples (LFS) for days 7 and 28. This might be due to the provision of the necessary mass transport conditions that trigger cellular growth and proliferation for the continuous flow cultures. Another possible explanation would be up-regulation of epidermal growth factor (EGF) due to perfusion induced stimulation that directs the enrichment of DNA content.[94]

Assessment of cellular metabolic activity showed significant differences in cell activity between regions 1 and 3 for both low flow samples (LFS) and flow samples (FS) at day

28, also showing a progressive decrease in activity over time. McGuigan *et al.*[438] observed a similar trend of a decrease in cellular metabolic activity over time with the human umbilical vein endothelial cells (HUVECs) seeded on polyethylene-based constructs. The slower growth associated with the lower cellular metabolic activity under continuous flow conditions correlates well with the cell density data. Reduced or slowing metabolic activity of the hGFs cultured on decellularized scaffolds and their controls has several possible explanations, including contact inhibition, a shift in environmental niche for the gingival fibroblasts due to depletion of oxygen, or other essential nutrient or metabolite.[439]

To elucidate the biological activity of the cultured hGFs *in vitro*, we furthered our studies by monitoring their expression levels for collagen types I and III (COL-I and COL-III), matrix metalloproteinase-1 and -2 (MMP-1, MMP-2), tissue inhibitor of MMP-1 (TIMP-1) and decorin. COL-I and COL-III are the most abundant ECM components of the gingival connective tissue.[37] The strongest up-regulation observed in HUV scaffolds (16.7-fold) was for COL-I that is essential for maintenance of tensile resistance and regulation of cell adhesion on the scaffold surface.[440, 441] Tissue COL- I content increases in the initial stages of wound healing due to the conversion of type III collagen to type I.[442] COL-III is not only involved in reinforcement and support of tissues, but also in vascular proliferation during the early wound healing period.[443] We found that flow-stimulated cultures did not demonstrate higher collagen producing activity compared to their static controls.

Decorin is a small leucine-rich proteoglycan (SLRP) that plays an important role in several biological events, including cell adhesion, proliferation and differentiation.[444, 445] In addition, decorin is also known to be an important mediator leading to the fibrillation process, affecting the size of the collagen fibrils and construct linkages between the collagen molecules.[446, 447] Interestingly, no significant upregulation of decorin was observed on any samples at day 7 or 28. We believe that this result could be related to the matrix transforming growth factor beta (TGFβ1) inhibiting decorin expression by the gingival fibroblasts.[448] TGFβ1 binds with high affinity to decorin to form inactive complexes.[449] Although the mechanism of action of TGFβ1 on the expression of decorin is dependent on the cell type,[450] over expression of TGFβ1 by the gingival fibroblasts may disturb the neutralization reaction with decorin, and thus suppress its expression.

Tissue remodeling events require the dynamic changes of cell-matrix interactions while regulating tissue homeostasis. An orchestrated cascade of event leads to the synthesis and degradation of extracellular proteins during remodeling. In this continuum, oral fibroblasts express the tissue degrading MMPs, such as MMP-1 and MMP-2 that cleave the bonds between collagen fibrils.[451, 452] As a regulatory action, tissue inhibitors of MMPs (TIMPs) function to suppress the activity of MMPs.[453] TIMP-1 has been proposed to be the major inhibitor of gingival tissue MMPs.[454] In addition, TIMP-1 has been suggested to be a mediator of cellular growth, differentiation and migration,[455] and renal fibrosis through inflammatory pathways.[456] It is inferred from our results that the continuous flow conditions activate the MMP-2 expression by the gingival fibroblasts, however, for the expression of MMP-1, no significant stimulatory effect by the flow conditions was noted. The studies also demonstrated a significant difference between

flow perfusion culture (5.4-fold upregulation) and static culture (no noticeable up or downregulation) in their mRNA expression levels for TIMP-1 only at day 7.

The real-time PCR results revealed regional and time-dependent changes in gene expression patterns. However, not all the regions remained above the detection level indicating relatively small RNA concentrations. To overcome this problem, small amounts of tissue RNA can be amplified using highly sensitive real-time RT-PCR techniques.[457, 458]

Histology and immunohistochemistry analyses confirm that the decellularization process effectively removed the cellular and nuclear components and the remaining HUV scaffold allowed the hGFs to attach on the scaffold surface, migrate and further proliferate. Immunolocalization of the hGFs was achieved by labeling the cells with anti-vimentin antibody. Vimentin is an intermediate filament protein of adult mammalian mesenchymal cells that plays an important role in cellular mechanics and cytoskeletal organization.[459, 460] Although not specific to human gingival fibroblasts (hGFs), positive staining for anti-vimentin in the hGF-seeded scaffolds demonstrated immunoreactivity of the protein in the cell cytoskeleton within the scaffold.[461] Cells within the 28-day bioreactor cultures were shown to migrate toward the HUV's lumenal surface in response to the nutrient gradient. Furthermore, immunolocalization in hGFs showed that cellular migration was greatly improved for the continuous flow samples (FS) compared to the low flow samples (LFS) over a 28 day culture period.

In this work, we have studied the influence of the regional variations in the bioreactor on the biological functioning of the hGFs that could be pronounced more for longer culture

durations. In addition, the current bioreactor design can be improved towards a biomimetic environment in several ways to reflect more realistic tissue integration for clinical applications, such as coating the bioreactor surfaces resembling the tooth surface (region 1) and the alveolar bone surface (region 3) with coating agents having similar composition, and circulating a blood-like fluid on the side of the bioreactor mimicking the wound site.

6.5. CONCLUSIONS

Dynamic tissue culture systems have been investigated and tested for their ability to modulate tissue repair and regeneration processes. These *in vitro* investigations are an indirect assessment of *in vivo* studies, however they are strong indicators of what we might expect with host cell/tissue. Evidence shows that mechanical stimulation coupled with the chemical composition gradients created through the scaffold enhances cell metabolic functioning, proliferation, differentiation and synthesis of the important ECM components. For future studies, *in vivo* assessments should be conducted to confirm the applicability of the HUV scaffold and the culture conditions.

CHAPTER 7

CONCLUSIONS

Tissue engineering requires the development of scaffolds and materials with a combination of biological and mechanical properties that facilitate appropriate cell-matrix interactions, and ultimately regenerate normal tissue structure and function. A further challenge, depending on the clinical situation, is that these complex biological events often must occur along with ongoing functional forces and movement. In these situations, appropriate matching of biomechanical properties between implanted materials and native tissues may be crucial.

While the studies described here may have broader clinical and biological implications, they were conducted within the context of periodontal guided tissue regeneration (GTR). In this widely employed technique, a physical barrier or scaffold is positioned between the gingival tissue and underlying bone defect. This is designed to provide a protected healing environment in which undifferentiated cells from the remaining periodontal ligament can repopulate and regenerate the defect, while the overlying barrier is gradually resorbed and incorporated into the adjacent tissues. While the feasibility and efficacy of this technique is supported by a number of clinical studies, results are not always predictable and post-operative complications, particularly barrier exposure, are common. It is obvious that the ideal materials and techniques have yet to be developed. A particular gap in knowledge is the relative lack of information regarding the

biomechanical properties of various oral tissues and how these compare to those of materials employed in periodontal GTR.

These studies began with a detailed analysis of the biomechanical properties of porcine oral soft tissues. It was found that the biomechanical properties of oral tissues were highly region-specific and correlated well with tissue architecture. Next, experiments were conducted on the human umbilical vein (HUV), as a potential scaffold material for use in periodontal GTR. Biomechanical analysis showed that the HUV mechanical properties were influenced greatly by its composite structure. Further, it was noted that the HUVs biomechanical characteristics were comparable to those of porcine tissues. Culturing human gingival fibroblasts on the HUV showed that the material demonstrated as a biologic barrier to promote cell migration and proliferation during the initial phases of tissue remodeling. In the final set of experiments, a novel bioreactor system was developed. This system provided individually adjustable flow chambers above and below the scaffold material in order to model the tissue compartments of a periodontal wound or defect. Using this system, concomitant improvement in the biological response of cells and tissue was achieved. Taken together, these studies exhibit promising results about the potential role of HUV in periodontal GTR and point toward several avenues for future periodontal research involving bioreactor technologies and many other clinical situations.

CHAPTER 8

SUMMARY AND FUTURE DIRECTIONS

In this study, the potential and further development of human umbilical vein (HUV)-derived scaffold as a guided tissue regeneration (GTR) membrane have been investigated. Besides its use as a GTR membrane, the HUV-derived scaffold could also be investigated for its application as an oral mucosal substitute. For that purpose, the co-culture of the HUV membrane with both human gingival fibroblasts (hGFs) on the ablumenal surface and the oral keratinocytes on the lumenal side is essential. Therefore, as further steps of the project, the potential of the decellularized HUV to support keratinization when seeded with oral keratinocytes on its lumenal side should be examined.

During the culture of the HUV membrane under static and dynamic conditions, the gas concentration of the culture environment was kept constant as 5% CO_2 and 95% air. Gas tensions are important modulators of wound healing. Therefore, the potential of the HUV and bioreactor as an ideal experimental system with which to further our understanding of important biological events such as the interaction of various oral tissue cells, hypoxia and wound healing within and across a complex natural tissue matrix needs to be investigated. By using the modified bioreactor and dual circuit process flow, the O_2 tension will be modulated and the regenerative capacity of the HUV bioscaffold will be quantified by assessing proliferation, migration and remodeling activity of hGF.

Bacterial contamination of implanted GTR membranes is particularly important in any attempt to regenerate oral tissues, where appropriate biological events must take place in the presence of oral bacteria, generally in the form of complex biofilms. This is a key clinical problem in periodontal GTR, where the physical barriers used often become exposed directly to the oral environment during early wound healing after periodontal surgery.[462] Clinical research indicates that early colonization of these materials does impair fibroblast migration into the healing periodontal wound.[463] *In vitro* work has shown that both periodontal pathogens and streptococcal organisms readily colonize both collagen and synthetic GTR barriers and interfere with periodontal ligament cell attachment.[464] In the light of these previous findings, a study for the quantification of bacterial invasion through the HUV bioscaffold should be conducted.

In addition to the continued assessment of the processed HUV as a novel periodontal soft tissue repair scaffold, there is the potential of the HUV and bioreactor as an ideal experimental system with which to further our understanding of important biological events such as the interaction of various oral tissue cells, and host-bacterial interactions within and across a complex natural tissue matrix. By continuing development of the tissue bioscaffold and bioreactor based perfusion culture system, a number of opportunities can be explored to enhance the performance of the soft tissue matrix, such as: Surgical implantation to assess biocompatibility and regenerative capacity of the tissue bioscaffold, Micro-encapsulation technology can be used to deliver time-released antibiotics or growth factors to enhance tissue repair.

References

1. Albandar JM, Kingman A. Gingival recession, gingival bleeding, and dental calculus in adults 30 years of age and older in the United States, 1988-1994. J Periodontol 1999;70:30-43.
2. Drisko CH. Trends in surgical and nonsurgical periodontal treatment. J Am Dent Assoc 2000;131:31S-38S.
3. Wang HL, Cooke J. Periodontal regeneration techniques for treatment of periodontal diseases. Dent Clin North Am 2005;49:637-659.
4. Alpiste Illueca FM, Buitrago Vera P, de Grado Cabanilles P, Fuenmayor Fernandez V, Gil Loscos FJ. Periodontal regeneration in clinical practice. Med Oral Patol Oral Cir Bucal 2006;11:E382-392.
5. O'Neal R, Wang HL, MacNeil RL, Somerman MJ. Cells and materials involved in guided tissue regeneration. Curr Opin Periodontol 1994:141-156.
6. Haney JM, Nilveus RE, McMillan PJ, Wikesjo UM. Periodontal repair in dogs: expanded polytetrafluoroethylene barrier membranes support wound stabilization and enhance bone regeneration. J Periodontol 1993;64:883-890.
7. Warrer K, Karring T. Guided tissue regeneration combined with osseous grafting in suprabony periodontal lesions. An experimental study in the dog. J Clin Periodontol 1992;19:373-380.
8. Chen FM, Zhang J, Zhang M, An Y, Chen F, Wu ZF. A review on endogenous regenerative technology in periodontal regenerative medicine. Biomaterials 2010;31:7892-7927.
9. Aukhil I, Nishimura K, Fernyhough W. Experimental regeneration of the periodontium. Crit Rev Oral Biol Med 1990;1:101-115.
10. Salonen JI, Persson GR. Migration of epithelial cells on materials used in guided tissue regeneration. J Periodontal Res 1990;25:215-221.
11. Locci P, Calvitti M, Belcastro S, Pugliese M, Guerra M, Marinucci L, Staffolani N, Becchetti E. Phenotype expression of gingival fibroblasts cultured on membranes used in guided tissue regeneration. J Periodontol 1997;68:857-863.

12. Alpar B, Leyhausen G, Gunay H, Geurtsen W. Compatibility of resorbable and nonresorbable guided tissue regeneration membranes in cultures of primary human periodontal ligament fibroblasts and human osteoblast-like cells. Clin Oral Investig 2000;4:219-225.
13. Bashutski JD, Wang HL. Periodontal and endodontic regeneration. J Endod 2009;35:321-328.
14. Mei F, Zhong J, Yang X, Ouyang X, Zhang S, Hu X, Ma Q, Lu J, Ryu S, Deng X. Improved biological characteristics of poly(L-lactic acid) electrospun membrane by incorporation of multiwalled carbon nanotubes/hydroxyapatite nanoparticles. Biomacromolecules 2007;8:3729-3735.
15. Zhang S, Huang Y, Yang X, Mei F, Ma Q, Chen G, Ryu S, Deng X. Gelatin nanofibrous membrane fabricated by electrospinning of aqueous gelatin solution for guided tissue regeneration. J Biomed Mater Res A 2009;90:671-679.
16. Stewart SF, Lyman DJ. Effects of a vascular graft/natural artery compliance mismatch on pulsatile flow. J Biomech 1992;25:297-310.
17. O'Brien T, Morris L, Walsh M, McGloughlin T. That hemodynamics and not material mismatch is of primary concern in bypass graft failure: an experimental argument. J Biomech Eng 2005;127:881-886.
18. Altman GH, Horan RL, Lu HH, Moreau J, Martin I, Richmond JC, Kaplan DL. Silk matrix for tissue engineered anterior cruciate ligaments. Biomaterials 2002;23:4131-4141.
19. Dey J, Xu H, Nguyen KT, Yang J. Crosslinked urethane doped polyester biphasic scaffolds: Potential for in vivo vascular tissue engineering. J Biomed Mater Res A 2010;95:361-370.
20. Bankowski E, Sobolewski K, Romanowicz L, Chyczewski L, Jaworski S. Collagen and glycosaminoglycans of Wharton's jelly and their alterations in EPH-gestosis. Eur J Obstet Gynecol Reprod Biol 1996;66:109-117.
21. Bartold PM, Narayanan AS. The biochemistry and physiology of the periodontium In: Wilson TG, Kornman KS, eds. Fundamentals of periodontics. Carol Stream: Quintessence Publishing Co., Inc.; 1996: 61-87.

22. Bourke KA, Haase H, Li H, Daley T, Bartold PM. Distribution and synthesis of elastin in porcine gingiva and alveolar mucosa. J Periodontal Res 2000;35:361-368.
23. Bratt P, Anderson MM, Mansson-Rahemtulla B, Stevens JW, Zhou C, Rahemtulla F. Isolation and characterization of bovine gingival proteoglycans versican and decorin. Int J Biochem 1992;24:1573-1583.
24. Gogiel T, Bankowski E, Jaworski S. Proteoglycans of Wharton's jelly. Int J Biochem Cell Biol 2003;35:1461-1469.
25. Larjava H, Hakkinen L, Rahemtulla F. A biochemical analysis of human periodontal tissue proteoglycans. Biochem J 1992;284:267-274.
26. Li WC, Zhang HM, Wang PJ, Xi GM, Wang HQ, Chen Y, Deng ZH, Zhang ZH, Huang TZ. Quantitative analysis of the microstructure of human umbilical vein for assessing feasibility as vessel substitute. Ann Vasc Surg 2008;22:417-424.
27. Shibutani T, Murahashi Y, Iwayama Y. Immunohistochemical localization of chondroitin sulfate and dermatan sulfate proteoglycan in human gingival connective tissue. J Periodontal Res 1989;24:310-313.
28. Valiyaveettil M, Achur RN, Muthusamy A, Gowda DC. Characterization of chondroitin sulfate and dermatan sulfate proteoglycans of extracellular matrices of human umbilical cord blood vessels and Wharton's jelly. Glycoconj J 2004;21:361-375.
29. Goktas S, Pierre N, Abe K, Dmytryk J, McFetridge PS. Cellular interactions and biomechanical properties of a unique vascular-derived scaffold for periodontal tissue regeneration. Tissue Eng Part A 2010;16:769-780.
30. Li WC, Ruan XZ, Zhang HM, Zeng YJ. Biomechanical properties of different segments of human umbilical cord vein and its value for clinical application. J Biomed Mater Res B Appl Biomater 2006;76:93-97.
31. Sobolewski K, Malkowski A, Bankowski E, Jaworski S. Wharton's jelly as a reservoir of peptide growth factors. Placenta 2005;26:747-752.
32. Hiramatsu M, Abe I, Minami N. Acid mucopolysaccharides in porcine gingiva. J Periodontal Res 1978;13:224-231.

33. Shabana AH, Ouhayoun JP, Sawaf MH, Forest N. A comparative biochemical and immunological analysis of cytokeratin patterns in the oral epithelium of the miniature pig and man. Arch Oral Biol 1989;34:249-259.
34. Pae A, Lee H, Kim HS, Kwon YD, Woo YH. Attachment and growth behaviour of human gingival fibroblasts on titanium and zirconia ceramic surfaces. Biomed Mater 2009;4:025005.
35. Stegemann JP, Nerem RM. Phenotype modulation in vascular tissue engineering using biochemical and mechanical stimulation. Ann Biomed Eng 2003;31:391-402.
36. Freed LE, Vunjak-Novakovic G. Tissue Engineering Bioreactors. In: Lanza RP, Langer RP, eds. Principles of tissue engineering. New York: Academic Press; 2000: 143-154.
37. Bartold PM, Narayanan AS. Biology of the periodontal connective tissues. Carol Stream: Quintessence Publishing Co, Inc.; 1998.
38. de Graaff J, van Winkelhoff AJ, Goene RJ. The role of Actinobacillus actinomycetemcomitans in periodontal disease. Infection 1989;17:269-271.
39. Zambon JJ, Umemoto T, De Nardin E, Nakazawa F, Christersson LA, Genco RJ. Actinobacillus actinomycetemcomitans in the pathogenesis of human periodontal disease. Adv Dent Res 1988;2:269-274.
40. Amano A. Molecular interaction of Porphyromonas gingivalis with host cells: implication for the microbial pathogenesis of periodontal disease. J Periodontol 2003;74:90-96.
41. Hasebe A, Yoshimura A, Into T, Kataoka H, Tanaka S, Arakawa S, Ishikura H, Golenbock DT, Sugaya T, Tsuchida N, Kawanami M, Hara Y, Shibata K. Biological activities of Bacteroides forsythus lipoproteins and their possible pathological roles in periodontal disease. Infect Immun 2004;72:1318-1325.
42. Tan KS, Song KP, Ong G. Bacteroides forsythus prtH genotype in periodontitis patients: occurrence and association with periodontal disease. J Periodontal Res 2001;36:398-403.

43. Ojima M, Hanioka T. Destructive effects of smoking on molecular and genetic factors of periodontal disease. Tob Induc Dis 2010;8:4.
44. Zee KY. Smoking and periodontal disease. Aust Dent J 2009;54:S44-50.
45. Tezal M, Grossi SG, Ho AW, Genco RJ. The effect of alcohol consumption on periodontal disease. J Periodontol 2001;72:183-189.
46. Tezal M, Grossi SG, Ho AW, Genco RJ. Alcohol consumption and periodontal disease. The Third National Health and Nutrition Examination Survey. J Clin Periodontol 2004;31:484-488.
47. Genco RJ, Loe H. The role of systemic conditions and disorders in periodontal disease. Periodontol 2000 1993;2:98-116.
48. Kim J, Amar S. Periodontal disease and systemic conditions: a bidirectional relationship. Odontology 2006;94:10-21.
49. Tuncer O, Mutlu S, Scully C, eds. Periodontal Tissue Destruction and Remodelling. Istanbul: Quintessence Ltd.; 2003.
50. Reners M, Brecx M. Stress and periodontal disease. Int J Dent Hyg 2007;5:199-204.
51. Green LW, Tryon WW, Marks B, Huryn J. Periodontal disease as a function of life events stress. J Human Stress 1986;12:32-36.
52. Chen FM, Jin Y. Periodontal tissue engineering and regeneration: current approaches and expanding opportunities. Tissue Eng Part B Rev 2010;16:219-255.
53. Squier CA, Johnson NW, Hopps RM. Human oral mucosa:development, structure and function. Oxford: Blackwell Scientific Publications; 1976.
54. Winning TA, Townsend GC. Oral mucosal embryology and histology. Clin Dermatol 2000;18:499-511.
55. Bartold PM, Wiebkin OW, Thonard JC. Glycosaminoglycans of human gingival epithelium and connective tissue. Connect Tissue Res 1981;9:99-106.
56. Bartold PM, Wiebkin OW, Thonard JC. Proteoglycans of human gingival epithelium and connective tissue. Biochem J 1983;211:119-127.

57. Bartold PM, Walsh LJ, Narayanan AS. Molecular and cell biology of the gingiva. Periodontol 2000 2000;24:28-55.
58. Meyer J, Squier CA, Gerson SJ, eds. The structure and function of oral mucosa. Oxford: Pergamon Press; 1984.
59. Slavkin HC, Bavetta LA. Developmental Aspects of Oral Biology. New York: Academic Press, Inc.; 1972.
60. Lozdan J. Studies on the mucogingival junction. Dent Pract Dent Rec 1970;20:379-384.
61. Redlich M, Shoshan S, Palmon A. Gingival response to orthodontic force. Am J Orthod Dentofacial Orthop 1999;116:152-158.
62. Porter K, Dooner JJ, Lopez A. Further study of elastic fibers in human attached gingiva. J Periodontol 1977;48:711-713.
63. Ginwalla TM, Da Cunha-Gomes B, Kumar AJ. Determination of the existence or otherwise of elastic fibres in human gingiva. J Indian Dent Assoc 1969;41:115-124.
64. Rosenbloom J, Abrams WR, Mecham R. Extracellular matrix 4: the elastic fiber. FASEB J 1993;7:1208-1218.
65. Jacob MP, Badier-Commander C, Fontaine V, Benazzoug Y, Feldman L, Michel JB. Extracellular matrix remodeling in the vascular wall. Pathol Biol (Paris) 2001;49:326-332.
66. Cleary EG, Gibson MA. Elastic tissue, elastin and elastin associated microfibrils. In: Comper WD, ed. Extracellular matrix. Amsterdam: Harwood Academic Press; 1996.
67. Fullmer HM, Lillie RD. The oxytalan fiber: a previously undescribed connective tissue fiber. J Histochem Cytochem 1958;6:425-430.
68. Chavrier C, Hartmann DJ, Couble ML, Herbage D. Distribution and organization of the elastic system fibres in healthy human gingiva. Ultrastructural and immunohistochemical study. Histochemistry 1988;89:47-52.
69. Meyer J, Gerson SJ. A Comparison of Human Palatal and Buccal Mucosa. Periodontics 1964;2:284-291.

70. Kydd WL, Stroud W, Moffett BC, Jr., Tamarin A. The effect of mechanical stress on oral mucoperiosteum of dogs. Arch Oral Biol 1969;14:921-933.
71. Dahllof G, Modeer T, Reinholt FP, Wikstrom B, Hjerpe A. Proteoglycans and glycosaminoglycans in phenytoin-induced gingival overgrowth. J Periodontal Res 1986;21:13-21.
72. Bartold PM, Wiebkin OW, Thonard JC. Proteoglycans in human gingiva: molecular size distribution in epithelium and in connective tissue. Arch Oral Biol 1982;27:1-7.
73. Purvis JA, Embery G, Oliver WM. Molecular size distribution of proteoglycans in human inflamed gingival tissue. Arch Oral Biol 1984;29:513-519.
74. Schroeder HE, Munzel-Pedrazzoli S, Page R. Correlated morphometric and biochemical analysis of gingival tissue in early chronic gingivitis in man. Arch Oral Biol 1973;18:899-923.
75. Moharamzadeh K, Brook IM, Van Noort R, Scutt AM, Thornhill MH. Tissue-engineered oral mucosa: a review of the scientific literature. J Dent Res 2007;86:115-124.
76. Butler WT, Birkedal-Hansen H, Beegle WF, Taylor RE, Chung E. Proteins of the periodontium. Identification of collagens with the [alpha1(I)]2alpha2 and [alpha1(III)]3 structures in bovine periodontal ligament. J Biol Chem 1975;250:8907-8912.
77. Sodek J, Limeback HF. Comparison of the rates of synthesis, conversion, and maturation of type I and type III collagens in rat periodontal tissues. J Biol Chem 1979;254:10496-10502.
78. Hakkinen L, Oksala O, Salo T, Rahemtulla F, Larjava H. Immunohistochemical localization of proteoglycans in human periodontium. J Histochem Cytochem 1993;41:1689-1699.
79. Mariotti A. The extracellular matrix of the periodontium: dynamic and interactive tissues. Periodontol 2000 1993;3:39-63.
80. Wang HM, Nanda V, Rao LG, Melcher AH, Heersche JN, Sodek J. Specific immunohistochemical localization of type III collagen in porcine periodontal

tissues using the peroxidase-antiperoxidase method. J Histochem Cytochem 1980;28:1215-1223.

81. Sodek J, McKee MD. Molecular and cellular biology of alveolar bone. Periodontol 2000 2000;24:99-126.
82. Bartold PM. A biochemical and immunohistochemical study of the proteoglycans of alveolar bone. J Dent Res 1990;69:7-19.
83. Birkedal-Hansen H, Butler WT, Taylor RE. Proteins of the periodontium. Characterization of the insoluble collagens of bovine dental cementum. Calcif Tissue Res 1977;23:39-44.
84. MacNeil RL, Thomas HF. Development of the murine periodontium. I. Role of basement membrane in formation of a mineralized tissue on the developing root dentin surface. J Periodontol 1993;64:95-102.
85. Reichert T, Storkel S, Becker K, Fisher LW. The role of osteonectin in human tooth development: an immunohistological study. Calcif Tissue Int 1992;50:468-472.
86. Yamamoto T, Domon T, Takahashi S, Arambawatta AK, Wakita M. Immunolocation of proteoglycans and bone-related noncollagenous glycoproteins in developing acellular cementum of rat molars. Cell Tissue Res 2004;317:299-312.
87. Wolf HF, Rateitschak EM, Rateitschak KH, Hassell TM. Periodontology. In: Rateitschak KH, Wolf HF, eds. Color atlas of dental medicine. New York; Thieme: 1989.
88. Nanci A, Bosshardt DD. Structure of periodontal tissues in health and disease. Periodontol 2000 2006;40:11-28.
89. Koka S, Reinhardt RA. Periodontal pathogen-related stimulation indicates unique phenotype of primary cultured human fibroblasts from gingiva and periodontal ligament: implications for oral health disease. J Prosthet Dent 1997;77:191-196.
90. Graves DT, Cochran D. The contribution of interleukin-1 and tumor necrosis factor to periodontal tissue destruction. J Periodontol 2003;74:391-401.

91. Sakaki H, Matsumiya T, Kusumi A, Imaizumi T, Satoh H, Yoshida H, Satoh K, Kimura H. Interleukin-1beta induces matrix metalloproteinase-1 expression in cultured human gingival fibroblasts: role of cyclooxygenase-2 and prostaglandin E2. Oral Dis 2004;10:87-93.
92. Barnett ML, Gilman RM, Charles CH, Bartels LL. Computer-based thermal imaging of human gingiva: preliminary investigation. J Periodontol 1989;60:628-633.
93. Narayanan AS, Page RC. Biosynthesis and regulation of type V collagen in diploid human fibroblasts. J Biol Chem 1983;258:11694-11699.
94. Narayanan AS, Page RC. Connective tissues of the periodontium: a summary of current work. Coll Relat Res 1983;3:33-64.
95. Page RC, Narayanan AS, Schroeder HE. Connective tissue composition and collagen synthesis in diseased and normal gingiva of adult dogs with spontaneous periodontitis. Arch Oral Biol 1980;25:727-736.
96. Flieder DE, Sun CN, Schneider BC. Chemistry of normal and inflamed human gingival tissues. Periodontics 1966;4:302-307.
97. Manakil JF, Sugerman PB, Li H, Seymour GJ, Bartold PM. Cell-surface proteoglycan expression by lymphocytes from peripheral blood and gingiva in health and periodontal disease. J Dent Res 2001;80:1704-1710.
98. Oksala O, Salo T, Tammi R, Hakkinen L, Jalkanen M, Inki P, Larjava H. Expression of proteoglycans and hyaluronan during wound healing. J Histochem Cytochem 1995;43:125-135.
99. Bartold PM, Page RC. The effect of chronic inflammation on gingival connective tissue proteoglycans and hyaluronic acid. J Oral Pathol 1986;15:367-374.
100. Gailit J, Clark RA. Wound repair in the context of extracellular matrix. Curr Opin Cell Biol 1994;6:717-725.
101. Wong ME, Hollinger JO, Pinero GJ. Integrated processes responsible for soft tissue healing. Oral Surg Oral Med Oral Pathol Oral Radiol Endod 1996;82:475-492.

102. Goslen JB. Wound healing for the dermatologic surgeon. J Dermatol Surg Oncol 1988;14:959-972.
103. Bartold PM, Narayanan AS. Molecular and cell biology of healthy and diseased periodontal tissues. Periodontol 2000 2006;40:29-49.
104. Knowles GC, McKeown M, Sodek J, McCulloch CA. Mechanism of collagen phagocytosis by human gingival fibroblasts: importance of collagen structure in cell recognition and internalization. J Cell Sci 1991;98:551-558.
105. Clark RAF, Ghosh K, Tonnesen MG. Tissue Engineering for Cutaneous Wounds Journal of Investigative Dermatology 2007;127:1018-1029.
106. Schultz GS, Wysocki A. Interactions between extracellular matrix and growth factors in wound healing. Wound Repair Regen 2009;17:153-162.
107. Barrientos S, Stojadinovic O, Golinko MS, Brem H, Tomic-Canic M. Growth factors and cytokines in wound healing. Wound Repair Regen 2008;16:585-601.
108. Bartold PM, Raben A. Growth factor modulation of fibroblasts in simulated wound healing. J Periodontal Res 1996;31:205-216.
109. van Beurden HE, Snoek PA, Von den Hoff JW, Torensma R, Kuijpers-Jagtman AM. Fibroblast subpopulations in intra-oral wound healing. Wound Repair Regen 2003;11:55-63.
110. Schroeder HE, Listgarten MA. The gingival tissues: the architecture of periodontal protection. Periodontol 2000 1997;13:91-120.
111. Kaigler D, Cirelli JA, Giannobile WV. Growth factor delivery for oral and periodontal tissue engineering. Expert Opin Drug Deliv 2006;3:647-662.
112. Giannobile WV. Periodontal tissue engineering by growth factors. Bone 1996;19:23S-37S.
113. Anusaksathien O, Giannobile WV. Growth factor delivery to re-engineer periodontal tissues. Curr Pharm Biotechnol 2002;3:129-139.
114. Hantash BM, Zhao L, Knowles JA, Lorenz HP. Adult and fetal wound healing. Front Biosci 2008;13:51-61.

115. Grazul-Bilska AT, Johnson ML, Bilski JJ, Redmer DA, Reynolds LP, Abdullah A, Abdullah KM. Wound healing: the role of growth factors. Drugs Today (Barc) 2003;39:787-800.
116. Murakami S, Takayama S, Ikezawa K, Shimabukuro Y, Kitamura M, Nozaki T, Terashima A, Asano T, Okada H. Regeneration of periodontal tissues by basic fibroblast growth factor. J Periodontal Res 1999;34:425-430.
117. Bertolami CN, Messadi DV. The role of proteoglycans in hard and soft tissue repair. Crit Rev Oral Biol Med 1994;5:311-337.
118. Jarvelainen H, Puolakkainen P, Pakkanen S, Brown EL, Hook M, Iozzo RV, Sage EH, Wight TN. A role for decorin in cutaneous wound healing and angiogenesis. Wound Repair Regen 2006;14:443-452.
119. Worapamorn W, Xiao Y, Li H, Young WG, Bartold PM. Differential expression and distribution of syndecan-1 and -2 in periodontal wound healing of the rat. J Periodontal Res 2002;37:293-299.
120. Maruyama H, Aoki A, Sasaki KM, Takasaki AA, Iwasaki K, Ichinose S, Oda S, Ishikawa I, Izumi Y. The effect of chemical and/or mechanical conditioning on the Er:YAG laser-treated root cementum: analysis of surface morphology and periodontal ligament fibroblast attachment. Lasers Surg Med 2008;40:211-222.
121. Terranova VP, Franzetti LC, Hic S, DiFlorio RM, Lyall RM, Wikesjo UM, Baker PJ, Christersson LA, Genco RJ. A biochemical approach to periodontal regeneration: tetracycline treatment of dentin promotes fibroblast adhesion and growth. J Periodontal Res 1986;21:330-337.
122. Baker PJ, Rotch HA, Trombelli L, Wikesjo UM. An in vitro screening model to evaluate root conditioning protocols for periodontal regenerative procedures. J Periodontol 2000;71:1139-1143.
123. Boyko GA, Melcher AH, Brunette DM. Formation of new periodontal ligament by periodontal ligament cells implanted in vivo after culture in vitro. A preliminary study of transplanted roots in the dog. J Periodontal Res 1981;16:73-88.

124. Lang H, Schuler N, Arnhold S, Nolden R, Mertens T. Formation of differentiated tissues in vivo by periodontal cell populations cultured in vitro. J Dent Res 1995;74:1219-1225.
125. Dogan A, Ozdemir A, Kubar A, Oygur T. Assessment of periodontal healing by seeding of fibroblast-like cells derived from regenerated periodontal ligament in artificial furcation defects in a dog: a pilot study. Tissue Eng 2002;8:273-282.
126. Dogan A, Ozdemir A, Kubar A, Oygur T. Healing of artificial fenestration defects by seeding of fibroblast-like cells derived from regenerated periodontal ligament in a dog: a preliminary study. Tissue Eng 2003;9:1189-1196.
127. Nakahara T, Nakamura T, Kobayashi E, Kuremoto K, Matsuno T, Tabata Y, Eto K, Shimizu Y. In situ tissue engineering of periodontal tissues by seeding with periodontal ligament-derived cells. Tissue Eng 2004;10:537-544.
128. Song AM, Shu R, Xie YF, Song ZC, Li HY, Liu XF, Zhang XL. A study of enamel matrix proteins on differentiation of porcine bone marrow stromal cells into cementoblasts. Cell Prolif 2007;40:381-396.
129. Liu Y, Zheng Y, Ding G, Fang D, Zhang C, Bartold PM, Gronthos S, Shi S, Wang S. Periodontal ligament stem cell-mediated treatment for periodontitis in miniature swine. Stem Cells 2008;26:1065-1073.
130. Bosshardt DD. Are cementoblasts a subpopulation of osteoblasts or a unique phenotype? J Dent Res 2005;84:390-406.
131. Kawaguchi H, Hirachi A, Hasegawa N, Iwata T, Hamaguchi H, Shiba H, Takata T, Kato Y, Kurihara H. Enhancement of periodontal tissue regeneration by transplantation of bone marrow mesenchymal stem cells. J Periodontol 2004;75:1281-1287.
132. Tobita M, Uysal AC, Ogawa R, Hyakusoku H, Mizuno H. Periodontal tissue regeneration with adipose-derived stem cells. Tissue Eng Part A 2008;14:945-953.
133. Han X, Amar S. Identification of genes differentially expressed in cultured human periodontal ligament fibroblasts vs. human gingival fibroblasts by DNA microarray analysis. J Dent Res 2002;81:399-405.

134. Giannopoulou C, Cimasoni G. Functional characteristics of gingival and periodontal ligament fibroblasts. J Dent Res 1996;75:895-902.
135. Ohshima M, Kuwata F, Otsuka K, Saito R, Sato K, Shioji S, Suzuki K. Alkaline phosphatase activities of cultured human periodontal ligament cells. J Nihon Univ Sch Dent 1988;30:208-217.
136. Somerman MJ, Archer SY, Imm GR, Foster RA. A comparative study of human periodontal ligament cells and gingival fibroblasts in vitro. J Dent Res 1988;67:66-70.
137. Somerman MJ, Foster RA, Imm GM, Sauk JJ, Archer SY. Periodontal ligament cells and gingival fibroblasts respond differently to attachment factors in vitro. J Periodontol 1989;60:73-77.
138. Oates TW, Maller SC, West J, Steffensen B. Human gingival fibroblast integrin subunit expression on titanium implant surfaces. J Periodontol 2005;76:1743-1750.
139. Burridge K. Substrate adhesions in normal and transformed fibroblasts: Organization and regulation of cytoskeletal, membrane and extracellular matrix components at focal contacts. Cancer Reviews 1986;4:18-78.
140. Burridge K, Molony L, Kelly T. Adhesion plaques: sites of transmembrane interaction between the extracellular matrix and the actin cytoskeleton. J Cell Sci Suppl 1987;8:211-229.
141. Iles RK. The Cell. In: Nargund VH, Raghavan D, Sandler HM, eds. Urological Oncology. London: Springer-Verlag; 2008: 3-36.
142. Payne JM, Cobb CM, Rapley JW, Killoy WJ, Spencer P. Migration of human gingival fibroblasts over guided tissue regeneration barrier materials. J Periodontol 1996;67:236-244.
143. Taba M, Jr., Jin Q, Sugai JV, Giannobile WV. Current concepts in periodontal bioengineering. Orthod Craniofac Res 2005;8:292-302.
144. Tsuruga E, Irie K, Sakakura Y, Yajima T. Tropoelastin expression by periodontal fibroblasts. J Dent Res 2002;81:198-202.

145. Birkedal-Hansen H, Cobb CM, Taylor RE, Fullmer HM. Synthesis and release of procollagenase by cultured fibroblasts. J Biol Chem 1976;251:3162-3168.
146. Yamasaki A, Rose GG, Mahan CJ. Collagen degradation by human gingival fibroblasts. I. In vivo phagocytosis. J Periodontal Res 1981;16:309-322.
147. Heath JK, Gowen M, Meikle MC, Reynolds JJ. Human gingival tissues in culture synthesize three metalloproteinases and a metalloproteinase inhibitor. J Periodontal Res 1982;17:183-190.
148. Stein E, Blaimauer K, Bauer S, Erovic BM, Turhani D, Thurnher D. High expression of integrin beta1 correlates with high proliferation capacity in oral keratinocytes. Wien Klin Wochenschr 2007;119:318-322.
149. Izumi K, Song J, Feinberg SE. Development of a tissue-engineered human oral mucosa: from the bench to the bed side. Cells Tissues Organs 2004;176:134-152.
150. Moriyama T, Asahina I, Ishii M, Oda M, Ishii Y, Enomoto S. Development of composite cultured oral mucosa utilizing collagen sponge matrix and contracted collagen gel: a preliminary study for clinical applications. Tissue Eng 2001;7:415-427.
151. Rouabhia M, Deslauriers N. Production and characterization of an in vitro engineered human oral mucosa. Biochem Cell Biol 2002;80:189-195.
152. Sanchez-Quevedo MC, Alaminos M, Capitan LM, Moreu G, Garzon I, Crespo PV, Campos A. Histological and histochemical evaluation of human oral mucosa constructs developed by tissue engineering. Histol Histopathol 2007;22:631-640.
153. Jones GL, Walton R, Czernuszka J, Griffiths SL, El Haj AJ, Cartmell SH. Primary human osteoblast culture on 3D porous collagen-hydroxyapatite scaffolds. J Biomed Mater Res A 2010;94:1244-1250.
154. Carrubba VL, Pavia FC, Brucato V, Piccarolo S, Ghersi G. PLLA biodegradable scaffolds for angiogenesis via Diffusion Induced Phase Separation (DIPS). The international journal of material forming 2008;1:623-626.
155. Rompen E, Domken O, Degidi M, Pontes AE, Piattelli A. The effect of material characteristics, of surface topography and of implant components and connections

on soft tissue integration: a literature review. Clin Oral Implants Res 2006;17:55-67.

156. Norotte C, Marga FS, Niklason LE, Forgacs G. Scaffold-free vascular tissue engineering using bioprinting. Biomaterials 2009;30:5910-5917.

157. Nabers CL. Long-term results of autogenous bone grafts. Int J Periodontics Restorative Dent 1984;4:50-67.

158. Ames JR, Ryan DE, Maki KA. The autogenous particulate cancellous bone marrow graft in alveolar clefts. A report of forty-one cases. Oral Surg Oral Med Oral Pathol 1981;51:588-591.

159. Garrett S. Periodontal regeneration around natural teeth. Ann Periodontol 1996;1:621-666.

160. Friedlaender GE. Bone grafts. The basic science rationale for clinical applications. J Bone Joint Surg Am 1987;69:786-790.

161. Anusaksathien O, Jin QM, Ma PX, Giannobile WV. Scaffolding in Periodontal Engineering. In: Ma PX, Elisseeff J, eds. Scaffolding in Tissue Engineering. Boca Raton: CRC Press Taylor & Francis Group; 2006: 437-454.

162. Yang YG, Sykes M. Xenotransplantation: current status and a perspective on the future. Nat Rev Immunol 2007;7:519-531.

163. Shetty V, Han TJ. Alloplastic materials in reconstructive periodontal surgery. Dent Clin North Am 1991;35:521-530.

164. Zeichner-David M. Regeneration of periodontal tissues: cementogenesis revisited. Periodontol 2000 2006;41:196-217.

165. Bartold PM, Narayanan AS. Biology of the Periodontal Connective Tissues. Illinois: Quintessence Publishing Co., Inc.; 1998.

166. Bartold PM, McCulloch CA, Narayanan AS, Pitaru S. Tissue engineering: a new paradigm for periodontal regeneration based on molecular and cell biology. Periodontol 2000 2000;24:253-269.

167. Nyman S, Lindhe J, Karring T, Rylander H. New attachment following surgical treatment of human periodontal disease. J Clin Periodontol 1982;9:290-296.

168. Wikesjo UM, Nilveus RE, Selvig KA. Significance of early healing events on periodontal repair: a review. J Periodontol 1992;63:158-165.
169. Gottlow J, Nyman S, Karring T, Lindhe J. New attachment formation as the result of controlled tissue regeneration. J Clin Periodontol 1984;11:494-503.
170. Minabe M. A critical review of the biologic rationale for guided tissue regeneration. J Periodontol 1991;62:171-179.
171. Gottlow J. Guided tissue regeneration using bioresorbable and non-resorbable devices: initial healing and long-term results. J Periodontol 1993;64:1157-1165.
172. Kamin S, Ghani SHA. Dehiscence Treated with Non-resorbable Gore-Tex Membrane-A Case Report. Annals of Dentistry, University Malaya 1996;3:61-64.
173. Murphy KG. Postoperative healing complications associated with Gore-Tex Periodontal Material. Part II. Effect of complications on regeneration. Int J Periodontics Restorative Dent 1995;15:548-561.
174. Proussaefs P, Lozada J. The use of resorbable collagen membrane in conjunction with autogenous bone graft and inorganic bovine mineral for buccal/labial alveolar ridge augmentation: a pilot study. J Prosthet Dent 2003;90:530-538.
175. Rothamel D, Schwarz F, Sculean A, Herten M, Scherbaum W, Becker J. Biocompatibility of various collagen membranes in cultures of human PDL fibroblasts and human osteoblast-like cells. Clin Oral Implants Res 2004;15:443-449.
176. Callan DP, Silverstein LH. Use of acellular dermal matrix for increasing keratinized tissue around teeth and implants. Pract Periodontics Aesthet Dent 1998;10:731-734.
177. Henderson RD, Drisko CH, Greenwell H. Root coverage using Alloderm acellular dermal graft material. J Contemp Dent Pract 1999;1:24-30.
178. Keith JD, Jr., Salama MA. Ridge preservation and augmentation using regenerative materials to enhance implant predictability and esthetics. Compend Contin Educ Dent 2007;28:614-621.

179. Sudarsan S, Arun KV, Priya MS, Arun R. Clinical and histological evaluation of alloderm GBR and BioOss in the treatment of Siebert's class I ridge deficiency. J Indian Soc Periodontol 2008;12:73-78.
180. Taskonak B, Ozkan Y. An alveolar bone augmentation technique to improve esthetics in anterior ceramic FPDs: a clinical report. J Prosthodont 2006;15:32-36.
181. Livesey SA, Herndon DN, Hollyoak MA, Atkinson YH, Nag A. Transplanted acellular allograft dermal matrix. Potential as a template for the reconstruction of viable dermis. Transplantation 1995;60:1-9.
182. Becker W, Becker BE, Berg L, Prichard J, Caffesse R, Rosenberg E. New attachment after treatment with root isolation procedures: report for treated Class III and Class II furcations and vertical osseous defects. Int J Periodontics Restorative Dent 1988;8:8-23.
183. Gottlow J, Nyman S, Lindhe J, Karring T, Wennstrom J. New attachment formation in the human periodontium by guided tissue regeneration. Case reports. J Clin Periodontol 1986;13:604-616.
184. Nygaard-Ostby P, Bakke V, Nesdal O, Nilssen HK, Susin C, Wikesjo UM. Periodontal healing following reconstructive surgery: effect of guided tissue regeneration using a bioresorbable barrier device when combined with autogenous bone grafting. A randomized controlled clinical trial. J Clin Periodontol 2008;35:37-43.
185. Nyman S, Gottlow J, Lindhe J, Karring T, Wennstrom J. New attachment formation by guided tissue regeneration. J Periodontal Res 1987;22:252-254.
186. Pontoriero R, Lindhe J, Nyman S, Karring T, Rosenberg E, Sanavi F. Guided tissue regeneration in degree II furcation-involved mandibular molars. A clinical study. J Clin Periodontol 1988;15:247-254.
187. Machtei EE, Grossi SG, Dunford R, Zambon JJ, Genco RJ. Long-term stability of Class II furcation defects treated with barrier membranes. J Periodontol 1996;67:523-527.

188. Becker W, Becker BE. Treatment of mandibular 3-wall intrabony defects by flap debridement and expanded polytetrafluoroethylene barrier membranes. Long-term evaluation of 32 treated patients. J Periodontol 1993;64:1138-1144.

189. Gottlow J, Nyman S, Karring T. Maintenance of new attachment gained through guided tissue regeneration. J Clin Periodontol 1992;19:315-317.

190. Machtei EE, Schallhorn RG. Successful regeneration of mandibular Class II furcation defects: an evidence-based treatment approach. Int J Periodontics Restorative Dent 1995;15:146-167.

191. Rutherford RB, Ryan ME, Kennedy JE, Tucker MM, Charette MF. Platelet-derived growth factor and dexamethasone combined with a collagen matrix induce regeneration of the periodontium in monkeys. J Clin Periodontol 1993;20:537-544.

192. Nakahara T, Nakamura T, Kobayashi E, Inoue M, Shigeno K, Tabata Y, Eto K, Shimizu Y. Novel approach to regeneration of periodontal tissues based on in situ tissue engineering: effects of controlled release of basic fibroblast growth factor from a sandwich membrane. Tissue Eng 2003;9:153-162.

193. Rutherford RB, Niekrash CE, Kennedy JE, Charette MF. Platelet-derived and insulin-like growth factors stimulate regeneration of periodontal attachment in monkeys. J Periodontal Res 1992;27:285-290.

194. Tatakis DN, Wikesjo UM, Razi SS, Sigurdsson TJ, Lee MB, Nguyen T, Ongpipattanakul B, Hardwick R. Periodontal repair in dogs: effect of transforming growth factor-beta 1 on alveolar bone and cementum regeneration. J Clin Periodontol 2000;27:698-704.

195. Ripamonti U, Reddi AH. Tissue engineering, morphogenesis, and regeneration of the periodontal tissues by bone morphogenetic proteins. Crit Rev Oral Biol Med 1997;8:154-163.

196. Portner R, Giese C. An Overview on Bioreactor Design, Prototyping and Process Control for Reproducible Three-Dimensional Tissue Culture. In: Marx U, Sandig V, eds. Drug Testing in vitro: Breakthroughs and Trends in Cell Culture Technology. Weinheim: Wiley-VCH; 2007.

197. Jaasma MJ, O'Brien FJ. Mechanical stimulation of osteoblasts using steady and dynamic fluid flow. Tissue Eng Part A 2008;14:1213-1223.
198. Kalyanaraman B, Supp DM, Boyce ST. Medium flow rate regulates viability and barrier function of engineered skin substitutes in perfusion culture. Tissue Eng Part A 2008;14:583-593.
199. Rose GG, Cattoni M. Human gingiva cultivated in circumfusion systems. Arch Oral Biol 1974;19:113-123.
200. Edel A, Faccini JM. Histologic changes following the grafting of connective tissue into human gingiva. Oral Surg Oral Med Oral Pathol 1977;43:190-195.
201. Grossman ES, Austin JC. The ultrastructural response to loading of the oral mucosa of the vervet monkey. Journal of Periodontal Research 1983;18:474-482.
202. Shama F, Sherman P. Identification of stimuli controlling the sensory evaluation of viscosity. Journal of Texture Studies 1973;4:111-118.
203. de Bruijne DW, Hendrickx HACM, Anderliesten L, de Looff J. Mouthfeel of foods. In: Dickinson E, Walstra P, eds. Food colloids and polymers:stability and mechanical properties. Cambridge: Royal Society of Chemistry; 1993.
204. Wennstrom JL, Lindhe J, Sinclair F, Thilander B. Some periodontal tissue reactions to orthodontic tooth movement in monkeys. J Clin Periodontol 1987;14:121-129.
205. Bouri A, Jr., Bissada N, Al-Zahrani MS, Faddoul F, Nouneh I. Width of keratinized gingiva and the health status of the supporting tissues around dental implants. Int J Oral Maxillofac Implants 2008;23:323-326.
206. Kim BS, Kim YK, Yun PY, Yi YJ, Lee HJ, Kim SG, Son JS. Evaluation of peri-implant tissue response according to the presence of keratinized mucosa. Oral Surg Oral Med Oral Pathol Oral Radiol Endod 2009;107:e24-28.
207. Miyasato M, Crigger M, Egelberg J. Gingival condition in areas of minimal and appreciable width of keratinized gingiva. J Clin Periodontol 1977;4:200-209.
208. Orban B. Clinical and histologic study of the surface characteristics of the gingiva. Oral Surg Oral Med Oral Pathol 1948;1:827-841.

209. Susi FR. Anchoring fibrils in the attachment of epithelium to connective tissue in oral mucous membranes. J Dent Res 1969;48:144-148.
210. Dolby AE, ed. Oral mucosa in health and disease. Oxford: Blackwell Scientific Publications; 1975.
211. Gibbs S, Ponec M. Intrinsic regulation of differentiation markers in human epidermis, hard palate and buccal mucosa. Arch Oral Biol 2000;45:149-158.
212. Orban B, Sicher H. The Oral Mucosa. Journal of Dental Education 1945;10:94-100.
213. Kullaa-Mikkonen A. Scanning electron microscopic study of surface of human oral mucosa. Scand J Dent Res 1986;94:50-56.
214. Clausen H, Vedtofte P, Moe D, Dabelsteen E. Keratin pattern in human and buccal and hard palate mucosa. Scand J Dent Res 1983;91:411-413.
215. Newcomb GM. An ultrastructural study of epithelial specialization at the porcine mucogingival junction. J Periodontal Res 1981;16:51-65.
216. Brill N, Maeda T, Stolze K. Does a temperature gradient exist across the mucogingival junction? J Oral Rehabil 1978;5:81-87.
217. Volchansky A, Cleaton-Jones P. Variations in oral temperature. J Oral Rehabil 1994;21:605-611.
218. Tanaka E, Inubushi T, Takahashi K, Shirakura M, Sano R, Dalla-Bona DA, Nakajima A, van Eijden TMGJ, Tanne K. Dynamic shear properties of the porcine molar periodontal ligament Journal of Biomechanics 2007;40:1477-1483.
219. Pini M, Wiskott HW, Scherrer SS, Botsis J, Belser UC. Mechanical characterization of bovine periodontal ligament. J Periodontal Res 2002;37:237-244.
220. Kydd WL, Mandley J. The stiffness of palatal mucoperiosteum. J Prosthet Dent 1967;18:116-121.
221. Heaney TG. A histological investigation of the influence of adult porcine gingival connective tissues in determining epithelial specificity. Arch Oral Biol 1977;22:167-174.

222. Pennati G. Biomechanical properties of the human umbilical cord. Biorheology 2001;38:355-366.
223. Soden PD, Kershaw I. Tensile testing of connective tissues. Med Biol Eng 1974;12:510-518.
224. Holzapfel GA. Determination of material models for arterial walls from uniaxial extension tests and histological structure. J Theor Biol 2006;238:290-302.
225. Fung YC. Biorheology of soft tissues. Biorheology 1973;10:139-155.
226. Fung YC. Biomechanics:Mechanical Properties of Living Tissues. New York: Springer-Verlag; 1993.
227. Daniel J, Abe K, McFetridge PS. Development of the human umbilical vein scaffold for cardiovascular tissue engineering applications. Asaio J 2005;51:252-261.
228. Cheng T, Dai C, Gan RZ. Viscoelastic properties of human tympanic membrane. Ann Biomed Eng 2007;35:305-314.
229. Druzinsky RE. The time allometry of mammalian chewing movements: chewing frequency scales with body mass in mammals. J Theor Biol 1993;160:427-440.
230. Kydd WL, Daly CH, Nansen D. Variation in the response to mechanical stress of human soft tissues as related to age. J Prosthet Dent 1974;32:493-500.
231. Beek M, Aarnts MP, Koolstra JH, Feilzer AJ, van Eijden TM. Dynamic properties of the human temporomandibular joint disc. J Dent Res 2001;80:876-880.
232. Lumpkins SB, Pierre N, McFetridge PS. A mechanical evaluation of three decellularization methods in the design of a xenogeneic scaffold for tissue engineering the temporomandibular joint disc. Acta Biomater 2008;4:808-816.
233. Natali AN, Pavan PG, Carniel EL, Dario P, Izzo I. Characterization of soft tissue mechanics with aging. IEEE Engineering in Medicine and Biology Magazine 2008;27:15-22.
234. Haslach HWJ. Nonlinear viscoelastic, thermodynamically consistent, models for biological soft tissue. Biomechanics and Modeling in Mechanobiology 2005;3:172-189.

235. Picton DC, Wills DJ. Viscoelastic properties of the periodontal ligament and mucous membrane. J Prosthet Dent 1978;40:263-272.
236. Appleton J, Heaney TG. A scanning electron microscope study of the surface features of porcine oral mucosa. J Periodontal Res 1977;12:430-435.
237. Tanaka E, Yamano E, Dalla-Bona DA, Watanabe M, Inubushi T, Shirakura M, Sano R, Takahashi K, van Eijden T, Tanne K. Dynamic compressive properties of the mandibular condylar cartilage. J Dent Res 2006;85:571-575.
238. Scapino RP. Biomechanics of prehensile oral mucosa. J Morphol 1967;122:89-114.
239. Avery JK. Oral Development and Histology. New York: Thieme Medical Publishers; 2002.
240. Landay MA, Schroeder HE. Differentiation in normal human buccal mucosa epithelium. J Anat 1979;128:31-51.
241. Schroeder HE. Oral Structural Biology. New York: Thieme Medical Publishers, Inc.; 1991.
242. Weinmann JP, Meyer J, Mardfin D, Weiss M. Occurrence and role of glycogen in the epithelium of the alveolar mucosa and of the attached gingiva. Am J Anat 1959;104:381-402.
243. Mercer EH. Keratin and Keratinization. New York: Pergamon Press; 1961.
244. Tanaka E, Kikuzaki M, Hanaoka K, Tanaka M, Sasaki A, Kawai N, Ishino Y, Takeuchi M, Tanne K. Dynamic compressive properties of porcine temporomandibular joint disc. Eur J Oral Sci 2003;111:434-439.
245. Kydd WL, Daly CH. The biologic and mechanical effects of stress on oral mucosa. J Prosthet Dent 1982;47:317-329.
246. Tanaka E, van Eijden T. Biomechanical behavior of the temporomandibular joint disc. Crit Rev Oral Biol Med 2003;14:138-150.
247. Lu XL, Mow VC, Guo XE. Proteoglycans and mechanical behavior of condylar cartilage. J Dent Res 2009;88:244-248.
248. Rahemtulla F. Proteoglycans of oral tissues. Crit Rev Oral Biol Med 1992;3:135-162.

249. Fleisch L, Austin JC. A histologic study of the response of masticatory and lining mucosa to mechanical loading in the vervet monkey. J Prosthet Dent 1978;39:211-216.
250. Kydd WL, Daly CH, Wheeler JB, 3rd. The thickness measurement of masticatory mucosa in vivo. Int Dent J 1971;21:430-441.
251. Fleisch L. A comparative study of the buccal and lingual gingival tissues of the vervet monkey. J Periodontal Res 1974;9:92-99.
252. Umeda T, Tamari Y, Nishimura M. Distribution of elastic fibers in oral mucosa of mammals. J Osaka Univ Dent Sch 1968;8:39-46.
253. Ohnemus U, Willers C, Bubenheim M, Horstkotte MA, Houdek P, Fischer F, Schmage P, Moll I, Brandner JM. An ex-vivo oral mucosa infection model for the evaluation of the topical activity of antifungal agents. Mycoses 2008;51:21-29.
254. Mickalites C, Orlowski WA. Study of the noncollagenous components of the periodontium J Dent Res 1977;56:1023-1026.
255. Rabinowitz JL, Rutberg M, Cohen DW, Marsh JB. Human gingival lipids. J Periodontal Res 1973;8:381-383.
256. Kulkarni U, Mahalingam R, Pather I, Li X, Jasti B. Porcine buccal mucosa as in vitro model: effect of biological and experimental variables. J Pharm Sci 2010;99:1265-1277.
257. Abbott WM, Megerman J, Hasson JE, L'Italien G, Warnock DF. Effect of compliance mismatch on vascular graft patency. J Vasc Surg 1987;5:376-382.
258. Bartz RL, Kamaric E, Noble PC, Lintner D, Bocell J. Topographic matching of selected donor and recipient sites for osteochondral autografting of the articular surface of the femoral condyles. Am J Sports Med 2001;29:207-212.
259. Osathanon T, Giachelli CM, Somerman MJ. Immobilization of alkaline phosphatase on microporous nanofibrous fibrin scaffolds for bone tissue engineering. Biomaterials 2009;30:4513-4521.
260. Ente G, Penzer PH. The umbilical cord: normal parameters. J R Soc Health 1991;111:138-140.

261. Dardik II, Ibrahim IM, Dardik H. Experimental and clinical use of human umbilical cord vessels as vascular substitutes. J Cardiovasc Surg (Torino) 1977;18:555-559.

262. Stehbens WE, Wakefield JS, Gilbert-Barness E, Zuccollo JM. Histopathology and ultrastructure of human umbilical blood vessels. Fetal Pediatr Pathol 2005;24:297-315.

263. Kadner A, Zund G, Maurus C, Breymann C, Yakarisik S, Kadner G, Turina M, Hoerstrup SP. Human umbilical cord cells for cardiovascular tissue engineering: a comparative study. Eur J Cardiothorac Surg 2004;25:635-641.

264. Palka J, Banikowski E, Jaworski S. An accumulation of IGF-I and IGF-binding proteins in human umbilical cord. Mol Cell Biochem 2000;206:133-139.

265. Rao CV, Li X, Toth P, Lei ZM. Expression of epidermal growth factor, transforming growth factor-alpha, and their common receptor genes in human umbilical cords. J Clin Endocrinol Metab 1995;80:1012-1020.

266. Engberg Damsgaard TM, Windelborg Nielsen B, Sorensen FB, Henriques U, Schiotz PO. Estimation of the total number of mast cells in the human umbilical cord. A methodological study. APMIS 1992;100:845-850.

267. Kafkasli A, Belfort MA, Giannina G, Vedernikov YP, Schaffner DL, Popek EJ. Histopathologic effects of meconium on human umbilical artery and vein: in vitro study. J Matern Fetal Med 1997;6:356-361.

268. Dardik H, Ibrahim IM, Sussman B, Kahn M, Israel M, Dardik I. Technical factors in the use of glutaraldehyde-tanned umbilical vein prosthesis for vascular reconstruction in the lower extremity Vascular Surgery 1981;15:51-60.

269. Aslan R, Sevin B, Dernek S, Manti Z. Human umbilical cord vein grafts for replacement of the superior vena cava. J Cardiovasc Surg (Torino) 1992;33:154-159.

270. Dardik H, Baier RE, Mennaghan M, Natiella J, Weinberg S, Turner R, Sussman B, Kahn M, Ibrahim IM, Dardik, II. Morphologic and biophysical assessment of long term human umbilical cord vein implants used as vascular conduits. Surg Gynecol Obstet 1982;154:17-26.

271. Dardik H, Dardik II. Successful arterial substitution with modified human umbilical vein. Ann Surg 1976;183:252-258.
272. Dardik H, Wengerter K, Qin F, Pangilinan A, Silvestri F, Wolodiger F, Kahn M, Sussman B, Ibrahim IM. Comparative decades of experience with glutaraldehyde-tanned human umbilical cord vein graft for lower limb revascularization: an analysis of 1275 cases. J Vasc Surg 2002;35:64-71.
273. Dardik HD, Ibrahim IM, Sprayregen S, Dardik, II. Clinical experience with modified human umbilical cord vein for arterial bypass. Surgery 1976;79:618-624.
274. Johnson WC, Lee KK. A comparative evaluation of polytetrafluoroethylene, umbilical vein, and saphenous vein bypass grafts for femoral-popliteal above-knee revascularization: a prospective randomized Department of Veterans Affairs cooperative study. J Vasc Surg 2000;32:268-277.
275. Wengerter K, Dardik H. Biological vascular grafts. Semin Vasc Surg 1999;12:46-51.
276. Dardik H. The threatened limb. Science & Medicine 1997;4:44-53.
277. Dardik H, Ibrahim IM, Baier R, Sprayregen S, Levy M, Dardik, II. Human umbilical cord. A new source for vascular prosthesis. JAMA 1976;236:2859-2862.
278. Ratto GB, Spinelli E, Lunghi C, Tomellini M, Sacco A, Motta G. Morphological evaluation of the human umbilical vein graft. An experimental study. Eur Surg Res 1983;15:151-160.
279. Sato O, Okamoto H, Takagi A, Miyata T, Takayama Y. Biodegradation of glutaraldehyde-tanned human umbilical vein grafts. Surg Today 1995;25:901-905.
280. Aalders GJ, van Vroonhoven TJ. Polytetrafluoroethylene versus human umbilical vein in above-knee femoropopliteal bypass: six-year results of a randomized clinical trial. J Vasc Surg 1992;16:816-823.

281. Dardik H, Ibrahim IM, Sussman B, Kahn M, Sanchez M, Klausner S, Baier RE, Meyer AE, Dardik, II. Biodegradation and aneurysm formation in umbilical vein grafts. Observations and a realistic strategy. Ann Surg 1984;199:61-68.
282. Esato K, Shintani K, Yasutake S. Modification and morphology of human umbilical cord vein as canine arterial bypass grafts. Ann Surg 1980;191:443-451.
283. Schmidt CE, Baier JM. Acellular vascular tissues: natural biomaterials for tissue repair and tissue engineering. Biomaterials 2000;21:2215-2231.
284. Dardik II, Dardik H. The fate of human umbilical cord vessels used as interposition arterial grafts in the baboon. Surg Gynecol Obstet 1975;140:567-571.
285. Gui L, Muto A, Chan SA, Breuer CK, Niklason LE. Development of decellularized human umbilical arteries as small-diameter vascular grafts. Tissue Eng Part A 2009;15:2665-2676.
286. Ott HC, Matthiesen TS, Goh SK, Black LD, Kren SM, Netoff TI, Taylor DA. Perfusion-decellularized matrix: using nature's platform to engineer a bioartificial heart. Nat Med 2008;14:213-221.
287. Schonmeyr B, Clavin N, Avraham T, Longo V, Mehrara BJ. Synthesis of a tissue-engineered periosteum with acellular dermal matrix and cultured mesenchymal stem cells. Tissue Eng Part A 2009;15:1833-1841.
288. Hudson TW, Liu SY, Schmidt CE. Engineering an improved acellular nerve graft via optimized chemical processing. Tissue Eng 2004;10:1346-1358.
289. Dahl SL, Koh J, Prabhakar V, Niklason LE. Decellularized native and engineered arterial scaffolds for transplantation. Cell Transplant 2003;12:659-666.
290. Brown BN, Barnes CA, Kasick RT, Michel R, Gilbert TW, Beer-Stolz D, Castner DG, Ratner BD, Badylak SF. Surface characterization of extracellular matrix scaffolds. Biomaterials 2010;31:428-437.
291. Gilbert TW, Sellaro TL, Badylak SF. Decellularization of tissues and organs. Biomaterials 2006;27:3675-3683.

292. Schaner PJ, Martin ND, Tulenko TN, Shapiro IM, Tarola NA, Leichter RF, Carabasi RA, Dimuzio PJ. Decellularized vein as a potential scaffold for vascular tissue engineering. J Vasc Surg 2004;40:146-153.
293. Cartmell JS, Dunn MG. Effect of chemical treatments on tendon cellularity and mechanical properties. J Biomed Mater Res 2000;49:134-140.
294. Chan RW, Rodriguez ML, McFetridge PS. The human umbilical vein with Wharton's jelly as an allogeneic, acellular construct for vocal fold restoration. Tissue Eng Part A 2009;15:3537-3546.
295. McFetridge PS, Daniel JW, Bodamyali T, Horrocks M, Chaudhuri JB. Preparation of porcine carotid arteries for vascular tissue engineering applications. J Biomed Mater Res A 2004;70:224-234.
296. Teebken OE, Bader A, Steinhoff G, Haverich A. Tissue engineering of vascular grafts: human cell seeding of decellularised porcine matrix. Eur J Vasc Endovasc Surg 2000;19:381-386.
297. Gloster ES, Stemerman MB, Spaet TH. Platelet interaction with human umbilical cord vascular basement membrane. Blood Vessels 1976;13:267-278.
298. Junek T, Baum O, Lauter H, Vetter K, Matejevic D, Graf R. Pre-eclampsia associated alterations of the elastic fibre system in umbilical cord vessels. Anat Embryol (Berl) 2000;201:291-303.
299. Romanowicz L, Jaworski S. Collagen of umbilical cord vein and its alterations in pre-eclampsia. Acta Biochim Pol 2002;49:451-458.
300. Patel A, Fine B, Sandig M, Mequanint K. Elastin biosynthesis: The missing link in tissue-engineered blood vessels. Cardiovasc Res 2006;71:40-49.
301. Sexton AJ, Turmaine M, Cai WQ, Burnstock G. A study of the ultrastructure of developing human umbilical vessels. J Anat 1996;188:75-85.
302. Kaem RI, Vtiurin BV, Zolotarevskii V, Kapanadze GI, Donetskii DA. [Morphology of a neonatal umbilical vein graft under prolonged experimental conditions]. Biull Eksp Biol Med 1985;100:485-489.

303. Nanaev AK, Kohnen G, Milovanov AP, Domogatsky SP, Kaufmann P. Stromal differentiation and architecture of the human umbilical cord. Placenta 1997;18:53-64.

304. Klein J, Meyer FA. Tissue structure and macromolecular diffusion in umbilical cord. Immobilization of endogenous hyaluronic acid. Biochim Biophys Acta 1983;755:400-411.

305. Romanowicz L, Sobolewski K. Extracellular matrix components of the wall of umbilical cord vein and their alterations in pre-eclampsia. J Perinat Med 2000;28:140-146.

306. Wang HS, Hung SC, Peng ST, Huang CC, Wei HM, Guo YJ, Fu YS, Lai MC, Chen CC. Mesenchymal stem cells in the Wharton's jelly of the human umbilical cord. Stem Cells 2004;22:1330-1337.

307. Franc S, Rousseau JC, Garrone R, van der Rest M, Moradi-Ameli M. Microfibrillar composition of umbilical cord matrix: characterization of fibrillin, collagen VI and intact collagen V. Placenta 1998;19:95-104.

308. Meyer FA, Laver-Rudich Z, Tanenbaum R. Evidence for a mechanical coupling of glycoprotein microfibrils with collagen fibrils in Wharton's jelly. Biochim Biophys Acta 1983;755:376-387.

309. Takechi K, Kuwabara Y, Mizuno M. Ultrastructural and immunohistochemical studies of Wharton's jelly umbilical cord cells. Placenta 1993;14:235-245.

310. Sobolewski K, Bankowski E, Chyczewski L, Jaworski S. Collagen and glycosaminoglycans of Wharton's jelly. Biol Neonate 1997;71:11-21.

311. Scantlebury TV. 1982-1992: a decade of technology development for guided tissue regeneration. J Periodontol 1993;64:1129-1137.

312. Brown B, Lindberg K, Reing J, Stolz DB, Badylak SF. The basement membrane component of biologic scaffolds derived from extracellular matrix. Tissue Eng 2006;12:519-526.

313. McFetridge PS, Bodamyali T, Horrocks M, Chaudhuri JB. Endothelial and smooth muscle cell seeding onto processed ex vivo arterial scaffolds using 3D vascular bioreactors. ASAIO J 2004;50:591-600.

314. Engbers-Buijtenhuijs P, Buttafoco L, Poot AA, Dijkstra PJ, de Vos RA, Sterk LM, Geelkerken RH, Vermes I, Feijen J. Biological characterisation of vascular grafts cultured in a bioreactor. Biomaterials 2006;27:2390-2397.
315. Quent VM, Loessner D, Friis T, Reichert JC, Hutmacher DW. Discrepancies between metabolic activity and DNA content as tool to assess cell proliferation in cancer research. J Cell Mol Med 2010;14:1003-1013.
316. Forsey RW, Chaudhuri JB. Validity of DNA analysis to determine cell numbers in tissue engineering scaffolds. Biotechnol Lett 2009;31:819-823.
317. Blaheta RA, Kronenberger B, Woitaschek D, Weber S, Scholz M, Schuldes H, Encke A, Markus BH. Development of an ultrasensitive in vitro assay to monitor growth of primary cell cultures with reduced mitotic activity. J Immunol Methods 1998;211:159-169.
318. Punshon G, Vara DS, Sales KM, Kidane AG, Salacinski HJ, Seifalian AM. Interactions between endothelial cells and a poly(carbonate-silsesquioxane-bridge-urea)urethane. Biomaterials 2005;26:6271-6279.
319. Abousleiman RI, Reyes Y, McFetridge P, Sikavitsas V. The human umbilical vein: a novel scaffold for musculoskeletal soft tissue regeneration. Artif Organs 2008;32:735-742.
320. Buurma B, Gu K, Rutherford RB. Transplantation of human pulpal and gingival fibroblasts attached to synthetic scaffolds. Eur J Oral Sci 1999;107:282-289.
321. Back SA, Khan R, Gan X, Rosenberg PA, Volpe JJ. A new Alamar Blue viability assay to rapidly quantify oligodendrocyte death. J Neurosci Methods 1999;91:47-54.
322. Al-Nasiry S, Geusens N, Hanssens M, Luyten C, Pijnenborg R. The use of Alamar Blue assay for quantitative analysis of viability, migration and invasion of choriocarcinoma cells. Hum Reprod 2007;22:1304-1309.
323. Fung YC. Elasticity of soft tissues in simple elongation. Am J Physiol 1967;213:1532-1544.
324. Ambrosio L, Netti PA, Nicolais L. Soft Tissue, In: Barbucci R, ed. Integrated biomaterials science. New York: Kluwer Academic/Plenum Publishers; 2002.

325. Fujita Y, Duncan NA, Lotz JC. Radial tensile properties of the lumbar annulus fibrosus are site and degeneration dependent. J Orthop Res 1997;15:814-819.
326. Hansen KA, Weiss JA, Barton JK. Recruitment of tendon crimp with applied tensile strain. J Biomech Eng 2002;124:72-77.
327. Johnson GA, Tramaglini DM, Levine RE, Ohno K, Choi NY, Woo SL. Tensile and viscoelastic properties of human patellar tendon. J Orthop Res 1994;12:796-803.
328. Gobin AS, Butler CE, Mathur AB. Repair and regeneration of the abdominal wall musculofascial defect using silk fibroin-chitosan blend. Tissue Eng 2006;12:3383-3394.
329. O'Cearbhaill ED, Barron V, McHugh PE. Characterisation of a collagen membrane for its potential use in cardiovascular tissue engineering applications. J Mater Sci Mater Med 2006;17:195-201.
330. Hoenicka M, Lehle K, Jacobs VR, Schmid FX, Birnbaum DE. Properties of the human umbilical vein as a living scaffold for a tissue-engineered vessel graft. Tissue Eng 2007;13:219-229.
331. Badylak SF. The extracellular matrix as a biologic scaffold material. Biomaterials 2007;28:3587-3593.
332. Comninou M, Yannas IV. Dependence of stress-strain nonlinearity of connective tissues on the geometry of collagen fibers. J Biomech 1976;9:427-433.
333. Elbischger PJ, Bischof H, Regitnig P, Holzapfel GA. Automatic analysis of collagen fiber orientation in the outermost layer of human arteries. Pattern Anal Appl 2004;7:269-284.
334. Holzapfel GA, Ogden RW, eds. Biomechanics of Soft Tissue in Cardiovascular Systems. New York: Springer; 2003:15-65.
335. Tower TT, Neidert MR, Tranquillo RT. Fiber alignment imaging during mechanical testing of soft tissues. Ann Biomed Eng 2002;30:1221-1233.
336. Dobrin PB. Mechanical properties of arteries. Physiological Reviews 1978;58:397-460.

337. Purslow PP, Wess TJ, Hukins DW. Collagen orientation and molecular spacing during creep and stress-relaxation in soft connective tissues. J Exp Biol 1998;201:135-142.
338. Saini S, Wick TM. Concentric cylinder bioreactor for production of tissue engineered cartilage: effect of seeding density and hydrodynamic loading on construct development. Biotechnol Prog 2003;19:510-521.
339. Rolfe P. Chemical sensing and control in cell & tissue bioreactors. Conf Proc IEEE Eng Med Biol Soc 2005;7:7486-7489.
340. Navarro FA, Mizuno S, Huertas JC, Glowacki J, Orgill DP. Perfusion of medium improves growth of human oral neomucosal tissue constructs. Wound Repair Regen 2001;9:507-512.
341. Shangkai C, Naohide T, Koji Y, Yasuji H, Masaaki N, Tomohiro T, Yasushi T. Transplantation of allogeneic chondrocytes cultured in fibroin sponge and stirring chamber to promote cartilage regeneration. Tissue Eng 2007;13:483-492.
342. Tran SC, Cooley AJ, Elder SH. Effect of a mechanical stimulation bioreactor on tissue engineered, scaffold-free cartilage. Biotechnol Bioeng 2011;108:1421-1429.
343. Walsh AJL, Lotz, J.C. Biological response of the intervertebral disc to dynamic loading. Journal of Biomechanics 2004;37:329-337.
344. Danciu TE, Gagari E, Adam RM, Damoulis PD, Freeman MR. Mechanical strain delivers anti-apoptotic and proliferative signals to gingival fibroblasts. J Dent Res 2004;83:596-601.
345. Grunheid T, Zentner A. Extracellular matrix synthesis, proliferation and death in mechanically stimulated human gingival fibroblasts in vitro. Clin Oral Investig 2005;9:124-130.
346. Zentner A, Panagiotis K, Heaney T. Early cellular reactions in mechanically stimulated gingival connective tissue. J Orofac Orthop 2001;62:476-487.
347. Theilig C, Bernd A, Leyhausen G, Kaufmann R, Geurtsen W. Effects of mechanical force on primary human fibroblasts derived from the gingiva and the periodontal ligament. J Dent Res 2001;80:1777-1780.

348. Bolcato-Bellemin AL, Elkaim R, Abehsera A, Fausser JL, Haikel Y, Tenenbaum H. Expression of mRNAs encoding for alpha and beta integrin subunits, MMPs, and TIMPs in stretched human periodontal ligament and gingival fibroblasts. J Dent Res 2000;79:1712-1716.
349. Hillmann G, Steinkamp-Zucht A, Geurtsen W, Gross G, Hoffmann A. Culture of primary human gingival fibroblasts on biodegradable membranes. Biomaterials 2002;23:1461-1469.
350. van der Pauw MT, Klein-Nulend J, van den Bos T, Burger EH, Everts V, Beertsen W. Response of periodontal ligament fibroblasts and gingival fibroblasts to pulsating fluid flow: nitric oxide and prostaglandin E2 release and expression of tissue non-specific alkaline phosphatase activity. J Periodontal Res 2000;35:335-343.
351. Elejalde CC, Kokini JL. The psychophysics of pouring, spreading and in-mouth viscosity Journal of Texture Studies 1992;23:315-336.
352. Kokini JL, Kadane JB, Cussler EL. Liquid texture perceived in the mouth Journal of Texture Studies 1977;8:195-218.
353. Kokini JL. Fluid and semi-solid food texture and texture-taste interactions. Food Technology 1985:86-94.
354. Bassett CA, Herrmann I. Influence of oxygen concentration and mechanical factors on differentiation of connective tissues in vitro. Nature 1961;190:460-461.
355. Pettigrew DW, Wang HM, Sodek J, Brunette DM. Synthesis of collagenolytic enzymes and their inhibitors by gingival tissue in vitro. Effect of endotoxin. J Periodontal Res 1981;16:637-645.
356. Niinikoski J. Effect of oxygen supply on wound healing and formation of experimental granulation tissue. Acta Physiol Scand Suppl 1969;334:1-72.
357. Papakonstantinou E, Aletras AJ, Roth M, Tamm M, Karakiulakis G. Hypoxia modulates the effects of transforming growth factor-beta isoforms on matrix-formation by primary human lung fibroblasts. Cytokine 2003;24:25-35.
358. Agocha A, Lee HW, Eghbali-Webb M. Hypoxia regulates basal and induced DNA synthesis and collagen type I production in human cardiac fibroblasts:

effects of transforming growth factor-beta1, thyroid hormone, angiotensin II and basic fibroblast growth factor. J Mol Cell Cardiol 1997;29:2233-2244.

359. Warren SM, Steinbrech DS, Mehrara BJ, Saadeh PB, Greenwald JA, Spector JA, Bouletreau PJ, Longaker MT. Hypoxia regulates osteoblast gene expression. J Surg Res 2001;99:147-155.

360. Griffith CK, George SC. The effect of hypoxia on in vitro prevascularization of a thick soft tissue. Tissue Eng Part A 2009;15:2423-2434.

361. Hopf HW, Gibson JJ, Angeles AP, Constant JS, Feng JJ, Rollins MD, Zamirul Hussain M, Hunt TK. Hyperoxia and angiogenesis. Wound Repair Regen 2005;13:558-564.

362. Vunjak-Novakovic G, Freshney RI. Culture of cells for tissue engineering. In: Freshney RI, ed. Culture of specialized cells. Hoboken: John Wiley & Sons; 2006.

363. Sen CK. Wound healing essentials: let there be oxygen. Wound Repair Regen 2009;17:1-18.

364. Hunt TK, Twomey P, Zederfeldt B, Dunphy JE. Respiratory gas tensions and pH in healing wounds. Am J Surg 1967;114:302-307.

365. Ninikoski J, Heughan C, Hunt TK. Oxygen and carbon dioxide tensions in experimental wounds. Surg Gynecol Obstet 1971;133:1003-1007.

366. Gray ML, Pizzanelli AM, Grodzinsky AJ, Lee RC. Mechanical and physiochemical determinants of the chondrocyte biosynthetic response. J Orthop Res 1988;6:777-792.

367. Polimeni G, Xiropaidis AV, Wikesjo UM. Biology and principles of periodontal wound healing/regeneration. Periodontol 2000 2006;41:30-47.

368. Wilkes RP, McNulty AK, Feeley TD, Schmidt MA, Kieswetter K. Bioreactor for application of subatmospheric pressure to three-dimensional cell culture. Tissue Eng 2007;13:3003-3010.

369. van Vliet T. On the relation between texture perception and fundamental mechanical parameters for liquids and time dependent solids. Food Quality and Preference 2002;13:227-236.

370. Percival RS, Challacombe SJ, Marsh PD. Flow rates of resting whole and stimulated parotid saliva in relation to age and gender. J Dent Res 1994;73:1416-1420.

371. Limbach LK, Li Y, Grass RN, Brunner TJ, Hintermann MA, Muller M, Gunther D, Stark WJ. Oxide nanoparticle uptake in human lung fibroblasts: effects of particle size, agglomeration, and diffusion at low concentrations. Environ Sci Technol 2005;39:9370-9376.

372. Gemmiti CV, Guldberg RE. Fluid flow increases type II collagen deposition and tensile mechanical properties in bioreactor-grown tissue-engineered cartilage. Tissue Eng 2006;12:469-479.

373. Levesque MJ, Nerem RM. The elongation and orientation of cultured endothelial cells in response to shear stress. J Biomech Eng 1985;107:341-347.

374. Coletti F, Macchietto S, Elvassore N. Mathematical modelling of three-dimensional cell cultures in perfusion bioreactors. Ind Eng Chem Res 2006;45:8158-8169.

375. Farsi NM. Signs of oral dryness in relation to salivary flow rate, pH, buffering capacity and dry mouth complaints. BMC Oral Health 2007;7:15.

376. Gallo LM, Nickel JC, Iwasaki LR, Palla S. Stress-field translation in the healthy human temporomandibular joint. J Dent Res 2000;79:1740-1746.

377. Lesch CA, Squier CA, Cruchley A, Williams DM, Speight P. The permeability of human oral mucosa and skin to water. J Dent Res 1989;68:1345-1349.

378. van Eyk AD, van der Bijl P. Comparative permeability of various chemical markers through human vaginal and buccal mucosa as well as porcine buccal and mouth floor mucosa. Arch Oral Biol 2004;49:387-392.

379. Squier CA, Johnson NW. Permeability of oral mucosa. Br Med Bull 1975;31:169-175.

380. Chotard-Ghodsnia R, Drochon A, Grebe R. A new flow chamber for the study of shear stress and transmural pressure upon cells adhering to a porous biomaterial. J Biomech Eng 2002;124:258-261.

381. Ichihara A, Suzuki H, Miyashita Y, Naitoh M, Hayashi M, Saruta T. Transmural pressure inhibits prorenin processing in juxtaglomerular cell. Am J Physiol 1999;277:R220-228.

382. Izumi K, Terashi H, Marcelo CL, Feinberg SE. Development and characterization of a tissue-engineered human oral mucosa equivalent produced in a serum-free culture system. J Dent Res 2000;79:798-805.

383. Del Fabbro M, Galardi E, Weinstein R, Bulfamante G, Miserocchi G. Fluid dynamics of gingival tissues. J Periodontal Res 1998;33:328-334.

384. Henskens YM, van den Keijbus PA, Veerman EC, Van der Weijden GA, Timmerman MF, Snoek CM, Van der Velden U, Nieuw Amerongen AV. Protein composition of whole and parotid saliva in healthy and periodontitis subjects. Determination of cystatins, albumin, amylase and IgA. J Periodontal Res 1996;31:57-65.

385. Dardik H. The role of synthetic grafts in femorotibial bypass. Surgical Rounds 1989;17-25.

386. Berthod F, Hayek D, Damour O, Collombel C. Collagen synthesis by fibroblasts cultured within a collagen sponge. Biomaterials 1993;14:749-754.

387. Black AF, Bouez C, Perrier E, Schlotmann K, Chapuis F, Damour O. Optimization and characterization of an engineered human skin equivalent. Tissue Eng 2005;11:723-733.

388. Kim YJ, Sah RL, Doong JY, Grodzinsky AJ. Fluorometric assay of DNA in cartilage explants using Hoechst 33258. Anal Biochem 1988;174:168-176.

389. Hoemann CD, Sun J, Chrzanowski V, Buschmann MD. A multivalent assay to detect glycosaminoglycan, protein, collagen, RNA, and DNA content in milligram samples of cartilage or hydrogel-based repair cartilage. Anal Biochem 2002;300:1-10.

390. Chirgwin JM, Przybyla AE, MacDonald RJ, Rutter WJ. Isolation of biologically active ribonucleic acid from sources enriched in ribonuclease. Biochemistry 1979;18:5294-5299.

391. Chomczynski P, Sacchi N. Single-step method of RNA isolation by acid guanidinium thiocyanate-phenol-chloroform extraction. Anal Biochem 1987;162:156-159.
392. Mentel R, Wegner U, Bruns R, Gurtler L. Real-time PCR to improve the diagnosis of respiratory syncytial virus infection. J Med Microbiol 2003;52:893-896.
393. Wilhelm J, Pingoud A. Real-time polymerase chain reaction. Chembiochem 2003;4:1120-1128.
394. Nolan T, Hands RE, Bustin SA. Quantification of mRNA using real-time RT-PCR. Nat Protoc 2006;1:1559-1582.
395. Qian H, Xiao Y, Bartold PM. Immunohistochemical localization and expression of fibromodulin in adult rat periodontium and inflamed human gingiva. Oral Dis 2004;10:233-239.
396. Gagliano N, Moscheni C, Dellavia C, Torri C, Stabellini G, Ferrario VF, Gioia M. Effect of cyclosporin A on human gingival fibroblast collagen turnover in relation to the development of gingival overgrowth: an in vitro study. Biomed Pharmacother 2004;58:231-238.
397. Tardif F, Ross G, Rouabhia M. Gingival and dermal fibroblasts produce interleukin-1 beta converting enzyme and interleukin-1 beta but not interleukin-18 even after stimulation with lipopolysaccharide. J Cell Physiol 2004;198:125-132.
398. Andrian E, Mostefaoui Y, Rouabhia M, Grenier D. Regulation of matrix metalloproteinases and tissue inhibitors of matrix metalloproteinases by Porphyromonas gingivalis in an engineered human oral mucosa model. J Cell Physiol 2007;211:56-62.
399. Livak KJ, Schmittgen TD. Analysis of relative gene expression data using real-time quantitative PCR and the 2(-Delta Delta C(T)) Method. Methods 2001;25:402-408.
400. Giulietti A, Overbergh L, Valckx D, Decallonne B, Bouillon R, Mathieu C. An overview of real-time quantitative PCR: applications to quantify cytokine gene expression. Methods 2001;25:386-401.

401. Kubista M, Andrade JM, Bengtsson M, Forootan A, Jonak J, Lind K, Sindelka R, Sjoback R, Sjogreen B, Strombom L, Stahlberg A, Zoric N. The real-time polymerase chain reaction. Mol Aspects Med 2006;27:95-125.
402. Pfaffl MW, Horgan GW, Dempfle L. Relative expression software tool (REST) for group-wise comparison and statistical analysis of relative expression results in real-time PCR. Nucleic Acids Res 2002;30:e36.
403. Teramura T, Fukuda K, Kurashimo S, Hosoi Y, Miki Y, Asada S, Hamanishi C. Isolation and characterization of side population stem cells in articular synovial tissue. BMC Musculoskelet Disord 2008;9:86-98.
404. Valarmathi MT, Yost MJ, Goodwin RL, Potts JD. The influence of proepicardial cells on the osteogenic potential of marrow stromal cells in a three-dimensional tubular scaffold. Biomaterials 2008;29:2203-2216.
405. Carson FL. Histotechnology. A Self-Instructional Text Chicago American Society of Clinical Pathologists; 1997.
406. Matos LL, Trufelli DC, de Matos MG, da Silva Pinhal MA. Immunohistochemistry as an important tool in biomarkers detection and clinical practice. Biomark Insights 2010;5:9-20.
407. Marriott NG, Gravani RB. Principles of Food Sanitation. New York: Springer; 2006:25-67.
408. May R, Sureban SM, Lightfoot SA, Hoskins AB, Brackett DJ, Postier RG, Ramanujam R, Rao CV, Wyche JH, Anant S, Houchen CW. Identification of a novel putative pancreatic stem/progenitor cell marker DCAMKL-1 in normal mouse pancreas. Am J Physiol Gastrointest Liver Physiol 2010;299:G303-310.
409. Yamashita S, Okada Y. Mechanisms of heat-induced antigen retrieval: analyses in vitro employing SDS-PAGE and immunohistochemistry. J Histochem Cytochem 2005;53:13-21.
410. Marshall-Taylor CE, Cartun RW, Mandich D, DiGiuseppe JA. Immunohistochemical detection of immunoglobulin light chain expression in B-cell non-Hodgkin lymphomas using formalin-fixed, paraffin-embedded tissues

and a heat-induced epitope retrieval technique. Appl Immunohistochem Mol Morphol 2002;10:258-262.

411. Lu A, Yu H, Chen K, Koide SS, Li X. Alteration in brain proteins following occlusion of the middle cerebral artery in rat. Life Sci 1999;65:493-500.

412. Qian-hua W, Shao-ping Z, Jian-wen Z, Yun Y, Li Z. Reduced expression of netrin-1 is associated with fetal growth restriction. Mol Cell Biochem 2011;350:81-87.

413. Daneshtalab N, Dore JJ, Smeda JS. Troubleshooting tissue specificity and antibody selection: Procedures in immunohistochemical studies. J Pharmacol Toxicol Methods 2010;61:127-135.

414. Goodpaster T, Legesse-Miller A, Hameed MR, Aisner SC, Randolph-Habecker J, Coller HA. An immunohistochemical method for identifying fibroblasts in formalin-fixed, paraffin-embedded tissue. J Histochem Cytochem 2008;56:347-358.

415. Radisic M, Park H, Chen F, Salazar-Lazzaro JE, Wang Y, Dennis R, Langer R, Freed LE, Vunjak-Novakovic G. Biomimetic approach to cardiac tissue engineering: oxygen carriers and channeled scaffolds. Tissue Eng 2006;12:2077-2091.

416. Meng L, Ye X, Fan M, Xiong X, Von den Hoff JW, Bian Z. Keratinocytes modify fibroblast metabolism in hereditary gingival fibromatosis. Arch Oral Biol 2008;53:1050-1057.

417. Poggi P, Rota MT, Boratto R. Microtubules and vimentin associated filaments (VIFs) in cultured human gingival fibroblasts (HGFs) after exposure to acrolein and acetaldehyde. Ann Anat 2001;183:159-163.

418. Li C, Li A, Li M, Xing Y, Chen H, Hu L, Tiozzo C, Anderson S, Taketo MM, Minoo P. Stabilized beta-catenin in lung epithelial cells changes cell fate and leads to tracheal and bronchial polyposis. Dev Biol 2009;334:97-108.

419. Nakamura Y, Miki Y, Suzuki T, Nakata T, Darnel AD, Moriya T, Tazawa C, Saito H, Ishibashi T, Takahashi S, Yamada S, Sasano H. Steroid sulfatase and

estrogen sulfotransferase in the atherosclerotic human aorta. Am J Pathol 2003;163:1329-1339.

420. Pfaffl MW. A new mathematical model for relative quantification in real-time RT-PCR. Nucleic Acids Res 2001;29:e45.

421. Hughes FJ, Ghuman M, Talal A. Periodontal regeneration: a challenge for the tissue engineer? Proc Inst Mech Eng H 2010;224:1345-1358.

422. Sowmya NK, Tarun Kumar AB, Mehta DS. Clinical evaluation of regenerative potential of type I collagen membrane along with xenogenic bone graft in the treatment of periodontal intrabony defects assessed with surgical re-entry and radiographic linear and densitometric analysis. J Indian Soc Periodontol 2010;14:23-29.

423. Kim EJ, Yoon SJ, Yeo GD, Pai CM, Kang IK. Preparation of biodegradable PLA/PLGA membranes with PGA mesh and their application for periodontal guided tissue regeneration. Biomed Mater 2009;4:055001.

424. Dardik H, Turner R. A clinicopathologic study of aneurysm formation of glutaraldehyde-tanned human umbilical vein grafts. J Vasc Surg 1990;12:221-222.

425. Nevelsteen A, D'Hallewin MA, Deleersnijder J, Wouters L, Suy R. The human umbilical vein graft in below-knee femoropopliteal and femorotibial surgery: an eight year experience. Ann Vasc Surg 1986;1:328-334.

426. Raithel D. Human umbilical cord vein for peripheral arterial reconstructive surgery. Angiology 1980;31:533-537.

427. Hou T, Xu J, Wu X, Xie Z, Luo F, Zhang Z, Zeng L. Umbilical cord Wharton's Jelly: a new potential cell source of mesenchymal stromal cells for bone tissue engineering. Tissue Eng Part A 2009;15:2325-2334.

428. Wang L, Ott L, Seshareddy K, Weiss ML, Detamore MS. Musculoskeletal tissue engineering with human umbilical cord mesenchymal stromal cells. Regen Med 2011;6:95-109.

429. Wang L, Tran I, Seshareddy K, Weiss ML, Detamore MS. A comparison of human bone marrow-derived mesenchymal stem cells and human umbilical cord-derived

mesenchymal stromal cells for cartilage tissue engineering. Tissue Eng Part A 2009;15:2259-2266.

430. Wang L, Zhao L, Detamore MS. Human umbilical cord mesenchymal stromal cells in a sandwich approach for osteochondral tissue engineering. J Tissue Eng Regen Med 2011;5:712-721.

431. Abousleiman RI, Reyes Y, McFetridge P, Sikavitsas V. Tendon tissue engineering using cell-seeded umbilical veins cultured in a mechanical stimulator. Tissue Eng Part A 2009;15:787-795.

432. Lumpkins SB, McFetridge PS. Regional variations in the viscoelastic compressive properties of the temporomandibular joint disc and implications toward tissue engineering. J Biomed Mater Res A 2009;90:784-791.

433. Ladd MR, Lee SJ, Atala A, Yoo JJ. Bioreactor maintained living skin matrix. Tissue Eng Part A 2009;15:861-868.

434. Stegemann JP, Hong H, Nerem RM. Mechanical, biochemical, and extracellular matrix effects on vascular smooth muscle cell phenotype. J Appl Physiol 2005;98:2321-2327.

435. Chao PH, Grayson W, Vunjak-Novakovic G. Engineering cartilage and bone using human mesenchymal stem cells. J Orthop Sci 2007;12:398-404.

436. Korber KH. Periodontal pulsation. J Periodontol 1970;41:382-390.

437. Murata H, Taguchi N, Hamada T, Kawamura M, McCabe JF. Dynamic viscoelasticity of soft liners and masticatory function. J Dent Res 2002;81:123-128.

438. McGuigan AP, Sefton MV. Design and fabrication of sub-mm-sized modules containing encapsulated cells for modular tissue engineering. Tissue Eng 2007;13:1069-1078.

439. Mooney R, Tawil B, Mahoney M. Specific fibrinogen and thrombin concentrations promote neuronal rather than glial growth when primary neural cells are seeded within plasma-derived fibrin gels. Tissue Eng Part A 2010;16:1607-1619.

440. Milam SB, Haskin C, Zardeneta G, Chen D, Magnuson VL, Klebe RJ, Steffenson B. Cell adhesion proteins in oral biology. Crit Rev Oral Biol Med 1991;2:451-491.

441. Barui A, Banerjee P, Das RK, Basu SK, Dhara S, Chatterjee J. Immunohistochemical Evaluation of p63, E-Cadherin, Collagen I and III Expression in Lower Limb Wound Healing under Honey. Evid Based Complement Alternat Med 2011;2011:239864.

442. Sidgwick GP, Bayat A. Extracellular matrix molecules implicated in hypertrophic and keloid scarring. J Eur Acad Dermatol Venereol 2011.

443. Brenda E, Marques A, Saldiva PHN, Davini MC, Pereira MD, Minami E, Ferreira MC. Analysis of the collagen content and tensile strength of the aponeurotic scar - an experimental study in pigs European Journal of Plastic Surgery 1999;22:28-35.

444. Iozzo RV, Murdoch AD. Proteoglycans of the extracellular environment: clues from the gene and protein side offer novel perspectives in molecular diversity and function. FASEB J 1996;10:598-614.

445. Yung S, Chan TM. Glycosaminoglycans and proteoglycans: overlooked entities? Perit Dial Int 2007;27:S104-109.

446. Lu P, Zhang GR, Song XH, Zou XH, Wang LL, Ouyang HW. Col V siRNA engineered tenocytes for tendon tissue engineering. PLoS One 2011;6:e21154.

447. Lewis JL, Krawczak DA, Oegema TR, Jr., Westendorf JJ. Effect of decorin and dermatan sulfate on the mechanical properties of a neocartilage. Connect Tissue Res 2010;51:159-170.

448. Uitto VJ, Larjava H. Extracellular matrix molecules and their receptors: an overview with special emphasis on periodontal tissues. Crit Rev Oral Biol Med 1991;2:323-354.

449. Hausser H, Groning A, Hasilik A, Schonherr E, Kresse H. Selective inactivity of TGF-beta/decorin complexes. FEBS Lett 1994;353:243-245.

450. Li X, Velleman SG. Effect of transforming growth factor-beta1 on decorin expression and muscle morphology during chicken embryonic and posthatch growth and development. Poult Sci 2009;88:387-397.

451. van den Akker J, Schoorl MJ, Bakker EN, Vanbavel E. Small artery remodeling: current concepts and questions. J Vasc Res 2010;47:183-202.

452. Aimes RT, Quigley JP. Matrix metalloproteinase-2 is an interstitial collagenase. Inhibitor-free enzyme catalyzes the cleavage of collagen fibrils and soluble native type I collagen generating the specific 3/4- and 1/4-length fragments. J Biol Chem 1995;270:5872-5876.

453. Suemitsu R, Yoshino I, Tomiyasu M, Fukuyama S, Okamoto T, Maehara Y. Serum tissue inhibitors of metalloproteinase-1 and -2 in patients with non-small cell lung cancer. Surg Today 2004;34:896-901.

454. Borsani E, Salgarello S, Mensi M, Boninsegna R, Stacchiotti A, Rezzani R, Sapelli P, Bianchi R, Rodella LF. Histochemical and immunohistochemical evaluation of gingival collagen and metalloproteinases in peri-implantitis. Acta Histochem 2005;107:231-240.

455. Perez-Amodio S, Tra WM, Rakhorst HA, Hovius SE,van Neck JW. Hypoxia preconditioning of tissue-engineered mucosa enhances its angiogenic capacity in vitro. Tissue Eng Part A 2011;17:1583-1593.

456. Cai G, Zhang X, Hong Q, Shao F, Shang X, Fu B, Feng Z, Lin H, Wang J, Shi S, Yin Z, Chen X. Tissue inhibitor of metalloproteinase-1 exacerbated renal interstitial fibrosis through enhancing inflammation. Nephrol Dial Transplant 2008;23:1861-1875.

457. Specht K, Richter T, Muller U, Walch A, Hofler MW. Quantitative gene expression analysis in microdissected archival tissue by real-time RT-PCR. J Mol Med (Berl) 2000;78:B27.

458. Lehmann U, Glockner S, Kleeberger W, von Wasielewski HF, Kreipe H. Detection of gene amplification in archival breast cancer specimens by laser-assisted microdissection and quantitative real-time polymerase chain reaction. Am J Pathol 2000;156:1855-1864.

459. Ethier CR, Simmons C. Introductory Biomechanics: From Cells to Organisms. Cambridge: Cambridge University Press; 2007.

460. Watson MA, Perry A, Budhraja V, Hicks C, Shannon WD, Rich KM. Gene expression profiling with oligonucleotide microarrays distinguishes World Health Organization grade of oligodendrogliomas. Cancer Res 2001;61:1825-1829.

461. Zhang WJ, Lin QX, Zhang Y, Liu CT, Qiu LY, Wang HB, Wang YM, Duan CM, Liu ZQ, Zhou J, Wang CY. The reconstruction of lung alveolus-like structure in collagen-matrigel/microcapsules scaffolds in vitro. J Cell Mol Med 2011;15:1878-1886.

462. Murphy KG. Postoperative healing complications associated with Gore-Tex Periodontal Material. Part I. Incidence and characterization. Int J Periodontics Restorative Dent 1995;15:363-375.

463. Lin SJ, Hou LT, Liu CM, Liao CS, Wong MY, Ho JY, Chang WK. Bacterial morphotypes and early cellular responses in clinically infected and non-infected sites after combination therapy of guided tissue regeneration and allograft. J Dent 2000;28:199-206.

464. Hung SL, Lin YW, Wang YH, Chen YT, Su CY, Ling LJ. Permeability of Streptococcus mutans and Actinobacillus actinomycetemcomitans Through guided tissue regeneration membranes and their effects on attachment of periodontal ligament cells. J Periodontol 2002;73:843-851.

Appendix A

STANDARD CURVE USED FOR THE ASSESSMENT OF DOUBLESTRANDED (ds)-DNA QUANTITY (PICOGREEN ASSAY)

The quantification of the double-stranded (ds)-DNA content within the tissue samples was done according to the manufacturer's protocol. Briefly, DNA standards were prepared by serially diluting λ DNA standard solution (100 μg/mL in TE buffer) in deionized (DI) water as follows:

Table A.1. Amounts and Concentrations Used for the λ DNA Standard Curve

Volume of standard used (μL)	Volume of DI water (μL)	Standard concentration obtained (μg/mL)
0	1000	0
1	999	0.1
3	997	0.3
10	990	1
30	970	3

Figure A-1 illustrates the standard curve obtained for λ DNA standard. The standard curve was obtained for each analysis.

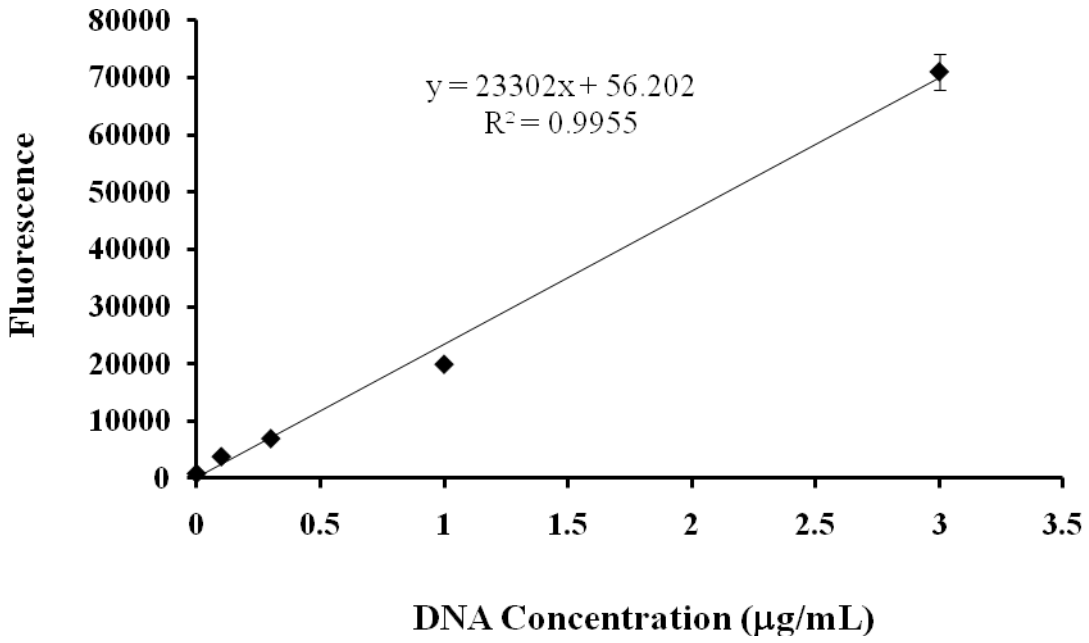

Figure A.1. λ DNA standard curve. The total concentration of DNA (μg/mL) was plotted against relative fluorescence units. The fluorescence was linear from 0.1 to 3 μg/mL with a correlation coefficient of 0.9955.